Optimization and Analysis of Lipid Nanoparticles for *in vivo* mRNA Delivery

By
Kevin John Kauffman

B.S. Chemical Engineering
The Ohio State University, 2012

SUBMITTED TO THE DEPARTMENT OF CHEMICAL ENGINEERING IN PARTIAL FULFILLMENT OF THE REQUIREMENTS FOR THE DEGREE OF

DOCTOR OF PHILOSOPHY
AT THE
MASSACHUSETTS INSTITUTE OF TECHNOLOGY

JUNE 2017

Signature redacted

Signature of Author: _____ Kevin J. Kauffman
Department of Chemical Engineering
May 9, 2017

Signature redacted

Certified by: _____ Daniel G. Anderson
Samuel A. Goldblith Professor of Applied Biology,
Chemical Engineering and Health Sciences & Technology
Thesis Supervisor

Signature redacted

Accepted by: _____ Daniel Blankschtein
Herman P. Meissner (1929) Professor of Chemical Engineering
Chairman, Committee for Graduate Students

Optimization and Analysis of Lipid Nanoparticles for *in vivo* mRNA Delivery

By

Kevin J. Kauffman

Submitted to the Department of Chemical Engineering on May 9th, 2017
in Partial Fulfillment of the Requirements for the Degree of Doctor of Philosophy

ABSTRACT

Messenger RNA (mRNA) therapeutics have the potential to treat a diverse array of diseases requiring protein expression, with applications in protein replacement therapies, immunotherapies, and genome engineering. However, the intracellular delivery of mRNA is challenging and necessitates a safe and effective delivery vector. Lipid nanoparticles (LNPs) have shown considerable promise for the delivery of small interfering RNAs (siRNA) to the liver but their utility as agents for mRNA delivery have only been recently investigated. New delivery materials for mRNA delivery are also being developed which have the potential to transfect non-liver targets, but the screening of these vectors *in vivo* is low-throughput and it is difficult to determine transfected cell types. There is a need both for efficacious, well-characterized mRNA delivery materials and for methods to facilitate *in vivo* screening of novel materials.

We first developed a generalized strategy to optimize LNP formulations for mRNA delivery to the liver using Design of Experiment methodologies. By simultaneously varying lipid ratios and structures, we developed an optimized formulation which increased the potency of eryrthopoietin-mRNA-loaded LNPs *in vivo* 7-fold relative to formulations previously used for siRNA delivery. Next, we explored the immune response and activity of base-modified LNP-formulated mRNA administered systemically *in vivo*. We observed indications of a previously-uncharacterized transient, extracellular innate immune response to mRNA-LNPs, including neutrophilia, myeloid cell activation, and up-regulation of four serum cytokines.

Although we have developed a more efficacious liver-targeting LNP, many mRNA therapies will require delivery to non-liver tissues. Using trial-and-error approaches, we discover novel formulations capable of inducing mRNA expression *in vivo* in the spleen, lung, and fat. To increase the throughput of *in vivo* screening, we report a new barcoding-based approach capable of evaluating the biodistribution and pharmacokinetics of many LNP formulations in a single mouse. Then, we develop a method that can identify mRNA expression delivered from LNPs in both bulk tissues and with single cell resolution.

Together, the work reported here contributes to the development of mRNA therapeutics by increasing mRNA-LNP potency and characterizing their immunogenicity *in vivo*. Furthermore, we hope the multiple *in vivo* screening methods described in this Thesis will accelerate the discovery of new delivery vectors capable of transfecting desired tissues and cell types.

Thesis Supervisor: Daniel G. Anderson
Title: Samuel A. Goldblith Associate Professor

ACKNOWLEDGMENTS

I would like to begin by thanking my advisor, Prof. Dan Anderson. Dan has been an excellent mentor who has supported me every step of the way, empowered me to explore my interests, and helped me to become a better scientist. Moreover, Dan has built a lab bursting with opportunities and full of incredibly creative, collaborative, and capable colleagues. I also want to thank Prof. Robert Langer and Prof. Phil Sharp for both their helpful discussions and their unparalleled expertise as members of my Thesis Committee.

It has been a privilege to work with many brilliant scientists from the Anderson and Langer Labs during my PhD; I have certainly stood on the shoulders of many giants. Although there are too many people to list here who have taught me skills, provided me guidance, and helped with experiments over the last five years, I would like to particularly acknowledge Robert Dorkin, Owen Fenton, Jimmy Kaczmarek, Sid Jhunjhunwala, Matt Webber, Danya Lavin, Benjamin Tang, Abigail Lytton-Jean, James Dahlman, Eric Wang, Mark Tibbitt, Asha Patel, Eric Appel, Guarav Sahay, Kevin Daniel, Piotr Kowalski, Hok Hei Tam, Roman Bogorad, Hao Yin, Omar Khan, and Luke Rhym. I have been extraordinarily fortunate to work with three outstanding technicians -- Faryal Mir, Jung Yang, and Shivani Bhadini -- and to have watched my undergraduate student Juan Hurtado grow into an exceptional young researcher. I also want to thank to Tara Fawaz and the support staff for keeping such a large lab running so smoothly.

Thank you to my undergraduate research advisor, Prof. Kristy Ainslie, for providing me three years of mentorship, teaching me how to be an independent researcher, and giving me the push to take a risk at MIT. I thank my high school chemistry teachers, Julie Summers and Bonnie Buddendeck as well. I also would have never had these research opportunities were it not for the support of funding and collaborators. I am grateful to Frank DeRosa and Mike Heartlein at Shire/RaNA for their advice and for providing many valuable materials for my research. I also thank the Skoltech/MIT Collaborative, Alnylam Pharmaceuticals, Biogen, and the Marble Center for Cancer Nanomedicine.

Many of my labmates have become steadfast friends during my time here, and I also want to acknowledge the support of my friends outside of lab. I want to give a special shout out to Nick Mozdzierz, who has been a tried and true friend, roommate, and climbing partner since Day 1 at MIT, and the rest of my ChemE friends -- Harry, Isaac, Monique, Sue Zanne, Justin, Abel, and Jose. Also thanks to the Sunday morning pickup basketball crew and my life-long friends from my beloved alma mater Ohio State -- Ben, Veda, Jerry, Justin, and Megan. (Go Bucks!)

Last and definitely not least, I want to thank my family and loved ones. Anthony, thanks for your patience and compassion. Jason, thanks for showing me how to be creative and kind. Mom, thanks for being my fiercest advocate over the years. Dad, thanks for inspiring me to be a scientist and for being my role model in all things. Maggie, thanks for the never-ending licking and for being the cutest little fur ball (she's a dog, in case anyone reading this thinks I'm weird.)

This PhD would not have been possible without the support and help of countless colleagues, friends, and family. Thank you to everyone, past and present.

TABLE OF CONTENTS

LIST OF FIGURES

LIST OF TABLES

Chapter 1

Introduction and Background

Portions of the work presented in this chapter were published as:
Kauffman, K.J., Webber, M.J., Anderson, D.G. "Materials for Non-viral Intracellular Delivery of Messenger RNA Therapeutics." *J. Control. Release*, **240**, 227-234, 2016.

1.1 Motivation

Aberrant protein expression is a frequent hallmark of many diseases, ranging from genetic disorders to cancer. Thus, the ability to control protein expression *in vivo* has broad therapeutic potential. Nucleic acids endogenously control and regulate intracellular protein expression via a number of established mechanisms. DNA can be transcribed to produce messenger RNA (mRNA), which in turn can be translated into specific proteins.[1] Alternatively, various RNA interference (RNAi) pathways exist in which oligonucleotides in the form of small interfering RNAs (siRNAs) or other types of RNAs silence protein expression.[2] In recent years, gene editing systems (e.g. CRISPR/Cas, zinc finger nucleases) have also emerged, which use programmable DNA nucleases to permanently and precisely manipulate the genome.[3]

Gene therapy uses nucleic acids to introduce beneficial protein or reduce levels of harmful protein for a therapeutic benefit. As of this writing, clinical trials in humans using therapeutic DNA, mRNA, and siRNA have shown promise in treating conditions as wide-ranging as hemophilia, Wiskott-Aldrich syndrome, B-cell lymphomas, macular degeneration, hypercholesterolemia, TTR-mediated amyloidosis, and melanoma.[4–6] Gene therapy is appealing because these and many other diseases can be treated at the genetic level without having to rely on traditional small-molecule therapeutics. However, a number of challenges must be addressed before gene therapy sees widespread clinical application, which will be discussed in the following sections.

1.1.1 Barriers to Intracellular Delivery of Nucleic Acids

To use nucleic acids therapeutically, a number of barriers must be overcome in the delivery of exogenous molecules.[7,8] Among these, barriers of entry into the cell in order to realize efficient intracellular delivery of nucleic acid presents perhaps the most formidable challenge. As nucleic acids are large, hydrophilic, anionic molecules, they cannot readily

traverse the hydrophobic lipid membrane of the cell.[9] Furthermore, the association of free nucleic acids with invading pathogens has resulted in the evolution of a number of innate defense mechanisms that include circulating nucleases, which degrade nucleic acids, and pattern recognition mechanisms that serve as activators of the innate immune system.[10,11] For these reasons, efficient delivery is often mediated by a vector to entrap, protect, and shuttle the nucleic acid payload across the cell membrane to enable access to the cytosol (for siRNAs and mRNAs) or the nucleus (for DNAs) in order for the nucleic acid to elicit its function. These delivery vectors for nucleic acids are made from diverse synthetic or natural materials (lipids, polymers, peptides, antibodies, small molecules, metals, etc.) and come in a variety of geometric architectures (nanoparticles, microparticles, conjugates, solid devices, hydrogels, etc.). The delivery material is crucial in achieving efficient and efficacious nucleic acid therapy.

Historically, early efforts to transfect cells led to the observation that positively-charged molecules, typically rich in protonating amine groups, could readily form electrostatic complexes with negatively-charged DNA, and further that the resulting nanocomplexes could enter cells and facilitate protein expression.[12] The evolution of these cationic delivery materials, beginning with initial efforts to use naturally-occurring molecules like protamine[13] and poly(L-lysine)[14] and extending to more recent examples of synthetic molecules specifically designed for gene delivery like poly(β-amino esters)[15] or DLinDMA[16] lipids, is the focus of the following sections. Following the discovery of siRNA in the late 1990s,[17] these and other delivery materials often proved useful in applications for siRNA delivery. In addition, a number of novel delivery materials were specifically designed for siRNA delivery, such as ionizable lipid-like molecules,[18,19] and these will be discussed in this Chapter as well.

1.1.2 Messenger RNA as a Therapeutic Modality

Recently, there has been great interest in the therapeutic use of mRNA,[20–23] which also requires effective delivery materials to reach its target. From a delivery perspective, there are inherent benefits to using mRNA instead of DNA. mRNA must only be delivered to the cytoplasm where cellular translation machinery is located; conversely, DNA requires transfection to the nucleus, which introduces the added physical barrier of the nuclear membrane. From a therapeutic perspective, protein expression arising from mRNA is more transient than that from DNA. From a safety perspective, mRNA does not carry the risk of genomic integration associated with DNA insertional mutagenesis.[24] Delivery of mRNA also offers many therapeutic directions beyond protein replacement/supplementation therapies. For example, the inherent immune-activating adjuvant properties of foreign RNAs can be leveraged for the intracellular delivery of mRNAs coding for specific antigens, which could be broadly applied in cancer immunotherapy,[25] prophylactic vaccines,[26] and allergy tolerization;[27] this particular use of mRNA is the most clinically advanced and thus constitutes the majority of the applications discussed here. Additionally, mRNAs have potential for use in the emerging field of genome editing and genomic engineering.[28,29]

1.2 Delivery Materials for mRNA Therapeutics

In this section of **Chapter 1**, the various classes of materials that have been used for nucleic acid delivery will be highlighted along with perspective on the use of these materials specifically for the therapeutic delivery of mRNA. Of note, viral vectors, which can also successfully deliver nucleic acids, have been extensively reviewed elsewhere[30,31] and are not discussed in this section. A recent review[22] extensively focused on the therapeutic potential and challenges surrounding mRNA as a drug, but did not describe in detail the specific delivery

materials that would facilitate its use. Here, we focus primarily on mRNA delivery materials, along with their mechanisms of action, routes of administration, and dosages for *in vivo* applications. The use of materials for mRNA delivery will be framed in the context of the history of their use in the delivery of other classes of nucleic acids, as many of these materials were initially designed for siRNA and DNA delivery applications. Materials are discussed in order of increasing complexity, starting with the delivery of naked mRNA, followed by protamine-based delivery systems, then lipid and polymer materials, and concluding with hybrid formulations.

1.2.1 Naked Oligonucleotides

Naked nucleic acids cannot readily cross cell membranes as a result of their size, charge, hydrophilicity, and degradability.[9] However, there exist some native mechanisms by which mRNA can translocate across the cell membrane without the use of a delivery material: studies performed *in vitro* have demonstrated the capability of cells to uptake naked mRNA via scavenger-receptor mediated endocytosis, and though most mRNA accumulates and degrades in lysosomal compartments, some intact mRNA is able to access the cytoplasm and express protein.[32] Common routes of transient membrane permeabilization, such as electroporation, provide another method to transfect cells with naked mRNA and is commonly used to study mRNA activity or immunogenicity *in vitro*[33] and *in vivo.*[34] Microinjection, in which mRNA is directly injected into the cell using a micropipette, is useful for efficient delivery of mRNA to single cells *in vitro.*[35] Other physical methods such as hydrostatic pressure transfection, sonoporation, and laser irradiation, have been used *in vitro* for DNA delivery[36] but are less commonly used for mRNA delivery. The use of a gene gun, in which naked mRNA is coated onto the surface of gold microparticles and pneumatically shot into a target cell at high speed, has also been described for mRNA transfection.[37]

Intravenous injection of unmodified mRNA without a delivery material leads to rapid degradation by ribonucleases and can activate the innate immune system.[11] Direct local injections of naked mRNA, e.g. subcutaneously,[38] intramuscularly,[39] or intranodally,[40] has shown some utility in applications in which an immune response is desired and relatively low levels of generated protein are required, such as for vaccination.[22] Some techniques have been demonstrated to improve naked mRNA potency; significant enhancements in both protein expression and duration were observed following intranodal injection of naked mRNA when dissolved in buffers containing calcium ions.[40] As of this writing, there have been dozens of preclinical studies and clinical trials in which the direct injection of mRNA was evaluated for cancer (melanoma, renal cell carcinoma), infectious diseases (influenza, tuberculosis), allergy tolerization (peanut, egg white), and protein replacement (anemia, asthma); these trials and others have been reviewed extensively elsewhere.[22] Thus, in some specific circumstances, the direct local injection of naked mRNA may have therapeutic utility.

Systemic delivery of naked siRNA to the liver, on the other hand, has been mediated through direct conjugation of targeting ligands to the siRNA molecule. In a report from 2004, Soutschek et al.[41] conjugated cholesterol to siRNA via the 3' end of the sense strand so as not to interfere with the antisense/RISC binding required for RNAi. Intravenous injection of the siRNA-cholesterol conjugate into mice at a high dose (50 mg/kg) resulted in silencing of an endogenous gene coding for apolipoprotein B and transfection was found to be mediated by lipoprotein trafficking.[42] Current state-of-the-art for liver-targeted siRNA conjugates uses direct conjugation of a triantennary GalNAc small molecule (**Fig. 1-1a**), a derivative of galactose which has remarkably high affinity for the asialoglycoprotein receptor found on heaptocytes.[43–45] GalNAc-conjugated siRNAs exhibit potent silencing in hepatocytes *in vivo* following subcutaneous administration at 5 mg/kg and are being evaluated in ongoing human clinical trials.[46,47]

Despite the success demonstrated for siRNA conjugates, to our knowledge direct small molecule conjugation approaches for mRNA delivery have not yet been reported. Differences in size, stability, and function between siRNA and mRNA contribute to making mRNA delivery via direct conjugation a more challenging endeavor. The molecular weight of therapeutically-relevant mRNA can be orders-of-magnitude larger than siRNA, and thus the relative targeting ligand to RNA size ratio is much smaller for mRNA conjugates, and the secondary structure of the mRNA may obscure the ligand from its cognate receptor. Another important difference is the existence of the siRNA sense strand, which offers a convenient route of chemical conjugation through terminal modification without impeding function, as only the antisense strand binds to the RISC complex.[48] Also, siRNA can be made routinely using established oligonucleotide synthesis techniques, enabling more control over orthogonal synthetic modification than is possible for mRNA which, owing to its length, is primarily produced via *in vitro* transcription[22] and thus presents significant challenges in controlling the location of potential modifications.

Furthermore, while siRNA can be protected against degradation by ribonucleases through chemical modifications to the RNA nucleotides and/or phosphodiester bonds[11,49] without significantly hindering the ability of siRNA to participate in the RNAi pathway, modifications to the bases of mRNA can be more challenging and alter ribosomal translation.[50,51] It should, however, be noted that several base modifications, such as pseudouridine (ψ) and 5-methylcytidine (5mC) (**Fig. 1-1b**), have been reported to be tolerated with decreased immunogenicity and may even increase net protein production compared to unmodified mRNAs in some settings.[52–54] There are a number of other design considerations in preparing mRNA for eventual therapeutic use. Typically, a 5' cap and polyadenylated 3' tail are used to increase the translation efficiency and also to protect against nuclease degradation.[55,56] Furthermore, the sequence of the untranslated regions (UTRs) of mRNA (which flank the coding region) can facilitate translation and stability.[57,58] A recent report describes sequence-engineered mRNA, in

which both the coding region and UTRs are optimized through iterative screening, resulting in significantly increased protein production.[59,60] There remains a need for new mRNA modification strategies that continue to further enhance potency, improve the efficiency of translation, and promote reduction in immunogenicity. It is anticipated that improvements in methodology to ensure mRNA stability, enable more robust and controlled synthesis, and understanding how orthogonal base modifications can be achieved without inhibiting translation could result in feasible and potentially clinically useful routes for direct conjugation of mRNA to facilitate systemic administration.

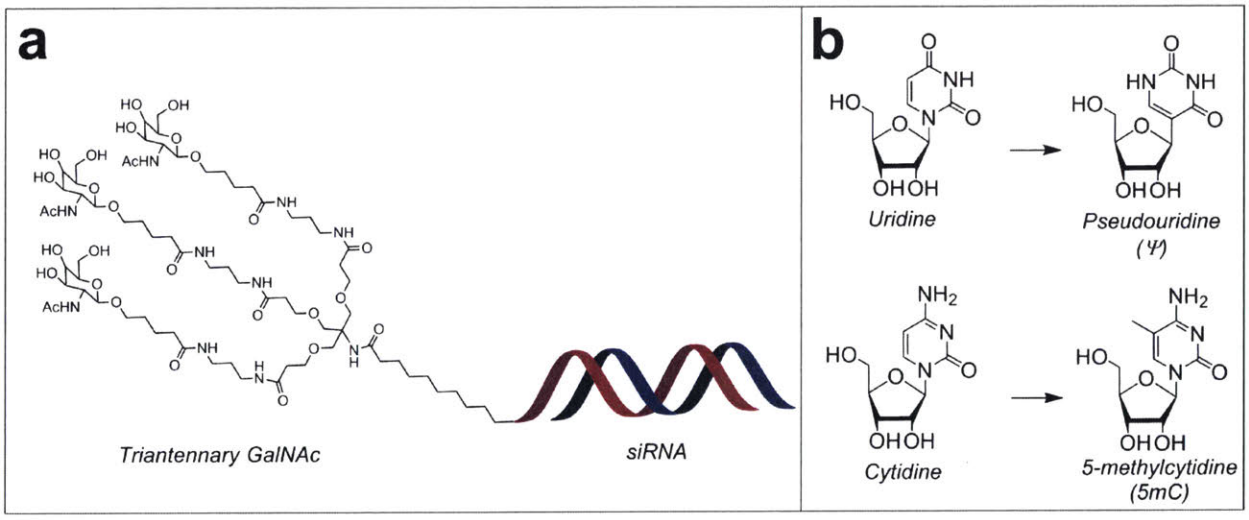

Figure 1-1. Direct oligonucleotide conjugates and strategies for modification. (**a**) Structure of triantennary GalNAc-siRNA direct conjugate in clinical trials. (**b**) Common base modifications for therapeutic mRNA to decrease immunogenicity and modulate translation.

1.2.2 Protamine-based Delivery Materials

Protamines, a family of small peptides (c.a. 4 kDa) derived from the sperm of fish, are arginine-rich molecules that form complexes with the negatively-charged backbone of DNA to condense the spermatid genome.[13] Because of their ability to bind to and form electrostatic

complexes with nucleic acids (**Fig. 1-2**), protamine was investigated in 1961 as one of the first materials for transfection of long RNAs.[61] Though there have been some reports of protamine-based siRNA delivery,[62] its use is more commonly associated with the delivery of longer RNAs, such as mRNA.[63] Protamine can complex with mRNA to form tightly-bound nanoparticles that are approximately 300 nm in diameter when a 2:1 protamine:mRNA weight ratio is used.[63,64] In its protamine-condensed form, mRNA is also protected against ribonuclease degradation,[65] though protamine complexation is known to heighten immune response both *in vitro* and *in vivo* compared to naked mRNA.[66] Single stranded RNAs are ligands for pattern recognition toll-like receptors TLR7 and TLR8,[67] and mRNA/protamine complexes also activate these pathways.[63–65] Although immune activation is not desirable for many applications of mRNA such as protein replacement therapy, it is an important property in the field of mRNA vaccines.

One example of an mRNA therapy is the RNActive© technology from CureVac, an mRNA vaccine which is prepared from a mixture of naked mRNA and protamine/mRNA complexes.[63] When delivered intradermally or intranodally, the naked mRNA encoding antigen enables expression while the protamine/mRNA complex also acts as an adjuvant. mRNA vaccination against infectious disease using this combination of naked mRNA with protamine-complexed mRNA to protect against the influenza virus in mice, ferrets, and pigs has been reported.[68] This approach has advanced through a number of clinical trials, with several more ongoing. An early clinical trial from 2005 (NCT00204607) first demonstrated the safety and immunogenicity of protamine/mRNA complexes in metastatic melanoma patients.[69] More recently, two ongoing clinical trials using RNActive© have been reported, including a trial using mRNA coding for six tumor-associated antigens (NY-ESO-1, MAGEC1, MAGEC2, 5 T4, survivin, MUC1) for treatment of patients with non-small cell lung cancer in combination with local radiation (NCT01915524).[70] Additionally, a trial using mRNA coding for four antigens overexpressed in prostate cancer (PSA, PSMA, PSCA, STEAP1) administered intradermally in

patients with prostate cancer demonstrated the vaccine to be well-tolerated and immunogenic.[71] The next generation of this prostate cancer mRNA vaccine is presently in a phase IIb trial (NCT01817738). The simplicity, facile synthesis, and self-adjuvanting properties of mRNA vaccine therapies have broach potential utility for enabling immunization towards a range of disease.

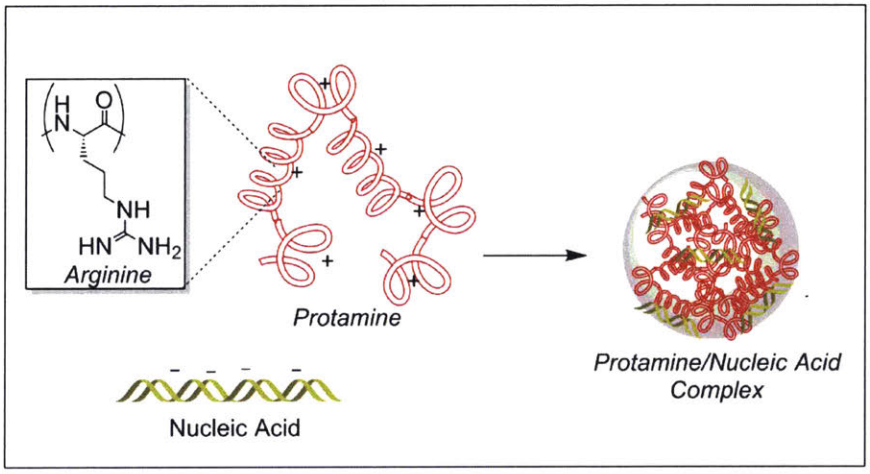

Figure 1-2. Protamine complexation with mRNA. Protamine, a cationic arginine-rich peptide, forms complexes with negatively-charged nucleic acids like mRNA.

1.2.3 Lipoplex and Lipid Nanoparticle Delivery Materials

Materials based on both synthetic and naturally derived lipids or lipid-like materials are commonly used for nucleic acid delivery.[72,73] Cationic lipids can form electrostatic complexes with negatively charged nucleic acids, leading to the formation of a "lipoplex" nanoparticle that can be endocytosed by cells (**Fig. 1-3a**). A number of commercially available transfection reagents, such as the Lipofectamine™ class of reagents, have been widely used *in vitro* for transfections of mRNA,[59,74] though these reagents can have limited utility *in vivo* due in part to their toxicity and poor transfection potency.

Proprietary cationic lipids MegaFectin™ and TransIT™ are two lipid-based transfection reagents reported to successfully deliver mRNA *in vivo*. Kormann et al.[74] reported that intravenous administration of MegaFectin™/mRNA lipoplexes in mice with incorporation of 2-thiouridine and 5mC into mRNA coding for red fluorescent protein (RFP) synergistically reduced innate immune system markers IFN-γ, IL-12, and IFN-α. Additionally, Karikó et al.[53] complexed mRNA encoding erythropoietin (EPO) with TransIT™ and by intraperitoneal administration demonstrated EPO protein expression along with a phenotypic increase in hematocrit and reticulocyte counts in studies performed in mice and rhesus macaques. Other more traditional lipids can also be used for lipoplex-mediated mRNA delivery, including the cationic 1,2-dioleoyl-3-trimethylammonium-propane (DOTAP) and the zwitterionic phospholipid 1,2-dioleoyl-sn-glycero-3-phosphoethanolamine (DOPE) (**Fig. 1-3c**), and a 1:1 mixture of DOTAP and DOPE was reported as an effective mRNA transfection reagent.[75,76]

Significant advances in siRNA potency were realized when cationic or ionizable lipids were co-formulated with additional excipients to form stabilized lipid nanoparticles (LNPs) (**Fig. 1-3b**). In LNP formulation, nucleic acid and cationic/ionizable lipids are often combined with naturally-occurring phospholipids to support lipid bilayer structure, cholesterol to increase lipid bilayer stability, and/or lipid-anchored polyethylene glycol (PEG) to limit opsonization and non-specific uptake and to increase the circulation half-life *in vivo*.[72] With some siRNA-loaded LNPs, it has been demonstrated that endogenous proteins such as apolipoprotein E (ApoE) can adsorb onto the particles to facilitate specific receptor-mediated endocytosis in liver hepatocytes.[77] Other siRNA-LNPs have been reported to be endocytosed by ApoE-independent mechanisms[78] or through conjugation of receptor-specific targeting ligands on the LNP surface.[77] Both endocytosis and potency of siRNA-LNPs are highly dependent on the specific cationic/ionizable lipid or lipid-like material used. It is postulated that ionizable lipids, which are

neutral at physiological pH but positively-charged in acidic endosomes, facilitates quick release of the RNA cargo from maturing endosomes through disruption of the endosomal membrane.[79]

Over the past decade, the emergence of novel synthetic lipids and lipid-like materials has been responsible for over 10,000-fold increases in siRNA potency in hepatocytes: whereas first-generation siRNA-cholesterol conjugates reported[41] in 2004 had an IC_{50} of approximately 50 mg/kg, LNPs made with a synthetic lipid-like material reported[80] in 2014 had an IC_{50} of approximately 0.002 mg/kg. Many of these lipids, though primarily used to this point for siRNA delivery, hold promise for the delivery of mRNA as well. One popular synthetic lipid used for *in vivo* siRNA delivery is DLinDMA (**Fig. 1-3c**). In 2006, DLinDMA co-formulated with the phospholipid DSPC, cholesterol, and lipid-anchored PEG produced an LNP capable of silencing a liver-specific gene with an IC_{50} dose of approximately 1.0 mg/kg in mice.[81] Six years later, a self-amplifying mRNA vaccine was delivered using the same DLinDMA/DSPC/cholesterol/PEG LNP formulation.[82] Whereas siRNAs are 21-23 bases long, the mRNA used in this study was 9 kilobases, highlighting the versatility of DLinDMA LNPs by efficiently delivering much larger nucleic acids. At mRNA doses of 1 to 10 μg administered intramuscularly in mice, the DLinDMA mRNA vaccine was able to both promote expression of the encoded protein antigen and also provide protection against a viral challenge comparable to that achieved by mRNA delivery using a standard alphavirus vector.

Again in the context of siRNA delivery, rational design has been used to increase the potency of synthetic lipids, including DLinDMA, by systematically varying structural elements in the head, linker, and tail regions of the lipid. Several new structural analogs have been synthesized through this approach, and though having only minor chemical differences, have demonstrated remarkable improvement in potency. These include synthesis of DLin-KC2-DMA, DLin-MC3-DMA, and L319 (**Fig. 1-3c**), which exhibited *in vivo* siRNA IC_{50} levels of 0.02, 0.005, and < 0.01 mg/kg, respectively, when formulated as LNPs.[19,83,84] Recently, Thess et al.[59] used

one of these rationally-designed ionizable lipids to encapsulate and deliver mRNA coding for EPO in mice, pigs, and non-human primates. Therapeutically relevant concentrations of EPO were achieved following intraperitoneal or intravenous injection of sequence-optimized mRNA, and it was further noted that mRNA delivery using LNPs mitigates much of the immunogenicity seen from mRNA administration, even when using mRNA with unmodified bases.

A complementary class of lipid-like materials, characterized by polyamine cores and multiple hydrophobic tail moieties, has also been developed for siRNA delivery through the use of combinatorial synthetic methodology and library screening.[18,80,85,86] Using this approach, thousands of new synthetic lipid-like materials can be generated and screened for potency through first identifying leads *in vitro* and then further evaluating lead compounds *in vivo*. This class of lipids, which includes C12-200, cKK-E12, and 503O13 (**Fig. 1-3c**), constitute some of the most potent materials for siRNA delivery that have been reported to date. In this Thesis, we will demonstrate the utility of these types of ionizable lipids to make highly efficacious mRNA-LNPs.

Another class of lipid-containing mRNA delivery nanoparticles is the cationic nanoemulsion (CNE). Whereas LNPs discussed previously were formulated via microfluidic mixing of an aqueous phase containing mRNA with an ethanol phase containing lipids,[87] CNEs are made through homogenization of aqueous and oil phases containing excipients to create a nanoemulsion with a cationic surface charge that can be subsequently complexed with mRNA (**Fig. 1-3d**). As a proof-of-concept, a cationic nanoemulsion prepared with the lipid DOTAP, squalene, sodium trioleate, and polysorbate 80 was reported to deliver a self-amplifying mRNA vaccine intramuscularly in multiple species.[88] In a follow-up study,[89] it was also demonstrated that this cationic nanoemulsion combined with self-amplifying mRNA encoding for the HIV Type 1 Envelope protein was well-tolerated and immunogenic in rhesus macaques at an mRNA dose of 50 μg.

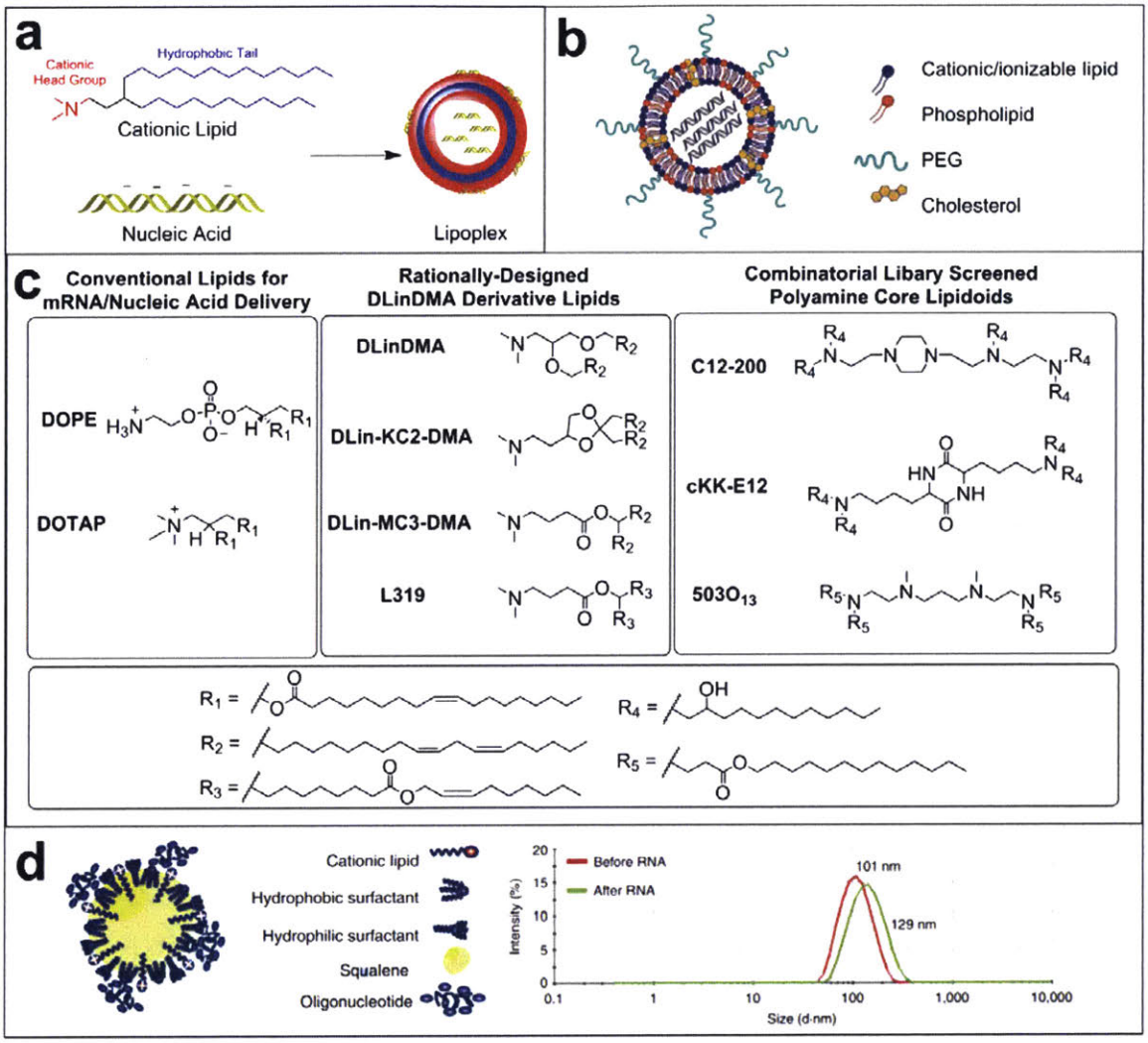

Figure 1-3. Lipid materials for mRNA and nucleic acid delivery. (**a**) Cationic lipids electrostatically bind to negatively-charged nucleic acids to form lipoplexes. (**b**) Lipid nanoparticles (LNPs) are formulated with a cationic/ionizable lipid, phospholipid, PEG, and cholesterol to form a stable nanoparticle encapsulating a nucleic acid (figure adapted from Kanasty et al.[90]). (**c**) Chemical structures of conventionally-used transfection lipids DOPE and DOTAP, rationally-designed DLinDMA and derivatives thereof, and polyamine core lipidoids discovered through combinatorial library screening. (**d**) Cationic nanoemulsions (CNE) can be prepared by homogenizing various excipients, and mRNA can be subsequently added to the CNE which results in an increased average particle size as measured by dynamic light spectroscopy (DLS) (figure adapted from Brito et al.[88]).

1.2.4. Polyplex and Polymer Nanoparticle Delivery Materials

Synthetic polymers, such as poly(lactic-*co*-glycolic) acid (PLGA), have been extensively used in drug delivery as micro- or nanoparticles in order to encapsulate and facilitate controlled

release of macromolecules.[91] Many cationic polymers have been investigated as agents to deliver both siRNA and DNA, with formation mechanisms that typically rely on electrostatic complexation which results in the formation of polyplex nanoparticles[7] (**Fig. 1-4a**). One polymer used in polyplex formation with nucleic acids is polyethyleneimine (PEI) (Fig. 1-4b), a highly cationic and water-soluble polymer that has branched, linear, or dendrimer architecture.[14,92,93] A linear PEI derivative that is commercially available, jetPEI™, though most commonly used for DNA and siRNA transfection has also been used for mRNA transfection.[75] Despite its frequent use, PEI is relatively cytotoxic and not degradable.[94] Other polymers with degradable moieties, such as poly(2-dimethylaminoethyl methacrylate) (PDMAEMA) (**Fig. 1-4b**), have also been used in the context of gene delivery,[95] as well as in a recent report demonstrating PDMAEMA/mRNA polyplexes for transfection *in vitro*.[96] Another common polymer historically used for DNA transfection is poly(L-lysine) (PLL) (**Fig. 1-4b**), but PLL/DNA complexes demonstrate high toxicity and poor transfection in comparison to other delivery materials.[97] Limited efforts toward the use of PLL for mRNA transfection did not result in detectable translation.[14]

A number of other classes of polymers have transitioned from use in siRNA/DNA delivery to mRNA delivery in recent years, and some examples are highlighted here, though this is not a comprehensive account of these technologies. Chitosan, a biopolymer found in the exoskeleton of crustaceans, is composed of repeating D-glucosamine and N-acetyl-D-glucosamine units (**Fig. 1-4b**). The primary amine group on the D-glucosamines can become positively charged at acidic pH and complex with negatively-charged nucleic acids to form polyplexes.[98] Chitosan and its derivatives have been most prevalent in the delivery of both DNA and siRNA[98,99] but have recently been investigated for the delivery of mRNA as well.[100]

Poly(β-amino esters) (PBAEs), which have been investigated for a range of gene delivery applications,[101] are ionizable, degradable polymers synthesized via the addition of diamines with diacrylates (**Fig. 1-4b**). Due to the simplicity of this reaction, thousands of

chemically distinct PBAEs have been synthesized over the past decade by combinatorial methods and screened for efficacy in delivery of plasmid DNA *in vitro*.[102–105] Amine groups on PBAEs become protonated in the acidic environment of the endosome, which has been theorized to disrupt endosomal membranes and promote escape of the nucleic acid payload. Recently, PBAE nanoparticles were coated with lipids and mRNA was subsequently electrostatically adsorbed onto particle surface.[106] The lipid/PBAE nanoparticles were capable of mRNA delivery both *in vitro* and intranasally at 4 μg doses *in vivo*. Another report studied the ability of PBAE/mRNA polyplexes to induce IFN-γ secretion in mice for vaccine applications, finding that lipoplex formulations activated the immune system better than PBAE polyplexes.[76] Later in this Thesis, we will present work on mRNA delivery using PBAE-lipid nanoparticles for lung delivery.

Polyaspartamides, made up of repeat aspartimide units with both primary and secondary cationic amides, were first used as drug delivery materials in the 1970s[107] and have since been used for gene delivery of both siRNA and DNA. Polyaspartamides for nucleic acid delivery are often synthetically modified, such as by adding a side chain group of 1,2-diaminoethane to a commonly-used polymer known as PAsp(DET) (**Fig. 1-4b**), and/or by forming a copolymer with polyethylene glycol (PEG) or polyethyleneimine, for example.[108–110] In recent years, polyaspartamides have also been explored for mRNA transfection. Baba et al.[111] synthesized a PEG-PAsp(DET) copolymer which formed polyplexes with mRNA coding for brain-derived neurotrophic growth factor (BDNF). Intranasal administration of the mRNA polyplex in mice induced with olfactory dysfunction demonstrated functional recovery. Another study investigated how polyaspartamide side chain modifications affected mRNA transfection efficacy *in vitro*, finding that polyaspartamides with odd numbers of aminoethylene repeats exhibited higher mRNA transfection efficacy than those with even numbers of aminoethylene repeats.[112] Interestingly, studies by the same group found the opposite effect for dependence on conjugate

number when these materials were formulated as DNA polyplexes[113] This surprising result is evidence that delivery materials and formulations previously used for DNA/siRNA delivery may require modifications when adapted for mRNA delivery.

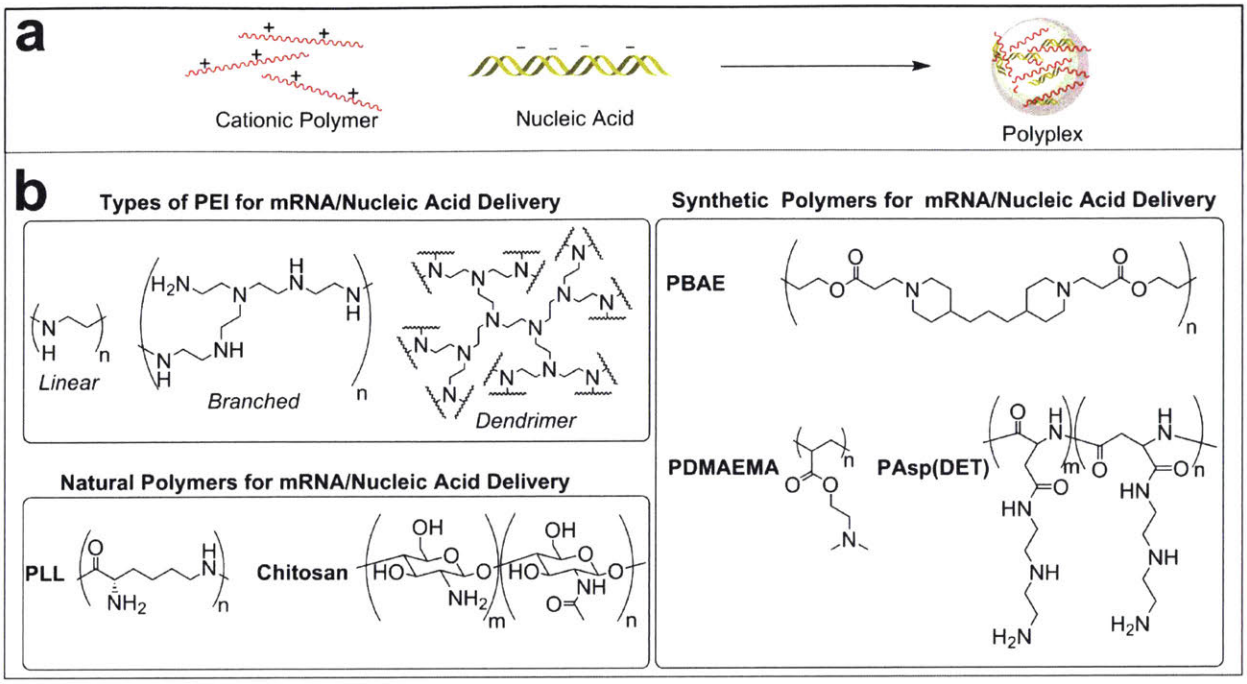

Figure 1-4: Polymer materials for mRNA and nucleic acid delivery. (**a**) Cationic polymers electrostatically bind to negatively-charged nucleic acids to form polyplexes. (**b**) Chemical structures of PEI, natural polymers, and synthetic polymers commonly used for mRNA transfection.

1.2.5 Hybrid Protamine-Lipid/Polymer Nanoparticles

Though we have individually categorized mRNA delivery materials, it is important to note that one can potentially combine different delivery materials to create "hybrid" formulations. One common strategy is to first complex nucleic acid with protamine to neutralize charge on the mRNA and provide nuclease protection, and subsequently deliver the resultant complex via a nanoparticle. The delivery of DNA/siRNA mixtures has been achieved using this hybrid approach[114,115] and a recent report demonstrated the potential of this approach for intravenous delivery of a lipid/protamine/mRNA (LPR) formulation with 10 μg mRNA coding for the suicide

gene herpes simplex virus 1-thymidine kinase (HSV1-tk) into xenograft tumor-bearing mice.[116] The LPR-delivered mRNA was reported to inhibit tumor growth and outperform a DNA treatment with the same formulation in terms of both efficacy and toxicity. Furthermore, while polymers previously described in this review were cationic in nature in order to complex with negatively charged mRNA, it is possible to deliver more electrostatically neutral mRNA/protamine complexes with nanoparticles made from a neutrally-charged polymer, such as polycaprolactone (PCL),[117] which would expand the types of polymers that could be used as mRNA delivery materials.

1.2.6 Summary and Perspective

In this section, we have endeavored to highlight the various classes of materials that have been demonstrated for nucleic acid delivery. Though the preponderance of use of these materials has been in cellular transfection of DNA or siRNA, a growing body of literature has supported the potential of various classes of delivery materials in mRNA-based therapy. Because of the inherent structural differences between mRNA and siRNA, improving mRNA delivery will certainly require further optimization in the materials used for delivery. This optimization will likely entail both reformulating existing materials as well as developing new materials.

The therapeutic potential of mRNA as a versatile strategy for treating a number of diseases or enabling protein-based immunotherapy underscores the need for continued development and refinement of mRNA delivery strategies. It is also worth noting that several companies are well on the way to commercialization of mRNA therapeutics using non-viral delivery materials, and a number of clinical trials as well as products existing across all phases of development are being actively pursued.[21,22] mRNA-based therapies have broad potential to

treat a range of important diseases, and the further development of delivery materials will be a key determinant of the success of these approaches.

1.3 Thesis Overview

In summary, the work presented in this Thesis aims to advance the field of therapeutic mRNA delivery by increasing the potency of mRNA-LNPs, understanding the resultant extracellular innate immune response, and demonstrating new methods for screening libraries of LNP formulations *in vivo.* The Thesis is divided into the following sections:

In **Chapter 2**, we first optimize existing liver-targeting lipid nanoparticle formulations specifically for the delivery of mRNA, thereby increasing the *in vivo* protein expression over 7-fold relative to the original formulation. Novel, rationally-designed ionizable lipids further improved mRNA potency *in vivo.* The general method we conceived here to screen materials *in vivo* could also potentially accelerate *in vivo* optimization of other formulations with large, multidimensional design spaces.

In **Chapter 3**, we then study the immune response to these mRNA-optimized lipid nanoparticle formulations and discover previously unreported indicators of a transient, extracellular innate immune response. Additionally, we find that pseudouridine modification of the mRNA altered neither the lipid nanoparticle immunogenicity nor efficacy *in vivo* and postulate that the effects of pseudouridine mRNA modification may depend on many variables, including delivery and mRNA properties.

In **Chapter 4**, we synthesize novel formulations capable of delivering mRNA to organs other than the liver. We show mRNA expression in the lungs and spleen following intravenous

administration and mRNA expression in the fat following subcutaneous administration, thus significantly expanding upon the number of organs treatable with mRNA therapies.

In **Chapter 5**, we describe a more generalized, barcoding-based approach for the discovery of nanoparticle formulations capable of delivering nucleic acid to a diverse array of tissues *in vivo.* Using this method, we analyze the biodistribution and pharmacokinetics of a library of lipid nanoparticles *in vivo.* In principle, this technology could be used to quickly evaluate thousands of nanoparticle formulations for gene therapy in a single mouse and greatly speed screening processes.

In **Chapter 6**, we report a new *in vivo* method using genetically-engineered mice which can, for the first time, identify mRNA expression in both bulk tissues and with single cell resolution following vectored mRNA delivery. This method is used to discover new cell types of transfection for mRNA lipid nanoparticles, including populations in the lungs and spleen. This mouse model may help contribute to mechanistic understandings of mRNA lipid nanoparticle delivery and optimize delivery vectors for wide-ranging clinical targets.

In **Chapter 7**, we conclude the Thesis by summarizing its contents and providing a future outlook for the field of mRNA delivery.

Chapter 2

Optimization of mRNA Lipid Nanoparticles with Design of Experiment

The work presented in this chapter was published as:

Kauffman, K.J.*, Dorkin, J.R.*, Yang, J.H., Heartlein, M.W., DeRosa, F., Mir, F.F., Fenton, O.S., Anderson, D.G. "Optimization of Lipid Nanoparticle Formulations for mRNA Delivery in vivo with Fractional Factorial and Definitive Screening Designs." *Nano Lett.*, **15**, 7300-7306, 2015.

Fenton, O.S., Kauffman K.J., McClellan, R.L., Appel, E.A., Dorkin, J.R., Tibbitt, M.W., Heartlein, M.W., DeRosa, F., Langer, R., Anderson, D.G. "Bioinspired Alkenyl Amino Alcohol Ionizable Lipid Materials for Highly Potent in vivo mRNA Delivery." *Adv. Mater.,* **28**, 2939-2943, 2016.

2.1 Introduction

Nucleic acids have tremendous therapeutic potential to modulate protein expression *in vivo* but must be delivered safely and effectively. Because the delivery of naked nucleic acids results in poor cellular internalization, rapid degradation, and fast renal clearance,[9,72] lipid nanoparticles (LNPs) have been developed to encapsulate and deliver nucleic acids to the liver. Most notably, the field has seen orders-of-magnitude potency advances in the delivery of 21 to 23 nucleotide-long double stranded small interfering RNAs (siRNAs) due in part to the creation of new synthetic ionizable lipids and lipid-like materials.[72] Whereas some of these novel lipids were synthesized with rational design approaches by systematically varying the lipid head and tail structures (e.g. DLin-KC2-DMA, DLin-MC3-DMA, L319),[19,83,84] other materials were discovered by creating large combinatorial libraries of lipid-like materials (e.g. C12-200, cKK-E12, 503O13).[80,85,86] When formulated into LNPs, these amine-containing ionizable lipids and lipid-like materials electrostatically complex with the negatively charged siRNA and can both facilitate cellular uptake and endosomal escape of the siRNA to the cytoplasm.[78,85] In particular, the ionizable lipid-like material C12-200 has been widely used to make siRNA-LNP formulations for various therapeutic applications *in vivo* to silence protein expression.[118–120]

In addition to the ionizable material, three other excipients are also commonly used to formulate LNPs: 1) a phospholipid, which provides structure to the LNP bilayer and also may aid in endosomal escape;[72,121] 2) cholesterol, which enhances LNP stability and promotes membrane fusion;[122,123] and 3) lipid-anchored polyethylene glycol (PEG), which reduces LNP aggregation and "shields" the LNP from non-specific endocytosis by immune cells.[124] The particular composition of the LNP can also have profound effects on the potency of the formulation *in vivo*. Several previous efforts to study the effect of formulation parameters on siRNA-LNP potency utilized the one-variable-at-a-time method,[125,126] in which formulation parameters were individually varied to maximize LNP potency; this approach, however, does

not allow for examination of potentially important second-order interactions between parameters. Inspired by statistical methodologies commonly used in the engineering and combinatorial chemistry literature,[127,128] we chose to utilize Design of Experiment (DOE) to better optimize LNP formulations for nucleic acid delivery. Using DOE, the number of individual experiments required to establish statistically significant trends in a large multi-dimensional design space are considerably reduced, which is particularly relevant for the economical screening of LNP formulations: *in vitro* screens are often poor predictors of *in vivo* efficacy with siRNA-LNPs,[129] and it would be both cost- and material-prohibitive to test large libraries of LNP formulations *in vivo*.

To demonstrate the application of Design of Experiment to LNP formulation optimization *in vivo*, we formulated LNPs with a different type of nucleic acid than siRNA. Recently, messenger RNA (mRNA) has been investigated for therapeutic protein production *in vivo*, including applications in cancer immunotherapy, infectious disease vaccines, and protein replacement therapy.[22,130] Unlike plasmid DNA, mRNA need only access the cytoplasm rather than the nucleus to enable protein translation and has no risk of inducing mutation through integration into the genome.[7] Because there are inherent chemical and structural differences between mRNA and siRNA in terms of length, stability, and charge density of the nucleic acid,[74] we hypothesized that LNP delivery formulations for mRNA may require significant variation from those developed for siRNA delivery. We further hypothesized that formulated mRNA may pack differently and with different affinity into nanoparticles than siRNA. To optimize LNP formulation parameters specifically for mRNA delivery, we developed a novel strategy in which we used Design of Experiment methodologies – including both Fractional Factorial and Definitive Screening Designs – to synthesize several smaller LNP libraries to screen *in vivo*. Using the formulation conditions of the original siRNA-LNPs as a starting point, each successive generation of library was designed to improve protein expression based upon the parameters in

the previous library that were found to correlate with improved efficacy. Through this approach, we aimed to develop an optimized C12-200 LNP with increased protein expression over the original LNP formulation.

2.2 mRNA Delivery with Original siRNA-Optimized LNP

The formulation process for synthesizing LNPs is described in **Figure 2-1**. The organic phase containing the lipids was mixed together with the acidic aqueous phase containing the nucleic acid in a microfluidic channel,[87] resulting in the formation of mRNA-loaded LNPs. We chose to use unmodified mRNA coding for Erythropoietin (EPO), a secreted serum protein that has previously been successfully translated *in vivo*[53,74]. It has further been recently reported[59] that LNP-delivered unmodified EPO mRNA is more potent than EPO mRNA with pseudouridine and/or 5-methylcytidine modifications *in vitro* and in mice. To establish a baseline from which to improve, EPO mRNA was first formulated into LNPs using the original formulation parameters previously published[85] for siRNA delivery *in vivo* (**Table 2-1**). The formulation was dosed intravenously at 15 μg of total mRNA per mouse, and resulted in an average EPO serum level of 963 ± 141 ng/mL at six hours post-injection.

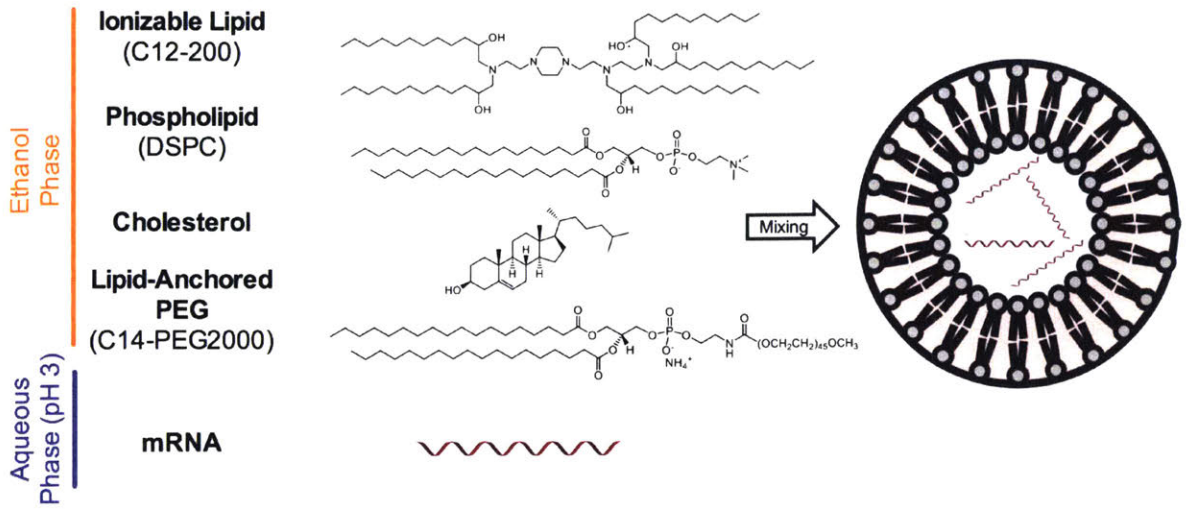

Figure 2-1. Formulation of lipid nanoparticles. Lipid nanoparticles (LNPs) are synthesized by the mixing of two phases: 1) a four-component ethanol phase containing ionizable lipid, helper phospholipid, cholesterol, and lipid-anchored PEG; 2) an acidic aqueous phase containing mRNA.

Table 2-1. Library A, B, and C formulation parameters

Parameter	Original Formulation	Library A	Library B	Library C
C12-200:mRNA Weight Ratio	5:1	2.5:1 to 7.5:1	7.5:1 to 12.5:1	5:1 to 25:1
Phospholipid	DSPC	DSPC, DSPE DOPC, DOPE	DSPC DOPE	DOPE
C12-200 Molar Composition	50%	40% to 60%	30% to 40%	35%
Phospholipid Molar Composition	10%	4% to 16%	16% to 28%	16%
Cholesterol Molar Composition	38.5%	21.5% to 55.5%	28.5% to 51.5%	46.5%
PEG Molar Composition	1.5%	0.5% to 2.5%	2.5% to 3.5%	2.5%

Phospholipid abbreviations: DS = 1,2- distearoyl -*sn*-glycero- (saturated tail), DO = 1,2-dioleoyl-*sn*-glycero- (Δ9-cis unsaturated tail), PC = 3-phosphocholine (primary amine head group), PE = 3-phosphoethanolamine (quaternary amine head group)

2.3 Optimization of mRNA LNPs with Design of Experiment

Some previous efforts to optimize nanoparticle formulations have involved varying each of the important parameters individually and then possibly combining each optimized parameter for an overall optimized formulation.[125,126,131] Because pilot experiments suggested strong second-order effects between parameters in our system, we chose instead to vary all five independent parameters simultaneously. In an attempt to maximize EPO expression in mice and thereby optimize the C12-200 LNPs for mRNA delivery, we chose to simultaneously vary the C12-200:mRNA weight ratio, the phospholipid identity, and the molar composition of the four-component LNP formulation. Three additional phospholipids structurally similar to DSPC but with differing head groups (primary vs. quaternary amine) and tail saturation (saturated vs. Δ9-cis unsaturated) were incorporated into the LNP formulations.

2.3.1 Library A: Definitive Screening Design

We designed the first library, Library A, to be centered around the original siRNA-optimized LNP formulation parameters (**Table 2-1**). With four three-level quantitative factors (C12-200:mRNA weight ratio and three independent formulation molar compositions) and one four-level qualitative factor (phospholipid type), this large five-dimensional design space required Design of Experiment to reduce the number of formulations (3 x 3 x 3 x 3 x 4 = 324) to a reasonable number for *in vivo* experiments. An initial library of fourteen formulations (coded A-01 through A-14, see **Table B.2-1** for parameters) was created using a Definitive Screening Design, a recently described economical Design of Experiment in which main effects are not confounded with two-factor interactions and non-linear correlations can be detected.[132] The purpose of this first screen was to sample the large design space in a controlled fashion to eliminate unimportant formulation parameters and/or find a local maximum in efficacy from which a second-generation library could be generated.

Out of fourteen formulations in Library A, two formulations (A-02 and A-09) resulted in higher EPO serum levels (6445 ± 1237 and 2072 ± 302 ng/mL, respectively) than the original formulation (**Fig. 2-2a)**. Although the results from Library A were insufficient to deduce statistically significant effects for EPO production *in vivo*, there were statistically significant ($p < 0.05$) orthogonal trends (**Fig. A.2-2)**. We hypothesize that the increased encapsulation efficiency with increasing C12-200:mRNA weight ratio (**Fig. A.2-2a**) is caused by better complexation of more positively-charged ionized C12-200 lipid with negatively-charged mRNA. We also observed decreased LNP size with increasing PEG composition (**Fig. A.2-2b**), a phenomenon that has been previously observed in the literature[126,133] and has been speculated to be caused by increased lipid bilayer compressibility and increased repulsive forces between liposomes.[134] The two top-performing formulations of Library A (A-02 and A-09) possessed similar attributes: increased weight ratio (7.5:1 vs. 5:1), increased phospholipid content (16% vs. 10%), and either DSPC or DOPE as the phospholipid; moreover, A-02 had decreased C12-200 content (40% vs. 50%) and A-09 had increased PEG content (2.5% vs. 1.5%).

2.3.2 Library B: Fractional Factorial Screening Design

A more robust second-generation library, Library B (coded B-15 to B-32, **Table B.2-1**), was generated using a L18-Taguchi Fractional Factorial Design[131] with new parameter ranges which shifted in the direction of the two top-performing LNPs from the first library (**Table 2-1**). Out of eighteen formulations in Library B, eleven formulations resulted in higher EPO serum levels than the original formulation (**Fig. 2-2a)**. The top-performing formulation was B-26 with an average serum EPO concentration of 7485 ± 854 ng/mL. A Standard Least Squares linear regression model was applied to the data from Library B and several statistically significant factors were found with respect to efficacy (**Table B.2-2**). Several second-order effects were found to be statistically significant as well, including the second-order interaction between DOPE and C12-200:mRNA weight ratio as shown by the best-fit line ($p < 0.05$) for DOPE in **Fig.**

2-2b. Additional description of the statistical model and significant effects may be found in the Supporting Information (**Table B.2-2, Fig. A.2-1**).

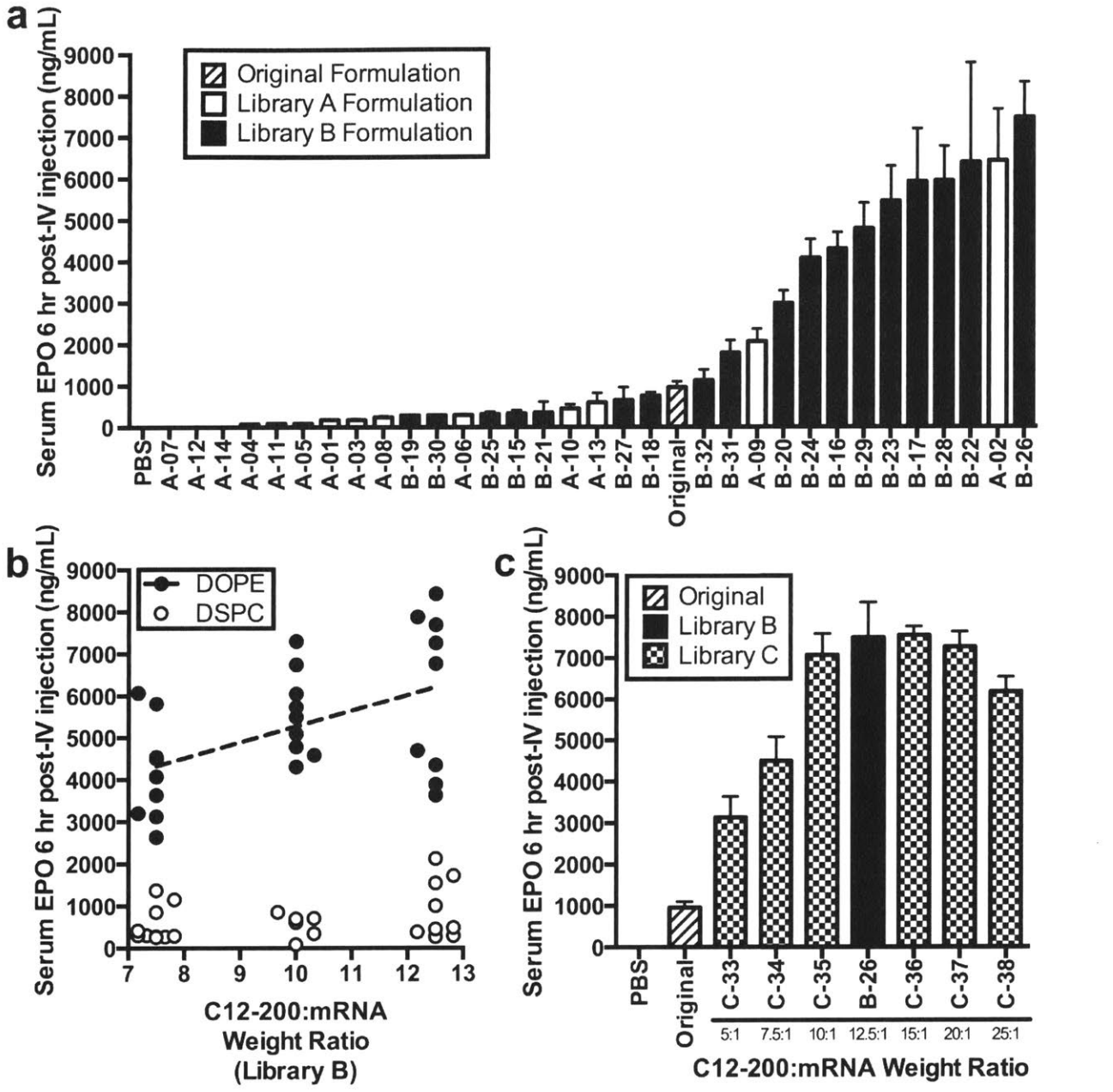

Figure 2-2. Efficacy results of LNPs in Libraries A, B, and C. (**a**) Serum EPO concentration six hours post-intravenous injection of 15 μg total mRNA for each formulation in Libraries A and B, including the original formulation (Data presented as mean + SD, $n = 3$). (**b**) A statistically significant trend of increasing serum EPO concentration was observed with increasing C12-200:mRNA weight ratio and with DOPE phospholipid for Library B formulations, independent of the other formulation parameters. Furthermore, a statistically significant second-order effect was observed between DOPE and increasing weight ratio, as

indicated by the larger relative slope of the DOPE best-fit line compared to the DSPC best-fit line. (1 data point = 1 mouse) (**c**) Serum EPO concentration six hours post-intravenous injection of 15 μg total mRNA for formulation B-26 and Library C, which had similar formulation parameters as B-26 with differing C12-200:mRNA weight ratios. (Data presented as mean + SD, n = 3).

The most apparent trend from Library B was that formulations with DOPE as the phospholipid resulted in significantly higher EPO production than formulations with DSPC, the original phospholipid (**Fig. 2-2b**). In fact, the presence of DOPE in the formulation was the single strongest predictor of *in vivo* efficacy in our study. Whereas DSPC contains a quaternary amine head group and a fully saturated tail, DOPE contains a primary amine head group and a tail with one degree of unsaturation. It has been reported that conical lipids, such as DOPE, tend to adopt the less stable hexagonal phase, while cylindrical lipids, such as DSPC, tend to adopt the more stable lamellar phase.[135] Upon fusion with the endosomal membrane, LNPs containing DOPE may reduce membrane stability, ultimately promoting endosomal escape.[136,137] Another possible explanation involves their different encapsulation efficiencies: independent of other varying formulation parameters, formulations with DSPC entrapped mRNA on average significantly better than DOPE (51% vs. 36%), so it may be possible that the stronger complexation of mRNA to lipid in DSPC LNPs hinders the subsequent de-complexation of mRNA from lipid once inside the cell, thus inhibiting translation of the mRNA to protein.

2.3.3 Library C: Maximizing Lipid:mRNA Weight Ratio with DOPE

As was initially hypothesized, we observed several second-order effects on EPO production between formulation parameters in Library B, most notably the synergistic effect between increasing the C12-200:mRNA weight ratio along with the use of DOPE as the phospholipid (**Fig. 2-2b**). In an effort to further increase *in vivo* potency, a third and final library was generated (Library C, **Table 2-1**) to exploit this discovered second-order effect. The top-performing formulation (B-26) from Library B was re-formulated with C12-200:mRNA weight

ratios varying from 5:1 to 25:1 (coded C33-C38, **Table B.2-1**). Surprisingly, increasing the weight ratio only increased the serum EPO concentration up to a certain point (**Fig. 2-2c**); it appears that increasing the weight ratio beyond 10:1 confers no significant efficacy advantage *in vivo*. Because no significant increases in EPO production were observed beyond 10:1 and to mitigate any concerns with possible lipid toxicity caused by increased lipid doses, we chose the 10:1 C12-200:mRNA weight ratio (C-35) as the final mRNA-optimized LNP formulation (**Table 2-2**).

Table 2-2. LNP characteristics of C-35 compared to the original formulation

	Original Formulation	**Optimized Formulation (C-35)**
C12-200:mRNA Weight Ratio	5:1	10:1
Phospholipid	DSPC	DOPE
C12-200 Molar Composition	50%	35%
Phospholipid Molar Composition	10%	16%
Cholesterol Molar Composition	38.5%	46.5%
C14 PEG 2000 Molar Composition	1.5%	2.5%
Serum EPO (ng/μL)	962 ± 141	7065 ± 513
Diameter (nm)	152	102
Polydispersity Index (PDI)	0.102	0.158
mRNA Encapsulation Efficiency (%)	24	43
pKa	7.25	6.96
Zeta Potential (mV)	-25.4	-5.0

Phospholipid abbreviations: DSPC = 1,2-distearoyl-sn-glycero-3-phosphocholine, DOPE = 1,2-dioleoyl-sn-glycero-3-phosphoethanolamine, Serum EPO reported as mean ± SD (n = 3) 6 hr after 15 μg total mRNA intravenous injection into mice

2.3.4 Evaluation of Methodology

Although only 14% (2 of 14) of the Library A formulations resulted in increased potency compared to the original parameters, 61% (11 of 18) of the Library B formulations and 100% of Library C formulations (6 of 6) did so (**Figs. 2-2a, 2-2c**). This suggests that formulation parameters can be optimized and are critically important for efficient mRNA delivery with C12-200 LNPs. Furthermore, the increasing percentage of formulations that performed better than

the original in each subsequent library demonstrates the predictive success of the generated statistical models (**Table B.2-2**). A flowchart of the complete methodology we developed for *in vivo* nanoparticle optimization can be found in **Figure A.2-3.**

2.3.5 Characterization of mRNA-Optimized LNP

The optimized formulation C-35 had the following formulation parameters: 10:1 C12-200:mRNA weight ratio with 35% C12-200, 16% DOPE, 46.5% cholesterol, and 2.5% C14-PEG2000 molar composition. The average efficacy of C-35 with 15 μg total EPO mRNA injection *in vivo*, 7065 ± 513 ng/mL, was increased over seven-fold compared to the original traditional LNP formulation (963 ± 141 ng/mL). C-35 was further characterized and compared to the original formulation with regard to size, polydispersity, encapsulation efficiency, and pKa (**Table 2-2**). No significant morphological differences were observed between the two formulations with Transmission Electron Microscopy (TEM) (**Figure A.2-4)**. Although others have reported increases in siRNA nanoparticle potency with decreasing size,[138] we found no such trend with all 38 mRNA formulations tested in our LNP system. Jayaraman et al.[83] found that pKa was an important characteristic in predicting the efficacy of liver-targeting siRNA LNPs with an optimal pKa of between 6.2 and 6.5. It appears that in our C12-200 mRNA system, the *in vivo* efficacy is not significantly correlated with pKa of the LNP, although the slightly lower pKa of C-35 (pKa = 6.96) compared to the original formulation (pKa = 7.25) may partially explain its improved efficacy. The surface charge of the LNP may also partially explain differences in efficacy: the optimized formulation C-35 is less negatively charged (zeta potential = -5.0 mV) than the original formulation (-25.4 mV). C-35 contains twice the amount of amine-rich ionizable lipid C12-200 than the original formulation, which is likely the predominant reason C-35 is more positively-charged. Although one study found no relationship between surface charge and hepatocellular delivery *in vivo* with siRNA-loaded lipid nanoparticles,[129] other reports have noted

that more positively-charged nanoparticles bind better to negatively-charged cellular membranes and this electrostatic interaction might facilitate uptake.[139]

In order to determine whether C-35 would similarly improve the efficacy of mRNAs with different lengths, we formulated LNPs with firefly luciferase (Luc) mRNA, an mRNA which has a coding region roughly three times longer than that of EPO mRNA (1653 vs. 582 nucleotides). Luciferase protein generated by C-35 LNPs was expressed predominately in the liver and likewise resulted in a statistically significant, approximately 3-fold increase in luciferase expression as measured by liver luminescence compared to the original formulation (**Fig. 3**). Although LNPs made with Luc mRNA had similar encapsulation efficiencies as those made with shorter EPO mRNA (**Tables 2-1, B.2-3**), we anticipate that significantly longer mRNAs would eventually become too large to effectively load into LNPs.

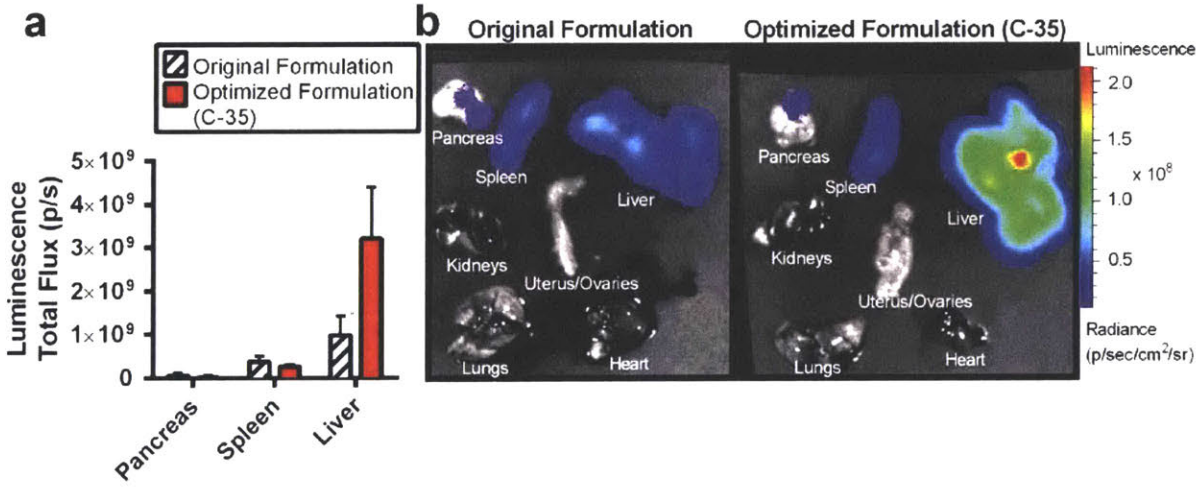

Figure 2-3. Efficacy and biodistribution of original and C-35 formulations with Luc mRNA. (**a**) Efficacy of original and C-35 LNP formulations synthesized with mRNA coding for Luciferase in three organs of interest as measured by total flux from luminescence 6 hr after intravenous injection of 15 μg total mRNA. (Data presented as mean + SD, n = 3). (**b**) Representative biodistribution image of luciferase expression for original and C-35 LNP in seven organs as measured with an IVIS imaging system 6 hr after intravenous injection of 15 μg total mRNA.

2.4 siRNA Delivery with mRNA-Optimized LNP

Having optimized the formulation for mRNA delivery, we then wanted to examine the potential for siRNA delivery with C-35 as compared to the original siRNA-optimized formulation. We formulated siRNA coding for Factor VII (FVII), a serum clotting factor expressed exclusively in hepatocytes, using both the C-35 LNP and the original LNP formulation to determine their relative silencing in hepatocytes. FVII levels were measured 72 hours after intravenous injection of siRNA-loaded LNPs ranging from 0.01 mg/kg to 0.1 mg/kg, and there was no significant difference between the original and optimized formulations at any dose (**Fig. 2-4, Table B.2-4**) despite having significantly different formulation parameters. The ED_{50} of both C-35 and the original formulations with FVII siRNA were approximately 0.03 mg/kg of total siRNA content, consistent with previous reports.[85]

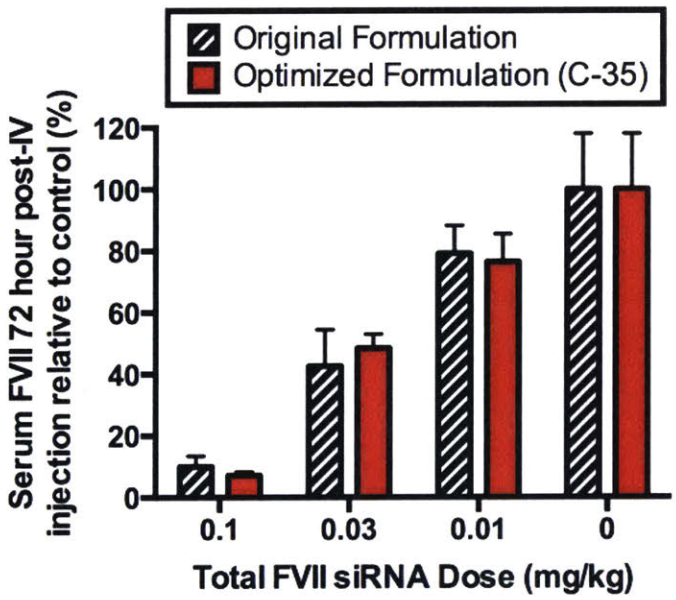

Figure 2-4. Efficacy of original and C-35 formulations with siRNA. Efficacy of original versus optimized C-35 formulation made with C12-200 and siRNA coding against Factor VII (FVII) protein as measured by serum FVII levels 72 hours post-intravenous injection of various doses of total siRNA. FVII levels were normalized with respect to PBS-injected control mice. (Data presented as mean + SD, n = 3).

Interestingly, siRNA-loaded LNPs may be more tolerant than mRNA-loaded LNPs of design space differences. Over the last decade in the siRNA delivery field, many groups have focused on developing new ionizable lipids to increase the potency of siRNA-LNPs but have generally used the same standard formulation parameters in consecutive studies.[19,80,83,85,86] The discovery of new ionizable lipids and lipid-like materials, however, is an endeavor which is often time- and material-intensive, requiring large-scale combinatorial libraries or chemically-difficult rational design approaches. Meanwhile, we have shown that for one of the most commonly used ionizable materials for siRNA delivery, C12-200, merely changing the formulation parameters can significantly increase the potency of the LNP when loaded with two different mRNAs of varying lengths, EPO or Luc (**Table 2-2**, **Fig 2-3**).

2.5 Alkenyl Amino Alcohol Ionizable Lipids for Increased Potency

Finally, we aimed to vary the ionizable lipid component of the optimized LNP to determine if mRNA potency *in vivo* could be further increased. Although the rational design of lipids had been described for siRNA delivery,[19,83,84] the rational design of ionizable lipids for mRNA delivery had not yet been reported. A new class of ionizable lipids based on alkenyl amino alcohols (AAA), which contain functional group combinations found in sphingosine and other bioactive molecules, were synthesized and formulated into LNPs with EPO mRNA.[140] The top-performing ionizable lipid from the library was OF-02 **(Fig. 2-5a)** and when formulated into mRNA-LNPs resulted in approximately 14,000 ng/mL of serum EPO at 6 hr post-i.v. injection **(Fig. 2-5b)**. The serum EPO concentration was approximately twice the concentration of similar mRNA-optimized C12-200 LNPs and to the best of our knowledge is the most potent mRNA delivery vehicle (based on EPO mRNA expression at equivalent doses) reported to date in the scientific literature. We tested other top-performing ionizable lipids previously used for siRNA

delivery (cKK-E12, 503O13, 304O13)[80,86] using the mRNA-optimized formulation with EPO mRNA, and OF-02 significantly outperformed these as well **(Fig. 2-5b)**.

Of particular note, the AAA with 2 *cis* alkenes in its lipid tails (OF-02, a derivative of linoleic acid) was the most potent AAA we tested for mRNA delivery, which matches a previous report showing that a class of two-tailed ionizable lipids were most potent for siRNA delivery when their tails also incorporated 2 *cis* alkenes.[16] As a result, we plan to incorporate 2 *cis* alkenes into the tails of future generations of ionizable lipids and rationally explore other structure/function trends in the lipid tails including degrees of saturation, tail length, and functional group incorporation. In all, this data also suggests that highly potent mRNA-LNPs can be generated via the optimization of both the lipid components of the LNP and the formulation parameters of the LNP.

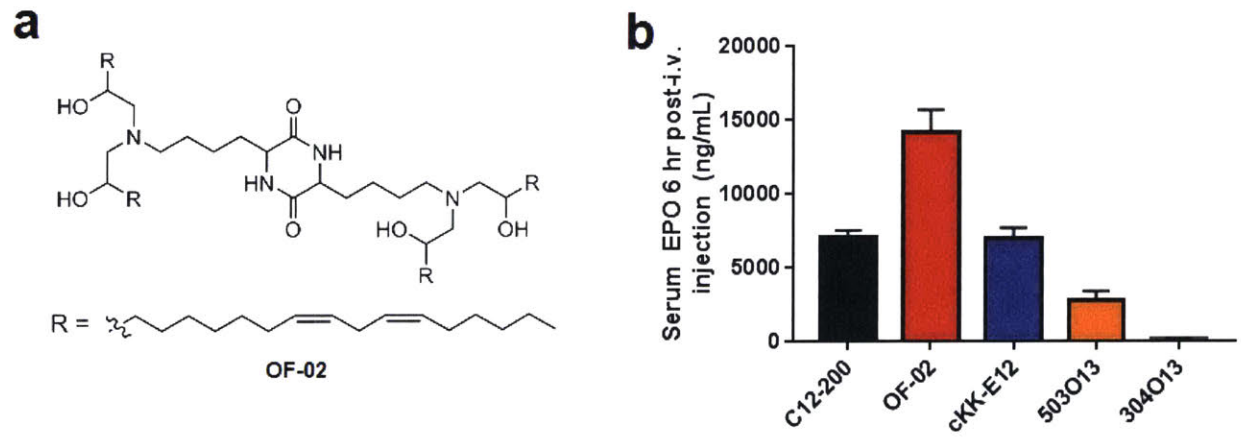

Figure 2-5. Alkenyl amino alcohols for potent mRNA delivery *in vivo*. (a) Structure of the lead AAA ionizable lipid tested, OF-02. **(b)** Serum EPO concentration six hours post-intravenous injection of 0.75 mg/kg (~15 µg) total mRNA for LNPs formulated using top-performing ionizable lipids. (Data presented as mean + std dev, $n = 3$).

2.6 Conclusions

In this study, we have demonstrated a new general method for optimizing previously-used siRNA lipid nanoparticle technology for a new class of RNA therapeutics and identified a

lead optimized formulation for mRNA delivery, coded C-35. To the best of our knowledge, this study represents the first optimization of nanoparticle potency *in vivo* using Design of Experiment principles. Although C-35 significantly improved mRNA delivery with mRNA's of two different lengths, C-35 was surprisingly equally as efficacious for siRNA delivery as the original siRNA-optimized formulation. Furthermore, the incorporation of a new ionizable lipid into the formulation further doubled the mRNA potency *in vivo*. We believe that the optimized formulations described here may provide a basis for further formulation optimization with other mRNA delivery materials as well. Furthermore, the generalized approach we described for *in vivo* optimization of multicomponent nanoparticle formulations may accelerate the discovery of more potent formulations with other materials and drug payloads.

2.7 Materials and Methods

Lipid Nanoparticle Synthesis. The ethanol phase was prepared by solubilizing with ethanol a mixture of C12-200 (prepared as previously described,[85] courtesy of Alnylam Pharmaceutics, Cambridge MA), 1,2-distearoyl-*sn*-glycero-3-phosphocholine (DSPC, Avanti Polar Lipids, Alabaster, AL), 1,2-distearoyl-*sn*-glycero-3-phosphoethanolamine (DSPE, Avanti), 1,2-dioleoyl-*sn*-glycero-3-phosphocholine (DOPC, Avanti), 1,2-dioleoyl-*sn*-glycero-3-phosphoethanolamine (DOPE, Avanti), cholesterol (Sigma), and/or 1,2-dimyristoyl-*sn*-glycero-3-phosphoethanolamine-N-[methoxy(polyethylene glycol)-2000] (ammonium salt) (C14-PEG 2000, Avanti) at pre-determined molar ratios. The aqueous phase was prepared in 10 mM citrate buffer (pH 3) with either EPO mRNA (human Erythropoietin mRNA, courtesy of Shire Pharmaceuticals, Lexington, MA), Luc mRNA (Firefly luciferase mRNA, Shire), or FVII siRNA (Factor VII siRNA,[80] Alnylam). Syringe pumps were used to mix the ethanol and aqueous phases at a 3:1 ratio in a microfluidic

chip device.[87] The resulting LNPs were dialyzed against PBS in a 20,000 MWCO cassette at 4°C for 2 hours.

mRNA Synthesis. mRNA was synthesized by *in vitro* transcription from a plasmid DNA template encoding the gene, which was followed by the addition of a 5' cap structure (Cap 1) using a vaccinia virus-based guanylyl transferase system. A poly(A) tail of approximately 300 nucleotides was incorporated via enzymatic addition employing poly-A polymerase. Fixed 5' and 3' untranslated regions were constructed to flank the coding sequences of the mRNA.

LNP Characterization. To calculate the nucleic acid encapsulation efficiency, a modified Quant-iT RiboGreen RNA assay (Invitrogen) was used as previously described.[16] The size and polydispersity (PDI) of the LNPs were measured using dynamic light scattering (ZetaPALS, Brookhaven Instruments). Zeta potential was measured using the same instrument in a 0.1x PBS solution. Size data is reported as the largest intensity mean peak average, which constituted >95% of the nanoparticles present in the sample. The pKa was determined using a TNS assay as previously described.[16] To prepare LNPs for Transmission Electron Microscopy (TEM), LNPs were dialyzed against water and negative staining was performed with 2% uranyl acetate. LNPs were then imaged with a Tecnai Spirit Transmission Electron Microscope (FEI, Hillsboro, OR).

Animal Experiments. All animal studies were approved by the M.I.T. Institutional Animal Care and Use Committee and were consistent with local, state and federal regulations as applicable. Female C57BL/6 mice (Charles River Labs, 18-22 grams) were intravenously injected with LNPs via the tail vein. After six hours or 72 hours, blood was collected via the tail vein with serum separation tubes and the serum was isolated by centrifugation. Serum EPO levels were measured using an ELISA assay (Human Erythropoietin Quantikine IVD ELISA Kit, R&D Systems, Minneapolis, MD). Serum FVII levels were measured using a chromogenic assay

(Biophen FVII, Aniara Corporation, West Chester, OH) and compared with a standard curve obtained from control mice. Six hours after administration of Luc mRNA LNPs, mice were administered an intraperitoneal injection of 130 µL of D-luciferin (30 mg/mL in PBS). After fifteen minutes, the mice were sacrificed and eight organs were collected (liver, spleen, pancreas, kidneys, uterus, ovaries, lungs, heart). The organs' luminescence were analyzed using an IVIS imaging system (Perkin Elmer, Waltham, MA) and quantified using LivingImage software (Perkin Elmer) to measure the radiance of each organ in photons/sec.

Statistics. Design of Experiment (DOE) was performed and statistical data was analyzed using JMP software (SAS, Cary, N.C.). In this study, statistical significance was defined as *p*-values less than 0.05. Three mice per formulation/dose (n = 3) were used for all *in vivo* experiments. For Library A, a $3^4 \times 2^2$ Definitive Screening Design[132] was used with 4 three-level quantitative factors (C12-200 RNA weight ratio, C12-200 mol%, phospholipid mol%, and PEG mol%) and 2 two-level qualitative factors for phospholipid tail group (DS =1,2-distearoyl-*sn*-glycero- and DO = 1,2-dioleoyl-*sn*-glycero-) and phospholipid head group (PC = 3-phosphocholine and PE = 3-phosphoethanolamine). For Library B, a $3^4 \times 2^1$ L-18 Taguchi Fractional Factorial Design[131] was used with 4 three-level quantitative factors (C12-200 RNA weight ratio, C12-200 mol%, phospholipid mol%, and PEG mol%) and 1 two-level qualitative factor for phospholipid (DSPC or DOPE). To make the Standard Least Squares regression model for Library B, a full model with all orthogonal and second-order effects was generated and subsequently reduced until only statistically significant effects remained in the model as determined by ANOVA. A post-hoc Tukey test was performed using JMP to verify that the two levels of phospholipid effect were statistically different ($p < 0.0001$). When comparing means between two groups, a Student's t-test was used assuming a Gaussian distribution and unequal variances. Further details about statistics and models used in this study, including ANOVA results, parameter estimates, residuals, etc. can be found in **Table B.2-2** and **Fig. A.2-1**.

2.7 Acknowledgments

This work was supported by Shire Pharmaceuticals (Lexington, MA) and the MIT Skoltech Initiative. The authors thank Nicki Watson at the W.M. Keck Microscopy Institute (Whitehead Institute, Cambridge, MA) for assistance in performing the TEM experiments. We also thank Prof. Sumona Mondal (Clarkson University) for performing a statistical review of the manuscript. The authors declare no competing financial interest.

Chapter 3

Evaluation of Efficacy and Immunogenicity of mRNA Lipid Nanoparticles

The work presented in this chapter was published as:

Kauffman, K.J., Mir, F.F., Jhunjhunwala, S., Kaczmarek, J.C., Hurtado, J.E., Yang, J.H., Webber, M.J., Kowalski, P.S., Heartlein, M.W., DeRosa, F., Anderson, D.G. "Efficacy and Immunogenicity of Unmodified and Pseudouridine-modified mRNA Delivered Systemically with Lipid Nanoparticles in vivo." *Biomaterials,* **109**, 78-87, 2016.

3.1 Introduction

Messenger RNA (mRNA) delivery is emerging as an attractive strategy for the treatment of a variety of diseases.[22] Nanoparticle delivery vehicles, including lipid nanoparticles (LNPs), polymer nanoparticles, viruses, and others, have been developed as tools to encapsulate and deliver RNAs into the cytoplasm, as naked nucleic acids cannot readily cross cell membranes.[7,30,141] *In vitro* transcribed (IVT) mRNA is known to activate various pattern recognition receptors, including toll-like receptors[10,142] (TLR3, TLR7, TLR8), RIG-I,[143] and RNA-dependent protein kinase (PKR),[54] leading to an antiviral immune response.[144] Synthetic base modifications have been reported to mitigate immunogenicity and improve the stability of small interfering RNAs (siRNAs)[49], and it has been hypothesized that similar strategies could also prove beneficial for mRNA therapeutics.[21] To reduce the immunogenicity and increase stability of therapeutic mRNAs, the use of naturally-occurring base modifications has been proposed, including pseudouridine,[52] 5-methylcytidine,[145] 2-thiouridine,[74] N^6-methyladenosine[51], and N^1-methylpseudouridine.[146] However, one disadvantage of base-modified mRNAs is the potential for decreased translational capacity of the mRNA.[52,147]

One common approach to mRNA base modifications is the 100% substitution of uridine with pseudouridine (PseudoU), which is sometimes used in combination with 5-methylcytidine replacement of cytidine.[116,130] Karikó and co-workers performed pioneering work with PseudoU modification to mRNA, finding that PseudoU-modified mRNAs resisted ribonuclease (RNase) degradation,[148] reduced activation of TLRs[10] and PKR[54], and interestingly resulted in improved translational efficacy both *in vitro* and *in vivo* compared to unmodified mRNAs when delivered with both liposomal and non-liposomal formulations.[52,53] However, Thess *et al.*[59] recently reported that that PseudoU modifications significantly diminished mRNA translation and that codon-optimized unmodified mRNAs did not upregulate three measured pro-inflammatory cytokines *in vivo* when delivered intraperitoneally with a lipid/polymer non-liposomal transfection

reagent. We hypothesize that these differing literature reports regarding the immunogenicity and efficacy of PseudoU-modified mRNAs *in vivo* (summarized in **Table 3-1**) may be due to 1) limited analysis[5] of the extracellular innate immune response to mRNAs *in vivo* and 2) the use of different delivery vehicles, methodologies, and material properties between studies. It has been previously demonstrated that delivery material properties[140,149–151] can dramatically affect the potency of encapsulated nucleic acids, and Pardi et al. recently reported that 1-methylpseudouridine-modified mRNA-LNPs have different kinetics and efficacy *in vivo* depending on the route of administration.[152]

The effect of PseudoU modifications on mRNA immunogenicity and efficacy remains an outstanding question with important implications for therapeutic application of mRNA. Therefore, in the present work we aimed to perform a thorough analysis of the extracellular innate immune response to and efficacy of mRNA with and without PseudoU modifications *in vivo* using mice. To maximize protein expression, mRNA was delivered intravenously[152] using LNPs based on the lipid-like material C12-200,[85,149] which have recently been studied therapeutically in a hemophilia B mouse model.[153] Our results indicate that PseudoU modification of mRNA does not measurably change the LNP physical properties and neither improves the efficacy nor reduces the immunogenicity of the mRNA-LNP when delivered systemically. Furthermore, at high mRNA doses we discovered indicators of a yet-uncharacterized, transient extracellular innate immune response to intravenously-delivered mRNA-LNPs, including cytokine elevation, neutrophilia, and myeloid cell activation in the blood and spleen. In all, these data do not indicate improved *in vivo* performance with PseudoU modification of mRNA, and suggest that unmodified mRNA may be at least as suitable for systemic mRNA-LNP administration.

3.2 mRNA Synthesis and LNP Formulation

mRNAs of three different sequences were synthesized with and without 100% pseudouridine (PseudoU) replacement of uridine (**Fig. 3-1a**). Following *in vitro* transcription (IVT), mRNA products were 5'-capped with Cap1 and 3'-polyadenylated, yielding mature mRNAs at their respective predicted lengths. (**Fig. 3-1b, Fig. A.3-1**). Electrophoresis size fractionation was performed on all synthesized mRNAs to confirm the absence of smaller length fragments (**Fig. A.3-2**). In general, we found that IVT PseudoU-modified mRNAs had significantly lower yields, typically half those of unmodified mRNAs **(Table B.3-1)**.

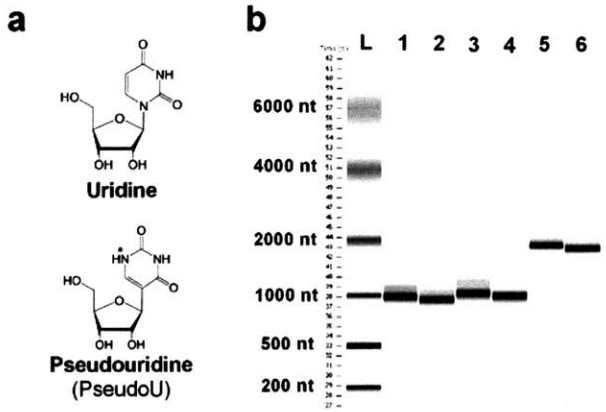

Figure 3-1. mRNA modification strategy and characterization. (**a**) Chemical structures of uridine and pseudouridine (PseudoU) bases, where (*) denotes the extra hydrogen-bond donor of PseudoU. (**b**) Electrophoresis size fractionation performed by an Agilent Bioanalyzer on all six fully 5'-capped and 3'-tailed mRNA's used in this study. L = ladder, 1 = unmodified scramble mRNA, 2 = PseudoU scramble mRNA, 3 = unmodified EPO mRNA, 4 = PseudoU EPO mRNA, 5 = unmodified Luc mRNA, 6 = PseudoU Luc mRNA.

PseudoU has an extra hydrogen-bond donor (shown as asterisk on **Fig. 3-1a**) that allows for increased local RNA stacking, more thermodynamically favorable duplex formation, and a more rigid sugar-phosphate backbone.[154,155] We observed that PseudoU-modified mRNAs migrate at a slightly lower observed molecular weight than their unmodified counterparts on Bioanalyzer **(Fig. 3-1b)** and agarose gel **(Fig. A.3-1)**, which could be attributed to the tighter packing and thus smaller hydrodynamic volume of PseudoU-modified mRNAs. However, this difference in

mRNA secondary structure imparted by PseudoU modifications does not affect mRNA loading into lipid nanoparticles (LNPs). When mRNAs were encapsulated into C12-200 LNPs (**Fig. A.3-3**) using formulation parameters previously optimized specifically for mRNA delivery,[149] all LNPs had similar diameters (approximately 80 nm, **Fig. 3-2a**) and mRNA encapsulation efficiencies (approximately 55-65%, **Fig 2b**) regardless of mRNA length or PseudoU modification. Visualized by Cryogenic Transmission Electron Microscopy, both unmodified and PseudoU-loaded mRNA LNPs had similar, spherical morphologies (**Fig. 3-2c,d**).

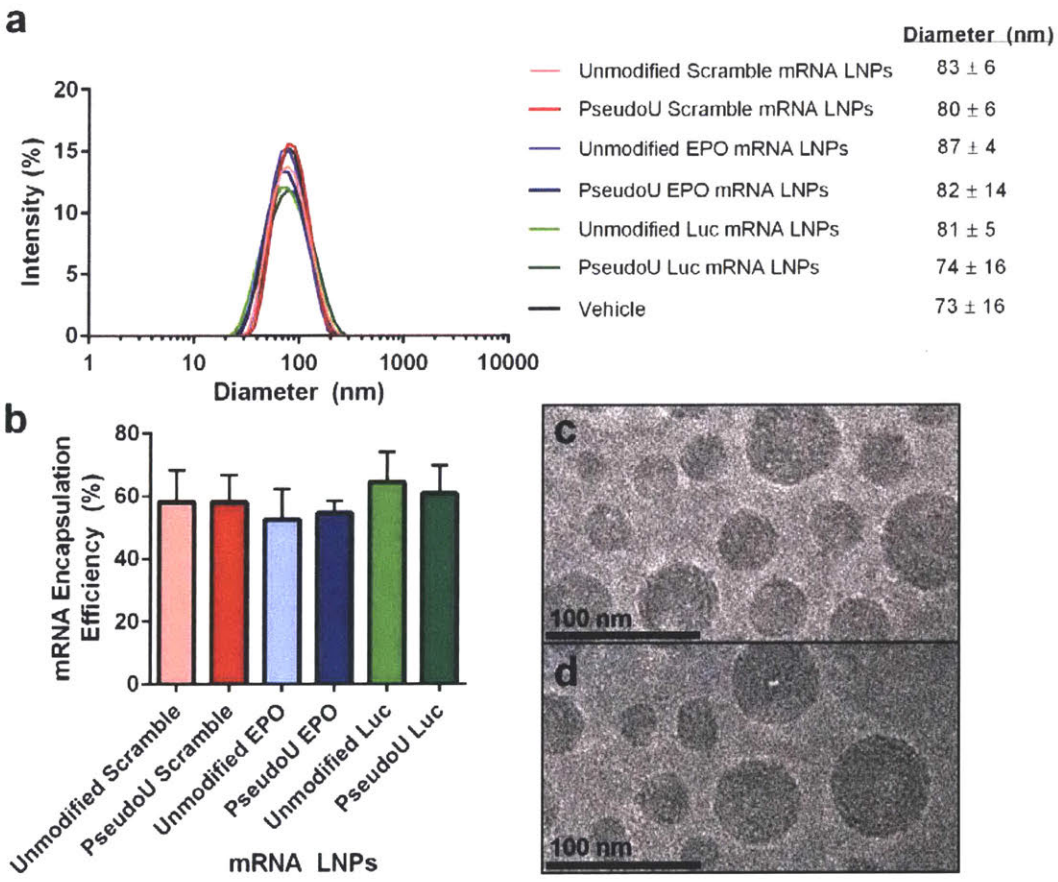

Figure 3-2. mRNA-loaded LNP synthesis and characterization. (**a**) Representative size distributions of all mRNA-loaded LNPs and LNP vehicle without mRNA. The legend includes average diameters, presented as mean +/- std. dev. (n = 5 for scramble mRNA's and vehicle, n = 3 for EPO and Luc mRNAs). (**b**) mRNA encapsulation efficiency of all mRNA-loaded LNPs. Data presented as mean +/- std. dev. (n = 5 for scramble mRNA's, n = 3 for EPO and Luc mRNA's). (**c**) Representative images of unmodified mRNA LNPs visualized by Cryo-EM. (**d**) Representative images of PseudoU mRNA LNPs visualized by Cryo-EM.

3.3 Efficacy of Unmodified vs. PseudoU-modified mRNA-LNPs

The effect of PseudoU modification on mRNA translation efficiency when delivered with LNPs was assessed both *in vitro* and *in vivo*. In this study, mRNAs coding for two proteins (i.e. mRNAs of different lengths) were tested: 1) Firefly luciferase (Luc), a model non-secreted luminescent protein, and 2) Erythropoietin (EPO), a secreted serum protein with therapeutic applications in anemia.[53] In HeLa cells *in vitro*, unmodified mRNA-LNPs were approximately twice as potent as PseudoU-modified mRNA-LNPs at multiple doses for both EPO-encoding (**Fig. 3-3a**) and Luc-encoding (**Fig. 3-3b**) mRNAs. In a similar experiment, Thess *et al.*[59] transfected HeLa cells with mRNA lipoplexes (Lipofectamine 2000) and reported that unmodified mRNAs led to significantly higher protein expression than PseudoU-modified mRNAs for both Luc and EPO. Here, we show a similar result across multiple doses *in vitro* using LNPs, which have better serum stability, longer circulation times, and are less prone to aggregation than lipoplexes *in vivo*[18,129].

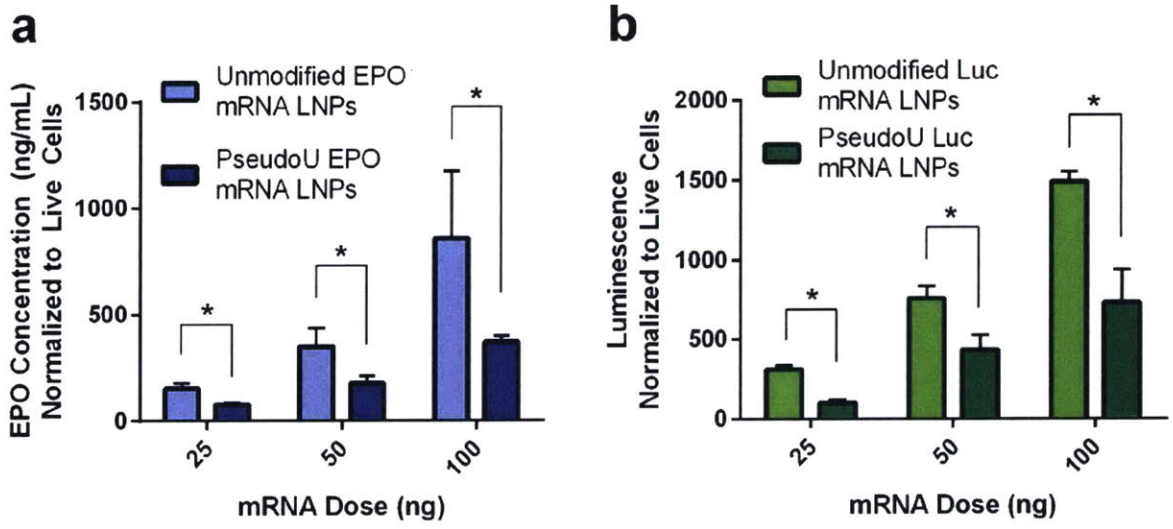

Figure 3-3. Unmodified vs. PseudoU-modified mRNA-LNP efficacy *in vitro*. (**a**) Supernatant EPO concentration as a function of dose for unmodified and PseudoU-modified EPO mRNA LNPs in HeLa cells 24 hr post-transfection. (**b**) Luciferase expression as a function of dose for unmodified and PseudoU-modified Luc mRNA LNPs in HeLa cells 24 hr post-transfection. Data presented as mean +/- std. dev. (n = 4). Asterisk represents a statistically significant difference.

LNPs formulated with either unmodified or PseudoU-modified mRNA were next evaluated for efficacy *in vivo* following systemic delivery. Contrasting the *in vitro* findings, no significant difference in EPO expression between unmodified and PseudoU EPO mRNA-loaded LNPs was observed following intravenous administration in mice at doses ranging between 0.125 mg/kg and 0.5 mg/kg **(Fig. 3-4a)**. To our knowledge, this is the first report that PseudoU modifications do not improve the potency of mRNA when delivered intravenously with LNPs in a mouse model. Similarly, no significant differences between unmodified and PseudoU Luc mRNA-loaded LNPs were observed for Luc expression in the spleen and liver **(Fig 4b)**, the only two organs which had measurable Luc expression for either treatment. Further, biodistribution was not altered by PseudoU modification of mRNA, as protein expression occurred predominately in the liver, consistent with previous reports.[85,149]

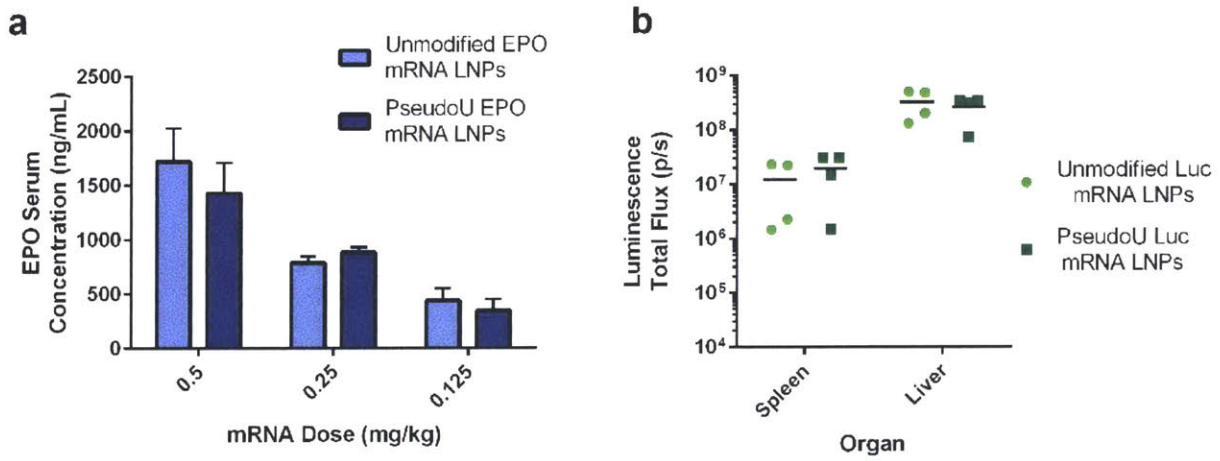

Figure 3-4. Unmodified vs. PseudoU-modified mRNA-LNP efficacy *in vivo.* (**a**) Serum EPO concentration as a function of dose for unmodified and PseudoU-modified EPO mRNA LNPs in mice 6 hr post-intravenous injection. Data presented as mean +/- std. dev. (n = 4). (**b**) Luciferase expression in spleen and liver for unmodified and PseudoU-modified Luc mRNA LNPs 6 hr post-intravenous injection at 0.1 mg/kg. Bar represents mean (n = 4).

3.4 Assessing Immunogenicity for Unmodified vs. PseudoU-modified mRNA-LNPs

The next objective was to determine if PseudoU modifications altered the immunogenicity of mRNA when delivered systemically *in vivo* using LNPs. Unmodified and PseudoU-modified mRNAs with a scrambled coding region of the same length as EPO were used to ensure that any immunogenicity was not in response to translated exogenous protein. Furthermore, LNPs formulated without mRNA were used as a control to parse out the immunogenicity of mRNA from that of the lipid delivery materials.

Previous studies[52,53,59] investigating the immunogenicity of PseudoU-modified mRNAs were limited to measuring a small number of common pro-inflammatory cytokines *in vivo* following administration of non-LNP formulations **(Table 3-1)**. Here, we measured a panel of over thirty cytokines in mouse serum six hours post-intravenous injection of mRNA-LNPs with and without PseudoU modifications (**Fig. 3-5a)**. When mRNA-LNPs were injected intravenously at high doses, we observed varying degrees of elevation in the levels of a variety of interleukins, colony stimulating factors, and chemokines at six hours post-injection relative to a control of LNPs without mRNA. The most upregulated cytokines (G-CSF, MCP-1, RANTES, MIG) were confirmed to be dependent on dose of mRNA **(Fig. 3-5b)**, and at sufficiently low doses of mRNA, cytokine response was minimal. Importantly, PseudoU-modified mRNA did not substantially reduce these serum cytokine levels compared to unmodified mRNA at six hours post-injection. Moreover, PseudoU modification of mRNA did not reduce mRNA-LNP liver enzymes alanine transaminase (ALT) and aspartate transaminase (AST) **(Fig. A.3-4)**.

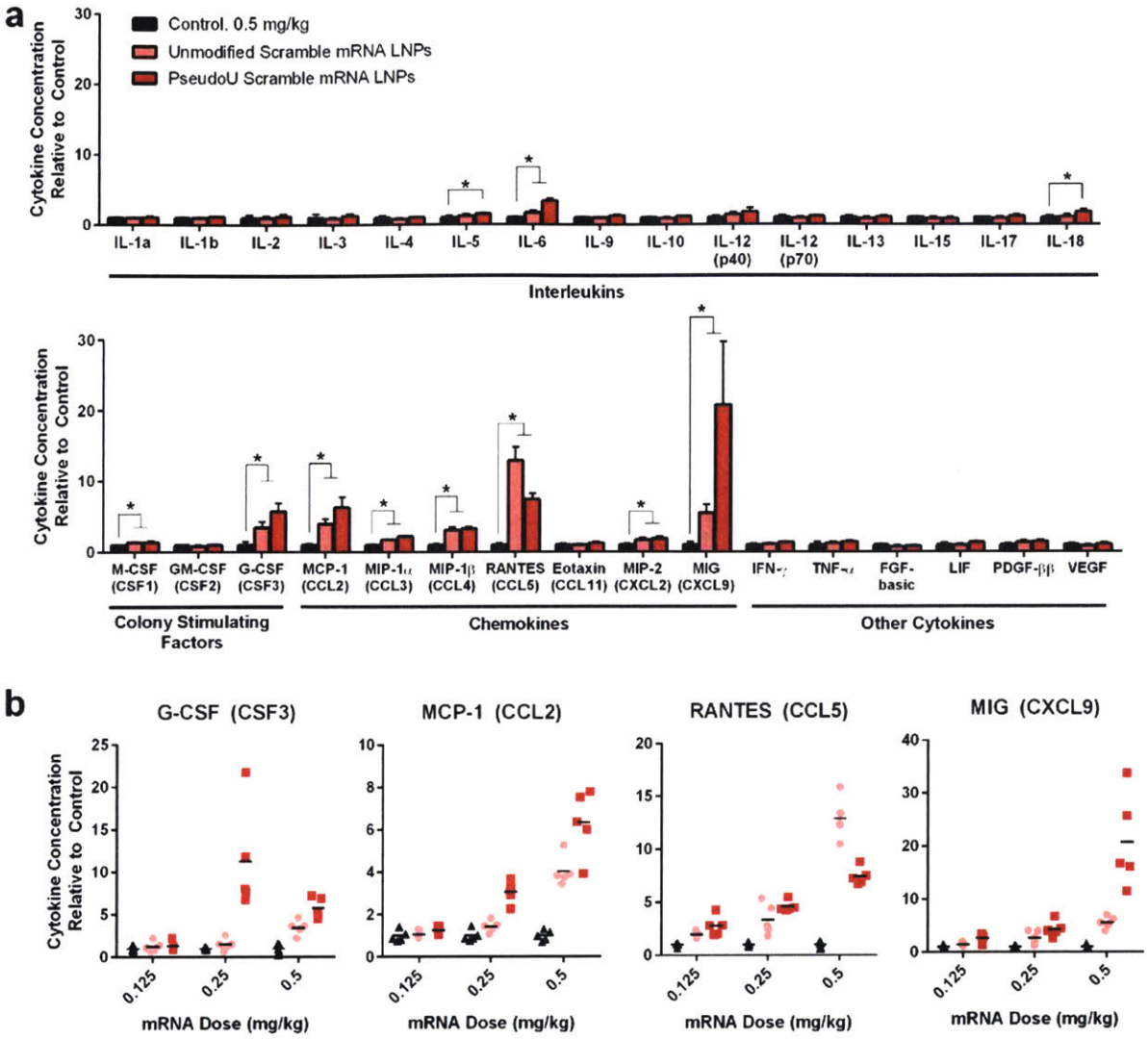

Figure 3-5. Cytokine response elicited by mRNA-LNPs *in vivo*. (**a**) Serum cytokine concentration 6 hr post-intravenous administration of mRNA-LNPs relative to the control (LNPs without mRNA) at an mRNA dose of 0.5 mg/kg (control injected at equivalent lipid dose). Data presented as mean +/- std. dev. (n = 5). Asterisk represents a statistically significant difference. (**b**) Serum G-CSF, MCP-1, RANTES, or MIG concentration 6 hr post-intravenous administration of mRNA-LNPs relative to the control (LNPs without mRNA) at various mRNA doses (control injected at equivalent lipid dose). Bar represents mean (n = 5). The legend in (a) applies to all panels.

The observation of elevated cytokines that are produced by and influence myeloid cells led us to question the effect of mRNA-LNPs on blood and splenic immune cell distribution and activity. Immune cell distributions in the blood and spleen were therefore measured at six hours

post-intravenous injection of mRNA-LNPs. At a sufficiently high dose of mRNA (0.5 mg/kg), we observed neutrophilia (increased percentage of neutrophils among total immune cells) in both the blood **(Fig. 3-6a)** and the spleen **(Fig. 3-6b)**. In addition, neutrophils in both the blood and spleen expressed significantly higher levels of cell-surface proteins that are markers for neutrophil activation, including CD14 and CD69, with CD11b also increased in the spleen **(Fig. 3-6c)**. Notably, neutrophil levels returned to baseline **(Fig. A.3-5a, b)** and activation markers were no longer upregulated 72 hours post-injection **(Fig. A.3-5c)**, suggesting that neutrophilia induced by mRNA administration is a transient response. Correspondingly, a small but statistically significant drop in non-neutrophil myeloid cells was observed at 6 hours post-intravenous administration of mRNA-LNPs **(Fig. 6a, b)**, with a return to baseline 72 hours post-injection **(Fig. A.3-5a, b).**

In the spleen, dendritic cells and macrophages expressed higher levels of the activation marker CD86, but not other markers such as MHC-II and CD80, at 6 hours post-injection **(Fig. 3-6c)** with a return to baseline 72 hours post-injection **(Fig. A.3-5c)**. Similar increased CD86 expression has been observed on bone marrow-derived dendritic cells following lipoplexed antigen-encoding mRNA administered subcutaneously in mice (Pollard *et al.*[76]). At 72 hours, the spleen mass had increased for both unmodified and PseudoU-modified mRNA-LNPs **(Fig. A.3-6)**, but no other differences were observed at 72 hours post-injection compared to vehicle-injected or PBS-injected mice. Prominently in this study, unmodified and PseudoU-modified mRNA-LNP administration resulted in similar changes in myeloid cell distribution and activation, suggesting that PseudoU modification does not reduce immune activation when mRNAs are delivered systemically with LNPs.

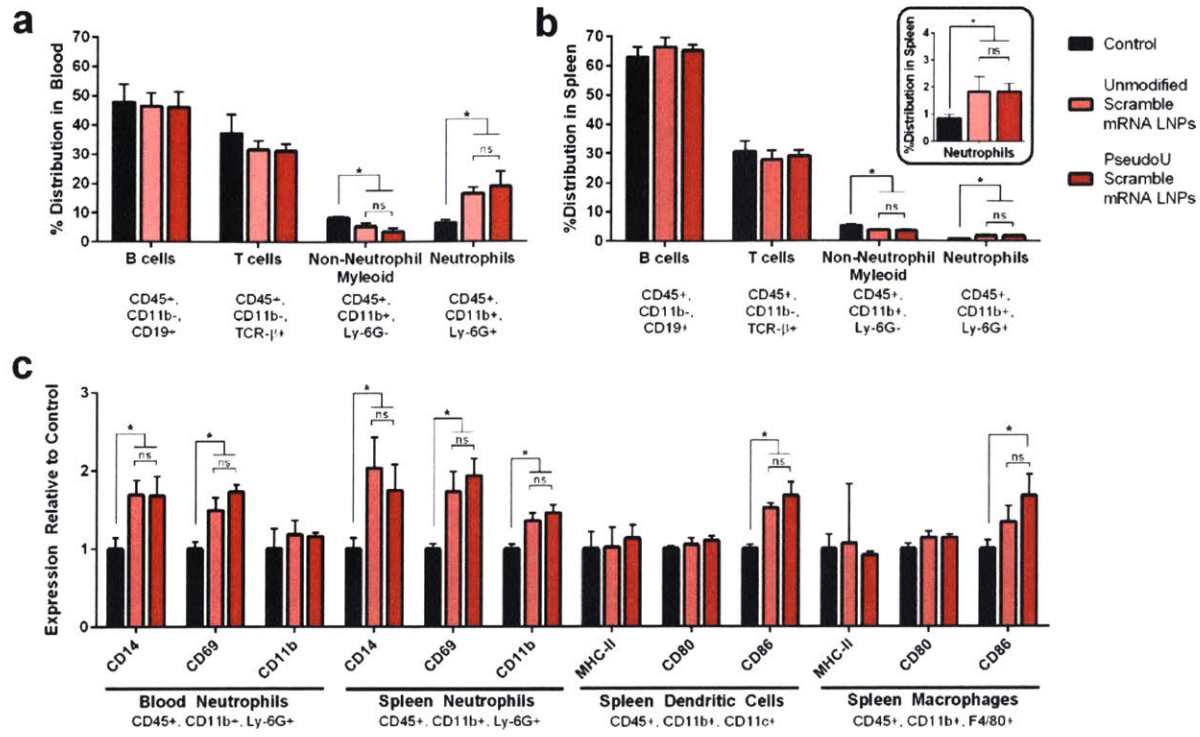

Figure 3-6: Neutrophilia and myeloid cell activation for mRNA-LNPs *in vivo*. Distribution of immune cell subsets in the blood (**a**) and spleen (**b**) measured by flow cytometry at 6 hour post-intravenous injection of mRNA-LNPs at 0.5 mg/kg mRNA dose (control LNPs without mRNA injected at equivalent lipid dose). (**c**) Increased expression of activation markers on neutrophils in the blood and spleen, and dendritic cells and macrophages in the spleen as measured by flow cytometry at 0.5 mg/kg mRNA dose (control LNPs without mRNA injected at equivalent lipid dose). All data presented as mean +/- std. dev. (n = 4).

3.5 Discussion

The broad use of mRNA in the clinic requires the development of safe and effective delivery systems. One method to vary mRNA potency and immunogenicity is through RNA base modifications, with 100% pseudouridine (PseudoU) replacement of uridine **(Fig. 3-1)** being the most commonly reported. The systemic use of mRNA requires a delivery vehicle to ensure cellular uptake, target specific tissues/cell types, and prevent mRNA degradation.[141] Recently, LNPs have been demonstrated as efficient mRNA delivery vehicles and have been studied *in vivo* in a therapeutic context[59,76,82]. Findings here demonstrate that the properties of mRNA-

loaded LNPs – specifically, encapsulation efficiency, diameter, and morphology – do not change as a result of PseudoU modification to the mRNA payload **(Fig. 3-2)** in spite of the different secondary structure imparted through PseudoU-modification of mRNA.

Table 3-1: Comparison of studies in the literature comparing efficacy of unmodified and PseudoU-modified mRNAs in mice

Publication	Kariko et al.[52], 2008	Kariko et al.[53], 2012	Thess et al.[59], 2015	Present, 2016
Delivery Vehicle	Lipofectin	TransIT	TransIT	LNP
Route of Administration	i.v.	i.p.	i.p.	i.v.
Primary Organ of Expression	Spleen	Spleen	Spleen	Liver
mRNA Codon-Optimized	No	Yes	Yes	No
mRNA HPLC-purified	No	Yes	No	No
mRNA 5' UTR	*Xen.* β-globin	TEV	HSD17B4	CMV
mRNA 3' UTR	*Xen.* β-globin	*Xen.* β-globin	ALB	hGH
Efficacy Findings	PseudoU more efficacious	PseudoU more efficacious	Unmodified more efficacious	Equal efficacy
Innate Immunogenicity Findings	Unmodified is immunogenic; PseudoU is non-immunogenic.	Unmodified is immunogenic; PseudoU is non-immunogenic.	Unmodified is non-immunogenic (PseudoU not tested)	Equal immunogenicity (high doses); equally non-immunogenic (low doses)
Criteria for Determining Innate Immunogenicity	1 cytokine tested (IFN-α)	3 cytokines tested (TNF-α, IL-6, IFN-γ)	3 cytokines tested (TNF-α, IL-6, IFN-γ)	30+ cytokines tested, blood/spleen neutrophilia, blood/ spleen myeloid cell activation

Note: TransIT is a commercial non-liposomal lipid/polymer transfection reagent. Abbreviations: CMV: cytomegalovirus, hGH: human growth hormone, HSD17B4: hydroxysteroid (17-β) dehydrogenase 4, ALB: albumin, TEV: tobacco etch virus, Xen.: Xenopus.

The literature contains different effects of PseudoU modification on mRNA immunogenicity and potency when delivered using a nanoparticle vehicle. While Karikó and colleagues reported that PseudoU modifications increased the efficacy of intravenously-administered, spleen-targeting lipofectin-complexed mRNA[52] and intraperitoneally-administered, spleen-targeting TransIT-complexed (a commercial non-liposomal lipid/polymer transfection

reagent) mRNA[53], Thess *et al.* have reported that PseudoU modifications *decreased* the efficacy of intraperitoneally-administered, codon-optimized mRNA delivered with TransIT[59]. As shown in **Table 3-1**, we hypothesize that these differences on the effect of PseudoU modifications result from some combination of four variables that are different from experiment-to-experiment: 1) delivery material (LNP vs. liposomal vs. non-liposomal lipid/polymer reagent), 2) route of administration (intravenous vs. intraperitoneal), 3) transfected cell type (liver vs. spleen), and 4) mRNA properties (different UTR's, codon-optimized,[60] HPLC-purified[156]).

In our experiments, we chose a delivery material (LNP) and route of administration (intravenous) with clinical potential and relatively high protein expression per dose of mRNA. Using these conditions, we sought to evaluate the effect of PseudoU mRNA modifications on efficacy by using two different mRNA sequences both *in vitro* **(Fig. 3-3)** and *in vivo*. **(Fig. 3-4)**. Our results indicate that 100% PseudoU modified and unmodified mRNAs have similar efficacies when delivered intravenously using these LNPs in wild-type mice, but interestingly, PseudoU mRNA-LNPs resulted in significantly lower translation *in vitro* in HeLa cells. *In vitro* experiments do not fully recapitulate the complexities of the *in vivo* environment, and a previous study found that the efficacy of siRNA-LNPs *in vitro* did not always correlate with the efficacy found *in vivo*.[129] In the case of mRNA-LNPs, the increased resistance imparted by PseudoU modifications to mRNA degradation may be more significant *in vivo,* or perhaps HeLa cells and hepatocytes process PseudoU-modified mRNAs differently.

In addition, increased levels of cytokines including MCP-1, RANTES, G-CSF, and MIG **(Fig. 3-5)** were observed following administration of high doses of both unmodified and PseudoU-modified mRNA-LNPs. Elevation of these cytokines has been previously implicated in the innate immune response to foreign nucleic acids: in human fetal membranes, viral ssRNA was found to upregulate MCP-1, RANTES, and G-CSF, among other cytokines (MIG was not tested).[157] Additionally, it was reported that MIG and RANTES were both significantly elevated

following mRNA transfection of A549 cells *in vitro*,[158] and the RANTES secretion from A549 cells did not appear to be significantly different between lipoplexed unmodified and PseudoU mRNA.[146] These four cytokines are involved in neutrophil recruitment and function: G-CSF controls neutrophil proliferation, differentiation, and trafficking,[159] and the other three (MCP-1, RANTES, MIG) are inflammatory chemokines, typically signaling recruitment of more myeloid cells such as neutrophils to sites of inflammation or infection.[160]

Indeed, neutrophilia and neutrophil activation were also observed in response to both unmodified and PseudoU-modified mRNA-LNPs at 6 hours post-injection **(Fig. 3-6)**. Neutrophilia and inflammatory cytokine response are commonly observed as part of an innate immune response to RNA-based viral infectious agents.[161] mRNA-loaded lipid nanoparticles share several structural similarities to some types of ssRNA viruses. Like mRNA-LNPs, ssRNA viruses can have spherical morphologies, a diameter on the order of 100 nm, and single-stranded RNA decorating the outside of the particle.[162] Cytokine production and neutrophilia have been observed in response to ssRNA viruses (including West Nile Virus,[163] SARS,[164] and Hantavirus[165]) through the activation of receptors that recognize pathogen-associated and damage-associated molecular patterns. Our data suggests that regardless of PseudoU modification, the innate immune system may interpret mRNA-laden LNPs at high enough doses through similar molecular pattern recognition mechanisms. However, of importance is the observation that these responses are hyper-acute (observed 6 hours post-injection) and transient (returned to baseline by 72 hours).

These findings provide additional perspective on the existing literature **(Table 3-1)** to provide a more comprehensive description of the *in vivo* extracellular innate immune response to mRNA-loaded LNPs. Our results suggest that intravenously-injected mRNA-LNPs can interact with phagocytic myeloid cells in the bloodstream and neutrophils specifically are activated and secrete several cytokines. Circulating neutrophils are also observed in higher

percentages and are activated in the spleen. We postulate that either activated neutrophils or blood monocytes which interact with mRNA-LNPs activate dendritic cells and macrophages in the spleen. Moreover, encapsulated mRNA is expressed predominately in the liver with some expression occurring in the spleen **(Fig. 3-7)**. Independent of conclusions based on mRNA modification, these results contribute mechanistic insight into the nature of the innate immune response elicited by therapeutic mRNAs in circulation. Further, this model suggests potential approaches to reduce this immune response by decreasing blood concentration of mRNA-LNPs and thereby minimizing their interaction with circulating myeloid cells. For example, it may be possible to mediate these effects through a gradual intravenous drip of mRNA-LNPs rather than bolus infusion.

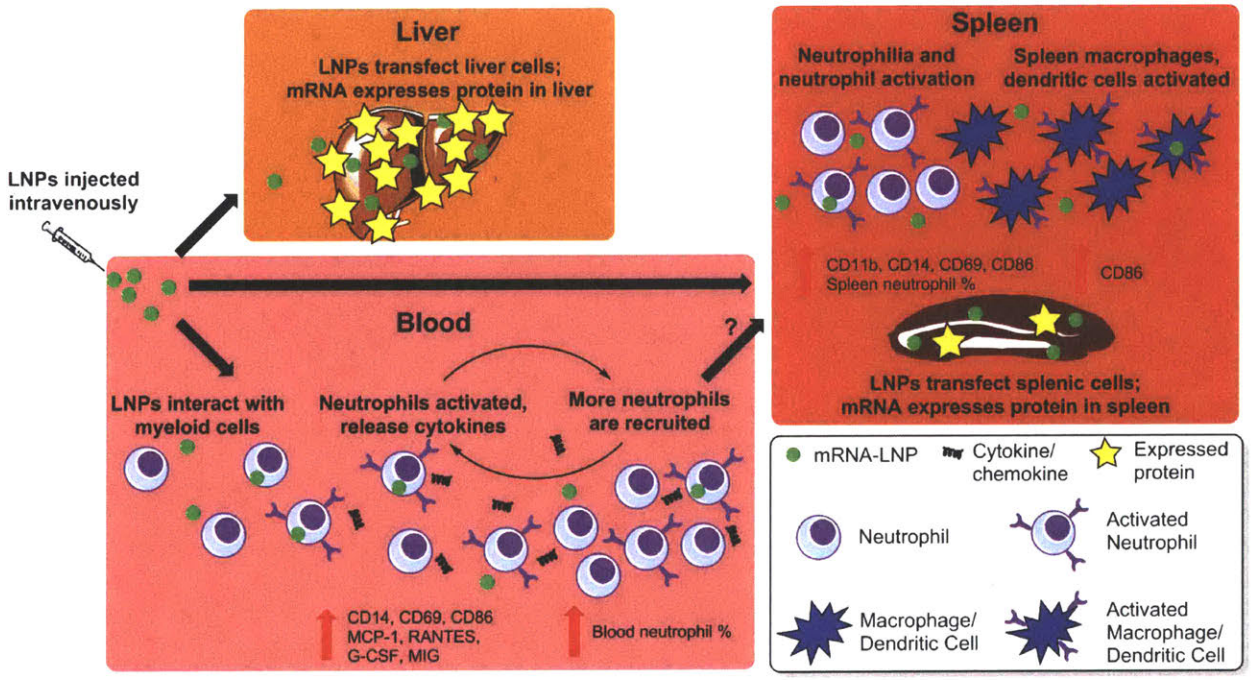

Figure 3-7: Hypothesized extracellular innate immune response to mRNA-LNPs injected systemically, regardless of PseudoU modification of mRNA.

Given that LNP encapsulation protects unmodified mRNAs from RNase degradation (**Fig. A.3-7**), the stability imparted by the PseudoU modifications against circulating RNases in

the bloodstream may be unnecessary when the mRNA is delivered with LNPs. It is also noteworthy that incorporation of PseudoU into mRNA significantly reduces IVT yields **(Table B.3-1)** and PseudoU triphosphate is currently much more expensive than uridine triphosphate when obtained commercially at small scales. Our results suggest that PseudoU modifications do not improve the efficacy or alter immunogenicity *in vivo*, and indicate that unmodified mRNAs may be preferred in future applications requiring systemic delivery of mRNA-LNPs. Future work will be necessary to determine if other mRNA base modifications do in fact improve efficacy or alter immunogenicity of the mRNA when delivered systemically with LNPs. For example, N(1)-methylpseudouridine has recently been reported[146] to result in significantly higher translation *in vivo* compared to unmodified mRNAs when delivered with lipofectamine/mRNA complexes via intramuscular and intradermal administration; however, it remains to be seen if these results change with different delivery vehicles, administration routes, and mRNA properties as listed in **Table 3-1**.

For certain therapeutic applications such as mRNA-based vaccines, an immune response to mRNA-LNPs may be desired. For other applications, an inappropriate immune response could result in unwanted toxicity. The immune responses observed here were measurable but transient in nature, with nearly all markers of immunogenicity returning to baseline levels after 72 hours. Additionally, while transient neutrophilia can be a sign of infection, it is not necessarily harmful in and of itself, as significant increases in neutrophil counts are also observed after vigorous exercise[166] or during pregnancy[167]. Furthermore, at low doses of mRNA-LNPs (0.125 mg/kg), no significant immune response was observed.

3.6 Conclusions

In conclusion, we have evaluated PseudoU-modified and unmodified mRNA when encapsulated in C12-200 LNPs by measuring nanoparticle physical properties, *in vitro* and *in vivo* potency, and *in vivo* immunogenicity. PseudoU modifications to mRNA did not result in changes to LNP size, morphology, or encapsulation efficiency. Furthermore, PseudoU modification of mRNA did not improve the efficacy of the mRNA-LNP *in vitro* or *in vivo*. Lastly, we identified three previously-unreported indicators of a modest and transient extracellular innate immune response to mRNA-LNPs – myeloid cell activation, neutrophilia, and cytokine elevation – but determined that PseudoU modification of mRNA does not reduce this immune response. In all, we report no benefit in these studies for using PseudoU-modified mRNAs when delivered systemically with lipid nanoparticles.

3.7 Materials and Methods

mRNA Synthesis. DNA plasmids (Invitrogen) containing a T7 promoter upstream of the sequences for luciferase (Luc), or erythropoietin (EPO), or scrambled EPO coding region (scramble) mRNA were used as templates for mRNA synthesis. DNA plasmids were linearized using restriction enzyme XbaI (New England Biolabs, Ipswich, MA) and transcribed using the HiScribe T7 RNA Synthesis Kit (New England Biolabs). To make pseudouridine-modified mRNA, uridine triphosphate was replaced with pseudouridine triphosphate (Trilink, San Diego, CA) during the transcription step. mRNA was capped with the Vaccinia Capping System (New England Biolabs), and the cap was modified to Cap1 using mRNA Cap 2'-O-Methyltransferase (New England Biolabs). PolyA tails were added to the RNA using a Poly(A) Polymerase Kit (New England Biolabs). All mRNAs were purified after the transcription and tailing steps using

MEGAClear RNA purification columns (Life Technologies, Beverly, MA). Concentration was determined using a NanoDrop 1000 (Thermo Scientific, Cambridge, MA).

mRNA Sequences. Final, purified mRNAs contained a 5' cap (Cap1), a 5' UTR consisting of a partial sequence of the cytomegalovirus (CMV) immediate early 1 (IE1) gene, a coding region as described below, a 3' UTR consisting of a partial sequence of the human growth hormone (hGH) gene, and a 3' polyA tail estimated to be approximately 100 nucleotides long.

EPO:

AUGGGGGUGCACGAAUGUCCUGCCUGGCUGUGGCUUCUCCUGUCCCUGCUGUCGCUC
CCUCUGGGCCUCCCAGUCCUGGGCGCCCCACCACGCCUCAUCUGUGACAGCCGAGUCC
UGGAGAGGUACCUCUUGGAGGCCAAGGAGGCCGAGAAUAUCACGACGGGCUGUGCUGA
ACACUGCAGCUUGAAUGAGAAUAUCACUGUCCCAGACACCAAAGUUAAUUUCUAUGCCU
GGAAGAGGAUGGAGGUCGGGCAGCAGGCCGUAGAAGUCUGGCAGGGCCUGGCCCUGC
UGUCGGAAGCUGUCCUGCGGGGCCAGGCCCUGUUGGUCAACUCUUCCCAGCCGUGGG
AGCCCCUGCAGCUGCAUGUGGAUAAAGCCGUCAGUGGCCUUCGCAGCCUCACCACUCU
GCUUCGGGCUCUGGGAGCCCAGAAGGAAGCCAUCUCCCCUCCAGAUGCGGCCUCAGCU
GCUCCACUCCGAACAAUCACUGCUGACACUUUCCGCAAACUCUUCCGAGUCUACUCCAA
UUUCCUCCGGGGAAAGCUGAAGCUGUACACAGGGGAGGCCUGCAGGACAGGGGACAGA
UGA

Scramble:

AUGGUUCGAGGGUGAACGAAGCGACUGUCUCGGCGGUUCCCCCUAGCCACGGGUGAGA
GAGUUGACGCCGCGAGUCGCGAGUGGACAGUGCGGCUGCGGCUCGGACGUUGACCGA
CAGUGAGAGGACCGGCACAGCAGAGCCCACACCUCCCGUCAGCCAUUCGCUACCUUGU
GAGGCGUUGGGACUCUUUUCCGGUGGGGAUCCGCCGAUCACGACGCCUUGCUAGACC
GGGGGCUGUGAAUCCACCCAAGAUCUUUAUCUGGCUGGGUGGCGACUGCGCGCUUGAC

GCGCGACCGACCCCGAGCAAAGUCAUAACAUAGUGGAGCCUGGUUGUGUGGCUGUCGA

AUACCCCUUUGGCGUGUUCAGGACGAAGGGGCGUCAUUUGUCACCGGUGAUCACCAUC

GUGCCAGACCGAGCGCACACUACACGAGCUGCUUAGACCGCAUAUCAUACGGAAGGGU

CUCCCUACUUCCCACGACUCCUUUUGACAGUUCUCACAUCCUCGUGAGUCAGCGCCCG

CGAGCCUAUUUUACGUGGCACUAGGCCUCCGACCCAGUCGCCUCACCACACGAAACCCU

GUA

Luc:

AUGGAAGAUGCCAAAAACAUUAAGAAGGGCCCAGCGCCAUUCUACCCACUCGAAGACGG

GACCGCCGGCGAGCAGCUGCACAAAGCCAUGAAGCGCUACGCCCUGGUGCCCGGCACC

AUCGCCUUUACCGACGCACAUAUCGAGGUGGACAUUACCUACGCCGAGUACUUCGAGAU

GAGCGUUCGGCUGGCAGAAGCUAUGAAGCGCUAUGGGCUGAAUACAAACCAUCGGAUC

GUGGUGUGCAGCGAGAAUAGCUUGCAGUUCUUCAUGCCCGUGUUGGGUGCCCUGUUCA

UCGGUGUGGCUGUGGCCCCAGCUAACGACAUCUACAACGAGCGCGAGCUGCUGAACAG

CAUGGGCAUCAGCCAGCCCACCGUCGUAUUCGUGAGCAAGAAAGGGCUGCAAAAGAUC

CUCAACGUGCAAAAGAAGCUACCGAUCAUACAAAAGAUCAUCAUCAUGGAUAGCAAGACC

GACUACCAGGGCUUCCAAAGCAUGUACACCUUCGUGACUUCCCAUUUGCCACCCGGCU

UCAACGAGUACGACUUCGUGCCCGAGAGCUUCGACCGGGACAAAACCAUCGCCCUGAU

CAUGAACAGUAGUGGCAGUACCGGAUUGCCCAAGGGCGUAGCCCUACCGCACCGCACC

GCUUGUGUCCGAUUCAGUCAUGCCCGCGACCCCAUCUUCGGCAACCAGAUCAUCCCCG

ACACCGCUAUCCUCAGCGUGGUGCCAUUUCACCACGGCUUCGGCAUGUUCACCACGCU

GGGCUACUUGAUCUGCGGCUUUCGGGUCGUGCUCAUGUACCGCUUCGAGGAGGAGCU

AUUCUUGCGCAGCUUGCAAGACUAUAAGAUUCAAUCUGCCCUGCUGGUGCCCACACUAU

UUAGCUUCUUCGCUAAGAGCACUCUCAUCGACAAGUACGACCUAAGCAACUUGCACGAG

AUCGCCAGCGGCGGGGCGCCGCUCAGCAAGGAGGUAGGUGAGGCCGUGGCCAAACGC

UUCCACCUACCAGGCAUCCGCCAGGGCUACGGCCUGACAGAAACAACCAGCGCCAUUCU

GAUCACCCCCGAAGGGGACGACAAGCCUGGCGCAGUAGGCAAGGUGGUGCCCUUCUUC

GAGGCUAAGGUGGUGGACUUGGACACCGGUAAGACACUGGGUGUGAACCAGCGCGGCG

AGCUGUGCGUCCGUGGCCCCAUGAUCAUGAGCGGCUACGUUAACAACCCCGAGGCUAC

AAACGCUCUCAUCGACAAGGACGGCUGGCUGCACAGCGGCGACAUCGCCUACUGGGAC

GAGGACGAGCACUUCUUCAUCGUGGACCGGCUGAAGAGCCUGAUCAAAUACAAGGGCU

ACCAGGUAGCCCCAGCCGAACUGGAGAGCAUCCUGCUGCAACACCCCAACAUCUUCGAC

GCCGGGGUCGCCGGCCUGCCCGACGACGAUGCCGGCGAGCUGCCCGCCGCAGUCGUC

GUGCUGGAACACGGUAAAACCAUGACCGAGAAGGAGAUCGUGGACUAUGUGGCCAGCC

AGGUUACAACCGCCAAGAAGCUGCGCGGUGGUGUUGUGUUCGUGGACGAGGUGCCUAA

AGGACUGACCGGCAAGUUGGACGCCCGCAAGAUCCGCGAGAUUCUCAUUAAGGCCAAG

AAGGGCGGCAAGAUCGCCGUGUAA

mRNA Characterization. mRNA samples were characterized using the E-Gel iBase Power System with E-Gel EX gels (ThermoFisher) under denaturing conditions with 90% formamide. Gels were imaged using a BioRad ChemiDoc MP imager. Size fractionation was performed with an Agilent 2100 BioAnalyzer (Santa Clara, CA) at an mRNA concentration of 0.6 μg/μL. An RNA ladder (200, 500, 1000, 2000, 4000, 6000 nt) was used to generate a standard curve to convert Bioanalyzer results from migration time to number of bases.

LNP Synthesis. C12-200 lipid nanoparticles (LNPs) were prepared as previously described.[149] Briefly, an ethanol phase containing a mixture of C12-200 (WuXi AppTec, Shanghai, China), 1,2-dioleoyl-*sn*-glycero-3-phosphoethanolamine (DOPE, Avanti Polar Lipids, Alabaster, AL), cholesterol (Sigma), and 1,2-dimyristoyl-*sn*-glycero-3-phosphoethanolamine-*N*-[methoxy(polyethylene glycol)-2000] (ammonium salt) (C14-PEG 2000, Avanti) at a 35:16:46.5:2.5 molar ratio was mixed with an aqueous phase containing 10 mM citrate buffer (pH 3) with mRNA at a 1:3 volume ratio in a microfluidic chip device.[87] To formulate control LNPs (vehicle only), no mRNA was included in the aqueous phase. The LNPs were then

dialyzed against PBS in a 20,000 MWCO cassette at 4°C for 2 hr and no further purification was performed. For consistency, unmodified mRNA-LNPs, PseudoU-modified mRNA LNPs, and control LNPs were formulated in parallel.

LNP Characterization. mRNA encapsulation efficiency (i.e. loading efficiency) was calculated by performing a modified Quant-iT RiboGreen RNA assay (Invitrogen) as previously described.[16] The diameter and polydispersity (PDI) of the LNPs were measured using dynamic light scattering (ZetaPALS, Brookhaven Instruments). Diameter is reported as the largest intensity mean peak average. LNPs prepared for cryogenic transmission electron microscopy (Cryo-TEM) were dialyzed against 0.1x PBS, deposited onto a lacey copper grid coated with a continuous carbon film, and cooled continuously by liquid nitrogen. Using a minimum dose method, imaging was performed using a JEOL 2100 FEG microscope (Jeol, Freising, Germany) operated at 200 kV and a magnification setting of 60,000.

mRNA RNase Degradation. RNase A (ThermoFisher) was incubated with mRNA or mRNA-LNPs at 62.5 mU RNase/μg mRNA in a buffer made of 20 mM Tris-HCl, 2 mM EDTA, 1 M NaCl at room temperature for 30 min. RNase was inactivated by adding 6.4 mU Proteinase K / μg mRNA and incubating at 55°C for 10 min. To extract mRNA from LNPs, an equal volume of phenol-chloroform was added, the tube was vortexed vigorously, and the aqueous phase (containing the mRNA) was extracted. mRNAs were characterized using E-Gel EX gels as previously described.

***In vitro* Experiments.** HeLa cells (ATCC, Manassas, VA) were cultured in high glucose Dulbecco's Modified Eagle's Medium (ThermoFisher) containing 10% fetal bovine serum and 1% penicillin-streptomycin and maintained at 37°C and 5% CO_2. For transfection experiments, cells were plated at 20,000 cells/well in a 96-well plate. After 24 hr, the media in each well was

replaced with 150 μL of media containing LNPs. After another 24 hr, assays were performed as described below.

For wells containing EPO mRNA-LNPs, 100 μL of supernatant was removed and measured for EPO concentration using an ELISA assay (Human Erythropoietin Quantikine IVD ELISA Kit, R&D Systems, Minneapolis, MD). Live cell number was quantified using the MultiTox-Fluor Multiplex Cytotoxicity Assay (Promega, Madison, WI). For wells containing Luc mRNA-LNPs, the live cell number was first quantified using the MultiTox-Fluor Multiplex Cytotoxicity Assay. Then, luminescence was measured using the Bright-Glo Luciferase Assay System (Promega). All assays were performed according to manufacturer guidelines, and luminescence/fluorescence was measured using a Tecan infinite M200 Pro microplate reader.

***In vivo* Experiments.** All animal studies were approved by the M.I.T. Institutional Animal Care and Use Committee and were consistent with local, state, and federal regulations as applicable. LNPs were administered to female C57BL/6 mice (Charles River Laboratories, 16 – 20 g) intravenously via the tail vein. For flow cytometry experiments, blood was collected via the tail vein into an EDTA-lined Microvette tube (Sarstedt, Nümbrecht, Germany). For experiments requiring serum, blood was collected via the tail vein into a serum separator tube and serum was isolated by centrifugation. Serum EPO concentration was measured using an ELISA assay as described above. Serum cytokine concentration was measured using the Bio-Plex Pro Mouse Cytokine kits (23-Plex Immunoassay and 9-Plex Assay, Bio-Rad, Hercules, CA) according to the manufacturer's instructions and read with a BioPlex-200 (Bio-Rad) plate reader. Serum liver enzyme concentrations were measured with a Beckman Olympus AU400 Serum Chemistry Analyzer by Charles River Laboratories (Wilmington, MA).

To determine luciferase levels, mice were administered an intraperitoneal injection of D-luciferin (130 μL, 30 mg/mL in PBS). After 15 min, the mice were sacrificed, organs were collected, and

organ luminescence was measured using an IVIS imaging system (PerkinElmer, Waltham, MA) and quantified using LivingImage software (PerkinElmer).

Flow Cytometry. To prepare blood single cell suspensions, 100 µL of blood was mixed with 1 mL of RBC Lysis buffer and incubated on ice for 10 min. To prepare spleen single cell suspensions, spleens were harvested from mice following euthanasia, manually ground up with forceps in PBS, and passed through a 70 µm filter. Following centrifugation and removal of supernatant, cells were re-suspended in 1 mL of RBC Lysis buffer and incubated for 10 min. Once single cell suspensions had been made, cells were fixed with 2% paraformaldehyde in flow buffer (PBS containing 0.5% BSA and 2 mM EDTA) for 15 min at 4°C.

Fixed cells were stained with up to eight of the following anti-mouse antibodies at a 1:300 dilution in flow buffer unless otherwise stated: TCR-β (clone H57-597), CD19 (clone 6D5), CD11b (clone M1/70), Ly-6G (clone 1A8), CD45 (clone 30-F11), CD69 (clone H1.2F3), CD14 (clone Sa14-2), MHC-II (I-A/I-E clone M5/114.15.2), CD80 (clone 16-10A1, 1:100 dilution), CD86 (clone GL-1, 1:100 dilution), F4/80 (clone BM8), CD11c (clone N418). All antibodies were purchased from Biolegend (San Diego, CA). Data was collected using a BD LSR II cytometer (BD Biosciences).

The following identifications of cell populations were used: 1) T cells: $CD45^+$, $CD11b^-$, $TCR\text{-}\beta^+$, 2) B cells: $CD45^+$, $CD11b^-$, $CD19^+$, 3) Neutrophils: $CD45^+$, $CD11b^+$, $Ly\text{-}6G^+$, 4) Non-neutrophil myeloid: $CD45^+$, $CD11b^+$, $Ly\text{-}6G^-$, 5) Macrophages: $CD45^+$, $CD11b^+$, $F4/80^+$, 6) Dendritic cells: $CD45^+$, $CD11b^+$, $CD11c^+$. Gating strategy is shown in **Fig. A.3-8.**

Statistics. When comparing two groups, a Student's *t* test was used assuming a Gaussian distribution with unequal variances. When performing multiple *t* tests for two groups (e.g. dose response and cytokines), multiple comparisons were corrected for using the Holm-Šidák method. For mouse studies, data presented is representative of one independent experiment.

Statistical significance was defined with an alpha level of 0.05. All statistical analyses were performed using GraphPad Prism 6 software.

3.8 Acknowledgements

This work was supported by Shire Pharmaceuticals (Lexington, MA). We wish to thank the Nanotechnology Materials Core Facility, Animal Imaging and Preclinical Testing Core, Flow Cytometry Core, and KI Genomics Core at the Koch Institute at MIT.

Chapter 4

Formulations for Non-Liver mRNA Delivery *in vivo*

Portions of the work presented in this chapter were or will be published as:

Fenton, O.S., Kauffman, K.J., Kaczmarek, J.C., McClellan, R.M., Jhunjhunwala, S., Tibbitt, M.W., Zeng, M.D., Appel, E.A., Dorkin, J.R., Mir, F.F., Yang, J.H., Oberli, M.A., Heartlein, M.W., DeRosa, F., Langer, R., Anderson, D.G. "Messenger RNA Lipid Nanoparticles Induce Protein Expression Within B Lymphocytes In Vivo." *In submission.*

Kaczmarek, J.C., Patel, A.K., Kauffman, K.J., Fenton, O.S., Webber, M.J., Heartlein, M.W., DeRosa, F., Anderson, D.G. "Polymer-Lipid Nanoparticles for Systemic Delivery of mRNA to the Lungs." *Angew. Chem.*, **128**, 14012-14016, 2016.

4.1 Introduction

Many materials have been developed for the delivery of mRNA and other nucleic acids to the liver following systemic administration. In **Chapters 2** and **3** of this Thesis, we primarily described the use of two lipids, C12-200 and OF-02, to mediate delivery of mRNA to the liver,[140,149] but many thousands of other lipids have been synthesized through both combinatorial[18,80,85] and rational design[19,83,84] approaches to deliver RNAs to the liver. Liver physiology greatly enhances its ability to be targeted by circulating therapeutics in the bloodstream like LNPs, as the liver is well-perfused via the hepatic portal vein. LNPs, which are typically less than 100 nm in diameter, can readily extravasate from the bloodstream into surrounding liver tissue through small holes (fenestrae) in sinusoidal endothelial cells.[90,168] Certain LNP chemistries also promote the binding of serum proteins (e.g. Apolipoprotein E) to the LNP surface which in turn leads to receptor-mediated endocytosis by hepatocytes.[77,80] Hepatocytes can also be actively targeted by incorporating specific ligands onto the LNP surface which bind to the receptors found exclusively on hepatocytes.[77,169] Fortunately, the liver presents an attractive therapeutic target for genetic therapies: liver disorders can disrupt glycogen storage, hormone secretion, and serum lipid concentrations, making the liver important for treating diabetes, clotting disorders, and heart disease.[170] Furthermore, the liver is ideal for many mRNA-based therapies because protein synthesis is a major function of hepatocytes.[171]

However, many nucleic acid based therapies will not require delivery to the liver and instead necessitate delivery to other tissues. Some specific examples of mRNA therapies requiring non-liver transfection include 1) heart delivery of mRNA encoding for paracrine factors to repair damage following myocardial infarction;[130] 2) lung delivery of mRNA encoding for correct copies of CFTR to treat cystic fibrosis[172] or mRNA encoding for gene-editing nucleases to treat surfactant protein B (SP-B) deficiency;[100] 3) tumor delivery of mRNA encoding for anti-

angiogenic proteins to treat localized cancers, such as pancreatic cancer;[173] 4) lymphatic (i.e. spleen, lymph nodes, thymus, and/or bone marrow) delivery of mRNA encoding for antigens to be applied in immunotherapies, infectious disease vaccines, and allergy tolerization.[22,174,175] There is a need to develop mRNA delivery materials capable of transfecting a diverse array of non-liver organs in order to realize many potential therapies.

A recent publication reported that both the surface charge and size of the LNP appear to play a factor in the relative delivery of mRNA-LNPs to the liver, spleen, and lung.[175] However, a complete understanding of how the chemical structure of ionizable lipids influences LNP biodistribution following systemic delivery *in vivo* is generally not well-understood in the literature and is likely to be an extraordinarily complex function of many variables. As such, it is difficult to "design" a material *a priori* to passively target a particular organ following systemic administration. In a subsequent Chapter (**Chapter 5**), we will report a novel method that allows the high-throughput, simultaneous screening of many materials in a single mouse to determine biodistribution. However in this current Chapter (**Chapter 4**), we discovered materials capable of selectively delivering mRNA to the spleen and lung following systemic administration through low-throughput, more traditional trial-and-error screening of new lipids and polymers. Furthermore, we describe the local administration of mRNA-LNPs in the muscle, fat, and subcutaneous space, which avoids much of the unpredictable targeting from intravenous injections.

4.2 Fatty Acid Derived Ionizable Lipids for Splenic Delivery

In **Chapter 2**, we described the ionizable lipid OF-02 which, when formulated into mRNA-LNPs, led to high levels of protein expression in the liver with minimal expression in the spleen. As reported by the Thesis of Owen Fenton,[176] a new library of ionizable lipids was

generated and codenamed OF-71 through OF-77. **(Fig. 4-1a)** These ionizable lipids had the same core of OF-02, but the hydrophobic tails were derived from fatty acids and contained hydrolysable ester bonds, which have been associated with lower toxicity in ionizable lipids compared to non-degradable tails. Early experiments revealed that these ionizable lipids generally formed stable LNPs when formulated with siRNA against Factor VII (FVII, a hepatocyte-specific protein) but had poor potency *in vivo* at doses as high as 0.1 mg/kg. However, when formulated into LNPs with Luc mRNA and administered to mice intravenously, many ionizable lipids in this library surprisingly showed luciferase expression in the spleen with lower expression in the liver **(Fig. 4-1b)**, thus explaining their poor ability to knockdown a liver-associated protein. Whereas the liver accounted for about 99% of the total luminescence from OF-02 mRNA-LNPs, about 85% of total luminescence from OF-77 mRNA-LNPs was in the spleen. It is not yet known why the presence of these fatty acid derived hydrophobic tails result in significantly increased spleen specificity, and a general understanding of structure/function for ionizable lipids is not yet well understood in the literature.

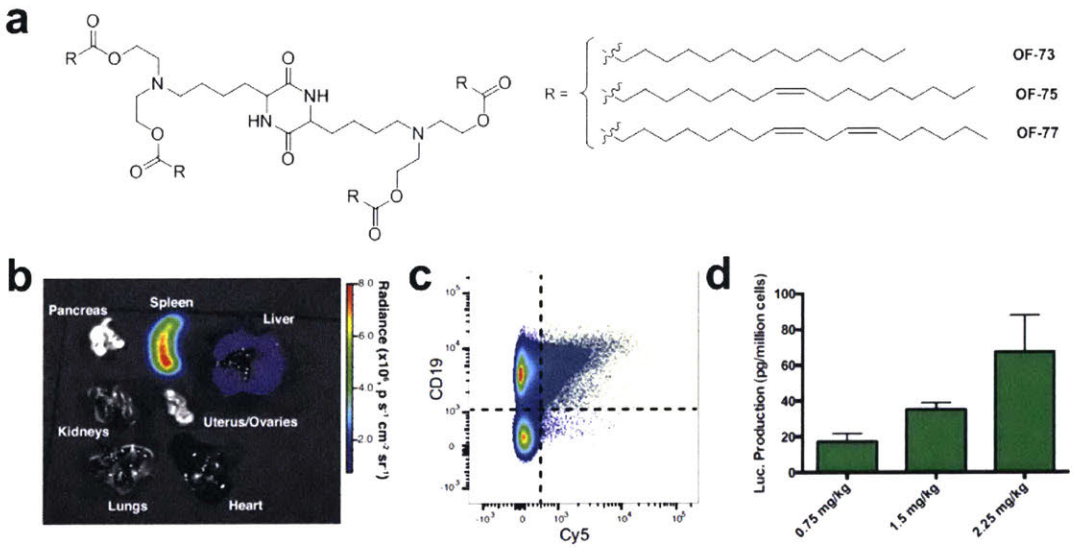

Figure 4-1. mRNA-LNPs for splenic targeting. (**a**) Chemical structure of ionizable lipid library OF-71 through OF-77 containing fatty acid derived tails with 3 representative tails shown (7 total in library). (**b**) Luminescence biodistribution 24 hr post-i.v. administration of OF-77 LNPs with Luc mRNA at a dose of 0.75 mg/kg. (**c**) Flow cytometry of CD45+ spleen cells isolated from mice treated with OF-77 LNPs containing Cy5-labelled mRNA, showing CD19 (B cell marker) vs. Cy5 (mRNA marker). (**d**) Luciferase protein in isolated B cells following i.v. administration of OF-77 LNPs with Luc mRNA at multiple doses.

The ability of OF-77 mRNA-LNPs to transfect the spleen led us to question what cell type was transfected. First, we formulated OF-77 with fluorescently-labelled mRNA, administered i.v. to mice, and isolated their spleens. We performed flow cytometry on splenic cells, discovering mRNA to be associated with a variety of splenic immune cells including lymphocytes, myeloid cells, and neutrophils; of note, approximately 8% of spleen B cells were labelled with our delivered mRNA (**Fig. 4-1c**). Next, to confirm actual translation of the delivered mRNA into functional protein in B cells, we formulated OF-77 with Luc mRNA and repeated the experiment at various doses. Here, we used immunomagnetic negative selection to isolate B cells and measured the luminescence of the B cells. Luciferase expression was observed in B cells in a linear dose response fashion **(Fig. 4-1d)**, reaching luciferase concentrations of 70 pg per million B cells at the 2.25 mg/kg OF-77 dose. Since B cells are key players in the adaptive immune response and diseases such as lymphomas, the ability of OF-77 mRNA-LNPs to transfect B cells has many important clinical applications.[26,177]

4.3 Polymer-Lipid Materials for Lung Delivery

Previous publications have described the use of a class of polymers called poly(β-amino esters) (PBAEs) for the delivery of DNA *in vitro* and *in vivo*.[102–105] PBAEs were first synthesized via the Michael addition of diacrylate monomers with amine monomers, and subsequent generations of PBAEs have added end-capping amines and hydrophobic alkyl amines to the polymer chain, each of which improved DNA delivery **(Fig. 4-2a)**. However, the poor serum stability of PBAE/DNA complexes limited their systemic *in vivo* application,[105] and the ability of PBAEs to deliver mRNA *in vivo* had not yet been explored.

As reported by Kaczmarek et al.,[178] a small library of PBAE polymers with varying monomers was synthesized, complexed with Luc mRNA, and applied to HeLa cells *in vitro*. The

addition of 7 mol% PEG-lipid to the formulation was found to significantly increase both *in vitro* potency and serum stability for most PBAEs tested. PEGylated DD90-C12-122 PBAE/mRNA nanoparticles were then administered intravenously to mice, resulting in protein expression nearly exclusively in the lung **(Fig. 4-2b)**. The selective delivery of mRNA and other nucleic acids to the lung has applications in various diseases including pulmonary hypertension, cystic fibrosis, and cancer.[172,179,180] Ongoing and future experiments indicate that PEGylated PBAE/mRNA nanoparticles delivered via nebulization are capable of transfecting the lung. Additionally, new classes of PBAE polymer chemistries are being explored in the context of mRNA delivery to the lung, including PBAEs which have a branched rather than linear structure.

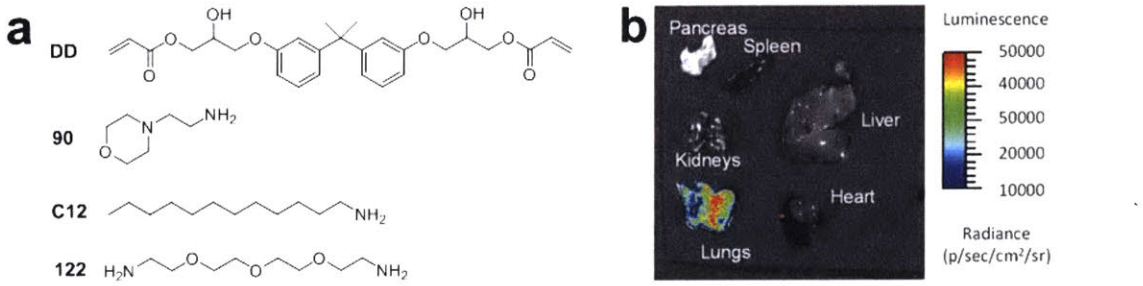

Figure 4-2. Polymer-lipid materials for delivery of mRNA to the lung. (**a**) Chemical structure of the components of the PBAE DD90-C12-122 which form a polymer through Michael addition reactions. In this representative PBAE, DD is the core diacrylate, 90 is the core amine, C12 is the hydrophobic amine, and 122 is the end-capping amine. (**b**) Luminescence biodistribution 24 hr post i.v. administration of Luc mRNA DD90-C12-122 NPs dosed at 0.5 mg/kg.

4.4 Locally-Administered Lipid Nanoparticles for Fat Delivery

Although intravenous administration of drugs allows for systemic delivery to many organs, it is not the most ideal administration route for certain applications, particularly those which require long-term dosing or the high throughput treatment of many people. For example, mRNA therapeutics hold great potential for easily adaptable prophylactic vaccines.[26,181] Unlike traditional vaccines which require months of development, mRNA vaccines could be conceived

and produced on a mass scale in a matter of days or weeks.[182] In one scenario, mRNA could encode for an antigen and lead to an adaptive immune response, generating antibody against the desired antigen after a certain time. In another scenario, mRNA could encode for antibody itself to result in a much faster but transient immunity against the antigen. A large-scale vaccination effort would likely require a more tolerable administration route than intravenous delivery. Examples of better clinically translatable administration routes include intraadipose, intramuscular and subcutaneous injections, which can be more easily and rapidly administered than intravenous infusions. However, we have not yet identified the efficacy of mRNA-LNPs *in vivo* using these non-intravenous injection methods. In the following sections, we will describe our initial studies into mRNA-LNP efficacy using these administration routes.

4.4.1 Intramuscular/Intraadipose Administration

As reporter mRNAs to measure efficacy, we used both luciferase (Luc) mRNA and Erythropoietin (EPO) mRNA to model the expression of non-secreted and secreted proteins respectively. We could not achieve detectable luciferase expression with Luc mRNA-LNPs after an intramuscular injection at 5 μg mRNA into the mouse quadriceps. It is possible that luciferase expression occurred deeper in the muscle and was not visible from the surface, but nonetheless, this experiment suggests that LNPs do not as readily transfect muscle cells. Interestingly, we have found that other delivery materials developed in our lab such as PBAEs[105] and ionizable dendrimers[151,182,183] are capable of transfecting muscle with mRNA; these other materials share a common trait in that they have a higher degree of cationic charge density than the lipids per unit mass, meaning a strong positive charge may be required to transfect muscle cells.

Early attempts at intraadipose injections with EPO mRNA-LNPs resulted in highly variable serum EPO expression in both the subcutaneous and visceral fat, approximately 100 ±

100 ng/mL and 400 ± 400 ng/mL respectively. The initial hypothesis was that due to the small size of these fatty areas in C57BL/6 mice, we were sometimes unintentionally performing intraperitoneal injections resulting in trafficking to and efficient expression in hepatocytes. To ensure that mRNA was only translated in adipose cells, we next injected the mammary fat pad of older female mice with Luc mRNA-LNPs. We observed that Luc expression occurred only in the mammary fat pad **(Fig. 4-3a)**, indicating that the mRNA-LNPs remained in the fat pad, could be expressed by adipose cells, and were not trafficked to other tissues. However, mammary fat pad injections were not ideal because 1) the mammary fat pad is fairly small in younger mice typically used for experiments and thus difficult to consistently inject, and 2) only small volumes (< 50 µL) can be administered. Therefore, we next investigated subcutaneous injections as much larger volumes can be tolerated in mice if required by the dose and the injection itself is much easier to consistently perform.

4.4.2 Subcutaneous Administration

We assessed the feasibility of subcutaneous administration of Luc mRNA-LNPs in nude immunocompetent mice in two different injection locations, the back and the flank. Durable luciferase expression is observed at the site of the injection for at least a week (**Fig. 4-3b)** at luminescence levels comparable to those obtained in the liver post-intravenous injection at equivalent doses. Furthermore, no difference in luciferase expression was observed between the two tested subcutaneous injection sites. Interestingly, a one-compartment pharmacokinetic model can be well-fit to the data,[184] from which a luciferase half-life of approximately 20 hr can be calculated. Next, a specialized Ai14/Cre mRNA mouse model (which is thoroughly described in **Chapter 6** of this Thesis) with two-photon excitation microscopy was used to confirm that fat cells near the injection site were indeed expressing the delivered mRNA (**Fig. 4-3c**).

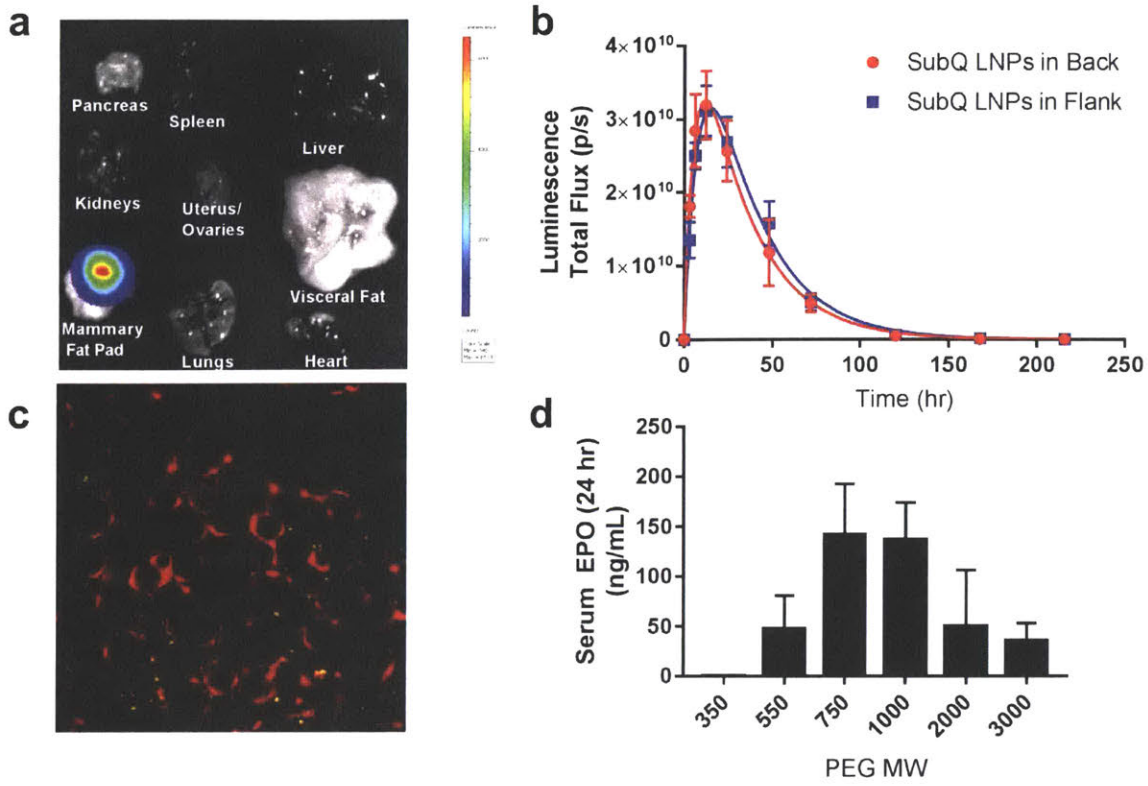

Figure 4-3. Intraadipose and subcutaneous administration of mRNA-LNPs. (**a**) Luminescence biodistribution 24 hr post administration of Luc mRNA-LNPs injected directly into the mammary fat pad of female C57BL/6 mice. (**b**) Luminescence timecourse after administration of Luc mRNA-LNPs injected subcutaneously into nude immunocompetent mice; curve fit is a one-compartment pharmacokinetic model. (**c**) Two photon excitation microscopy of skin/fat near injection site of subcutaneously administered mRNA-LNPs using the Ai14/Cre mRNA model described in Chapter 6; tdTomato expression (red) indicates where mRNA translation has occurred. (**d**) Serum EPO concentration 24 hr post-subcutaneous administration of 5 μg EPO mRNA-LNPs with varying PEG-lipid MW.

Although tissue luciferase expression was similar between Luc mRNA-LNPs delivered subcutaneously and intravenously, EPO mRNA-LNPs delivered subcutaneously suffered from orders-of-magnitude lower serum expression compared to those delivered intravenously. We first attempted to optimize the delivery vehicle for the subcutaneous space by varying the PEG molecular weight on the PEG-lipid component of the LNP; PEGylation influences nanoparticle diffusion,[185,186] so we hypothesized that lower MW PEGs would lead to less particle diffusion out of the subcutaneous space, thus becoming more concentrated at the site of injection and transfecting more adipose cells. The PEG MW on the PEG-lipid does influence serum EPO

levels **(Fig. 4-3d)** as predicted with higher serum EPO concentration with decreasing PEG MW until a PEG MW of 750; it should be noted that LNPs formed with PEG-lipids with PEG MW less than 750 were turbid, indicating poor particle formation. However, the approximate 2-fold improvement in using PEG 750 and PEG 1000 did not account for the orders-of-magnitude lower EPO serum levels, so we hypothesize that poor secretion of the translated EPO protein from fat cells (as opposed to hepatocytes) was the problem.

Future work will aim to address these secretion issues through optimization of the mRNA itself, particularly for antibody-encoding mRNAs with vaccine applications. One idea is to incorporate different signaling peptides into the mRNA (e.g. gLuc, EPO, IL2, adiponectin) which may lead to better secretion from cells which do not endogenously secrete antibody. It is also hypothesized that separate delivery of the antibody light and heavy chains may lead to greater antibody expression than a single mRNA encoding for the entire antibody.

4.5 Conclusions

We have demonstrated transfection of non-liver tissues with mRNA using new delivery materials and administration routes. A new class of ionizable lipids featuring fatty acid derived tails was found to selectively transfect the spleen with mRNA following systemic administration and also transfected splenic B cells in a dose-dependent fashion. PEGylated polymer-lipid nanoparticles selectively delivered mRNA to the lung following systemic administration. In addition, previously-described mRNA-LNPs are capable of adipose cell transfection following subcutaneous administration, although work is needed to optimize this system and make its results more consistent.

4.6 Materials and Methods

OF-77 mRNA-LNP Formulation. The detailed synthesis of OF-77 and related ionizable lipids are described in the Thesis of Owen Fenton.[176] An organic phase consisting of a mixture of OF-77, 1,2-dioleoyl-*sn*-glycero-3-phosphoethanolamine (DOPE, Avanti Polar Lipids, Alabaster, AL), cholesterol (Sigma), and 1,2-dimyristoyl-*sn*-glycero-3-phosphoethanolamine-N-[methoxy-(polyethyleneglycol)-2000] (ammonium salt) (C14 PEG 2000, Avanti) at a molar ratio of 35:16:46.5:2.5 and an OF-77:mRNA weight ratio of 10:1 was prepared in ethanol. An aqueous phase consisting of Luc mRNA (Shire Pharmaceuticals) or Cy5-labelled Luc mRNA (TriLink Biotechnologies) was prepared in 10 mM citrate buffer. The ethanol and aqueous phases were mixed at a 1:3 volume ratio in a microfluidic chip device using syringe pumps as previously described.[87] Resultant LNPs were dialyzed against PBS in a 20,000 MWCO cassette at 4°C for 2 hr.

PEGylated DD90-C12-122 mRNA Nanoparticle Formulation. The detailed synthesis of DD90-C12-122 is described in Kaczmarek et al.[178] An organic phase consisting of a mixture of DD90-C12-122 and C14 PEG 2000 at a molar ratio of 93:7 and a DD90-C12-122/mRNA N/P ratio of 57 was prepared in ethanol. An aqueous phase consisting of Luc mRNA (Shire Pharmaceuticals) was prepared in sodium acetate buffer, pH 5.2. The ethanol and aqueous phases were mixed at a 1:3 volume and subsequently dialyzed as described above.

mRNA-LNP Formulations for Intraadipose, Intramuscular, and Subcutaneous Administration. mRNA-LNPs were prepared identically to the formulation for OF-77 as described above, except the ionizable lipid cKK-E12 as reported by Dong et al.[80] (prepared by Shire Pharmaceuticals) was used in place of OF-77.

Nanoparticle Characterization. mRNA concentration in mRNA-LNPs was determined using a modified Quant-iT Ribogreen RNA assay (Thermo Fisher) as previously described.[16] mRNA

concentration in PEGylated DD90-C12-122 mRNA nanoparticles was determined similarly but required heparin to fully disassemble the nanoparticle as described in Kaczmarek et al.[178] The diameter and polydispersity (PDI) of the LNPs were measured using dynamic light scattering (ZetaPALS, Brookhaven Instruments). Diameter is reported as the largest intensity mean peak average.

***In vivo* Experiments.** All animal studies were approved by the M.I.T. Institutional Animal Care and Use Committee and were consistent with local, state, and federal regulations as applicable. mRNA nanoparticles were administered to female C57BL/6 mice (Charles River Laboratories, 16 – 20 g) via tail vein intravenous injection, intramuscular injection into the quadriceps, intraadipose injection into the mammary fat pad, or subcutaneous injection into the back or flank. For timecourse luciferase experiments, mRNA-LNPs were administered subcutaneously to female SKH1-Elite mice (Charles River Laboratories, 16 – 20 g), an immunocompetent, hairless strain of mice. Unless otherwise noted, cKK-E12 and OF-77 mRNA LNPs were administered at 0.75 mg/kg.

To determine luciferase levels, mice were administered an intraperitoneal injection of D-luciferin (130 µL, 30 mg/mL in PBS). For terminal experiments, after 15 min, the mice were sacrificed, organs were collected, and organ luminescence was measured using an IVIS imaging system (PerkinElmer, Waltham, MA) and quantified using LivingImage software (PerkinElmer). For timecourse experiments, mice were anesthetized with 2.5% isoflurane and imaged 15 min after D-luciferin injection.

For EPO measurement, blood was collected via the tail vein into a serum separator tube and serum was isolated by centrifugation. Serum EPO concentration was measured using an ELISA assay (Human Erythropoietin Quantikine IVD ELISA Kit, R&D Systems, Minneapolis, MD).

Flow Cytometry/B cell Isolation. Single cell suspensions of mouse spleens were generated and flow cytometry was performed as previously described in **Chapter 3.** B cells from mice injected with Luc mRNA OF-77 LNPs were isolated from the spleen using the EasySep Mouse B Cell Isolation kit (Stemcell Technologies, Seattle, WA). The cell purity was verified by flow cytometry to be >98% B cells. Isolated B cells were then plated in a 96-well plate at 2 million cells / well, and the luciferase expression was quantified using a Bright-Glo Luciferase Assay (Promega, Madison, WI). Luminescence was measured with a Tecan infinite M200 Pro microplate reader. A standard curve of luciferase protein was used to convert luminescence to luciferase concentration.

Ai14/Cre mRNA Mouse Model for Subcutaneous Administration. cKK-E12 mRNA-LNPs formulated with Cre mRNA were administered subcutaneously to Ai14 mice at a 5 μg mRNA dose. After 48 hr, the mice were euthanized, the hair surrounding the injection site was removed and the skin/fat was excised. Two-photon excitation microscopy was then performed on the skin/fat. Full details regarding the Ai14/Cre mRNA mouse model and two-photon excitation microscopy procedures can be found in **Chapter 6**.

4.7 Acknowledgments

This work was supported by Shire Pharmaceuticals (Lexington, MA), MassBiologics (Boston, MA), and the Marble Center for Cancer Nanomedicine and the Cancer Center Support (core) Grant P30-CA14051.

Chapter 5

Barcoded Nanoparticles for High Throughput *in vivo* Biodistribution Analysis

The work presented in this chapter was published as:

Dahlman, J.E.*; Kauffman, K.J.*; Xing, Y.*; Shaw, T.E.; Mir, F.F.; Dlott, C.C.; Langer, R.; Anderson, D.G.; Wang, E.T. "Barcoded Nanoparticles for High Throughput in vivo Discovery of Targeted Therapeutics." *Proc. Natl. Acad. Sci. U.S.A.,* **114**, 2060-2065, 2017.

5.1 Introduction

The clinical and scientific potential of nucleic acid therapies is limited by inefficient drug delivery to target cells. Drug delivery vehicles must avoid clearance by the immune and reticuloendothelial systems, access the correct organ, and enter specific cells within a complex tissue microenvironment.[9,187,188] At each of these steps, anatomical structures and biological molecules can actively engage the vehicles and influence their final destination. For example, fenestrations in endothelial cells lining the liver may improve access to hepatocytes, tight junctions in brain endothelial cells inhibit delivery across the blood brain barrier, the basement membrane in renal tubules can disassemble cationic delivery vehicles, and serum proteins can bind nanoparticles in the blood and affect their interactions with target cells.[77,189–191] It is not currently possible to recapitulate the totality of this complex process in cell culture.

Thousands of nanoparticles with distinct chemical structures and properties have been synthesized to overcome drug delivery obstacles and control nanoparticle biodistribution.[18,19,80,85,151,192–194] Due to the expensive and laborious nature of *in vivo* experiments, the current practice is to characterize these diverse nanoparticle "libraries" in cell culture, before selecting a small number to test *in vivo*.[18,19,80,85,151,192–194] However, *in vitro* transfection can be a poor predictor of *in vivo* transfection, and *in vitro* screens cannot predict whole body biodistribution, which influences off-target effects.[129,195]

We sought to develop a system which increases the number of nanoparticles testable *in vivo*. To increase the throughput of *in vivo* studies, we used a rapid microfluidic mixing system to encapsulate nucleic acid barcodes inside nanoparticles, and administered them as a single pool to mice (**Fig. 5-1a,b**). We recovered the barcodes from tissues and cells, and used deep sequencing to obtain counts for those barcodes in each sample of interest.[196] Deep sequencing is a high throughput, cost-effective method to precisely quantitate nucleic acid species; it has led to the identification of molecules or peptides with specific biological activities, and enabled

pooled screening with shRNAs, cDNAs, and labeled pools of RNA.[197–199] By associating specific nanoparticles with unique DNA barcode sequences, we can now reliably measure the biodistribution of many nanoparticles in a single animal (**Fig. 5-1c**).

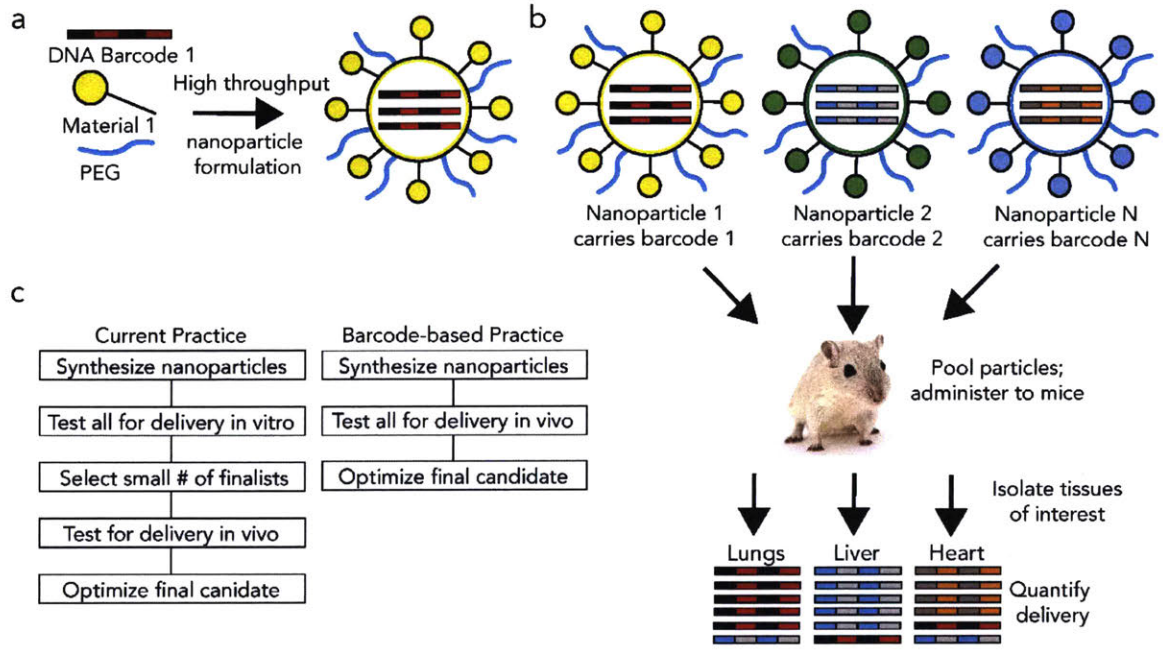

Figure 5-1. DNA barcoded nanoparticles for high throughput in vivo nanoparticle delivery. **(a)** Using high throughput fluidic mixing, nanoparticles are formulated to carry a DNA barcode. **(b)** Many nanoparticles can be formulated in a single day; each nanoparticle chemical structure carries a distinct barcode. Particles are then combined and administered simultaneously to mice. Tissues are then isolated, and delivery is quantified by sequencing the barcodes. In this example, Nanoparticle 1 delivers to the lungs, Nanoparticle 2 delivers to the liver, and Nanoparticle N delivers to the heart. **(c)** This enables multiplexed nanoparticle-targeting studies in vivo, improving upon the current practice, which relies on *in vitro* nanoparticle screening to identify lead candidates.

5.2 Validation of Barcoding System *in vivo*

We formulated chemically distinct lipid nanoparticles (LNPs) so they each carried a unique DNA barcode oligonucleotide (**Fig. 5-1a**). We pooled the different nanoparticle formulations together, and injected the pool intravenously into mice (**Fig. 5-1b**). At different time points, we isolated tissues or cells and recovered the oligonucleotides. We used polymerase chain reaction (PCR) with indexed primers to amplify the oligonucleotides and label each tissue/animal (**Table B.5-1**), and performed deep sequencing. By counting the nanoparticle-

associated barcode sequences obtained from each tissue, we measured the relative biodistribution of many nanoparticles simultaneously (**Fig. 5-1c**).

We first tested this approach using nanoparticles with known abilities to target nucleic acids to lung and liver (**Fig. 5-2a**).[85,151,200–202] For these experiments, we analyzed barcode distribution four hours after injection, a length of time sufficient for these LNPs to be cleared by the bloodstream.[151] We formulated four different nanoparticles with four different DNA barcodes. One barcode was formulated with LNPs made with the lipid C12-200; these "liver-targeting" LNPs deliver nucleic acids to hepatocytes at doses of nucleic acid as low as 0.01 mg/kg.[85] Three other barcodes were formulated with LNPs made with the lipid 7C1; these "lung-targeting" LNPs deliver nucleic acids to pulmonary endothelial cells at doses as low as 0.01 mg/kg.[151] As expected, barcodes delivered by 7C1 particles were enriched ~4.5 to 10-fold in the lung relative to liver, as compared to barcodes delivered by C12-200; these results were consistent across all four mice (**Fig. 5-2b**). Formulation details for all nanoparticles analyzed are listed in **Table B.5-2.**

Interpretation of results following injection of pooled nanoparticles requires that there is minimal re-assortment of nanoparticles following formulation. To assess whether particle mixing occurred, we repeated the previous experiment, but allowed the particles to mix for 24 hours prior to injection. We observed the same delivery efficiencies (**Fig. 5-2c**), suggesting that for these particles and this time scale, appreciable mixing or 'hybrid' nanoparticle formation does not occur, and that nanoparticle barcode content is not differentially lost into the buffer over time.

Encouraged by these results, we assessed the sensitivity of our assay. We formulated seven identical C12-200 LNPs, so that each formulation carried a distinct barcode. We then mixed the formulations together so that the abundance of each barcode-containing particle varied, spanning a range of 0.0001 mg/kg to 0.5 mg/kg, forming an "*in vivo* standard curve." Barcode counts in both lung and liver correlated linearly to the dose of injected LNP four hours

after injection **(Fig. 5-2d, Fig. A.5-1a)**. These data demonstrate that DNA barcodes delivered by LNPs can be accurately measured at doses as low as 0.0001 mg/kg DNA barcode for each particle. Notably, sequencing at greater depth may allow for lower doses to be measured.

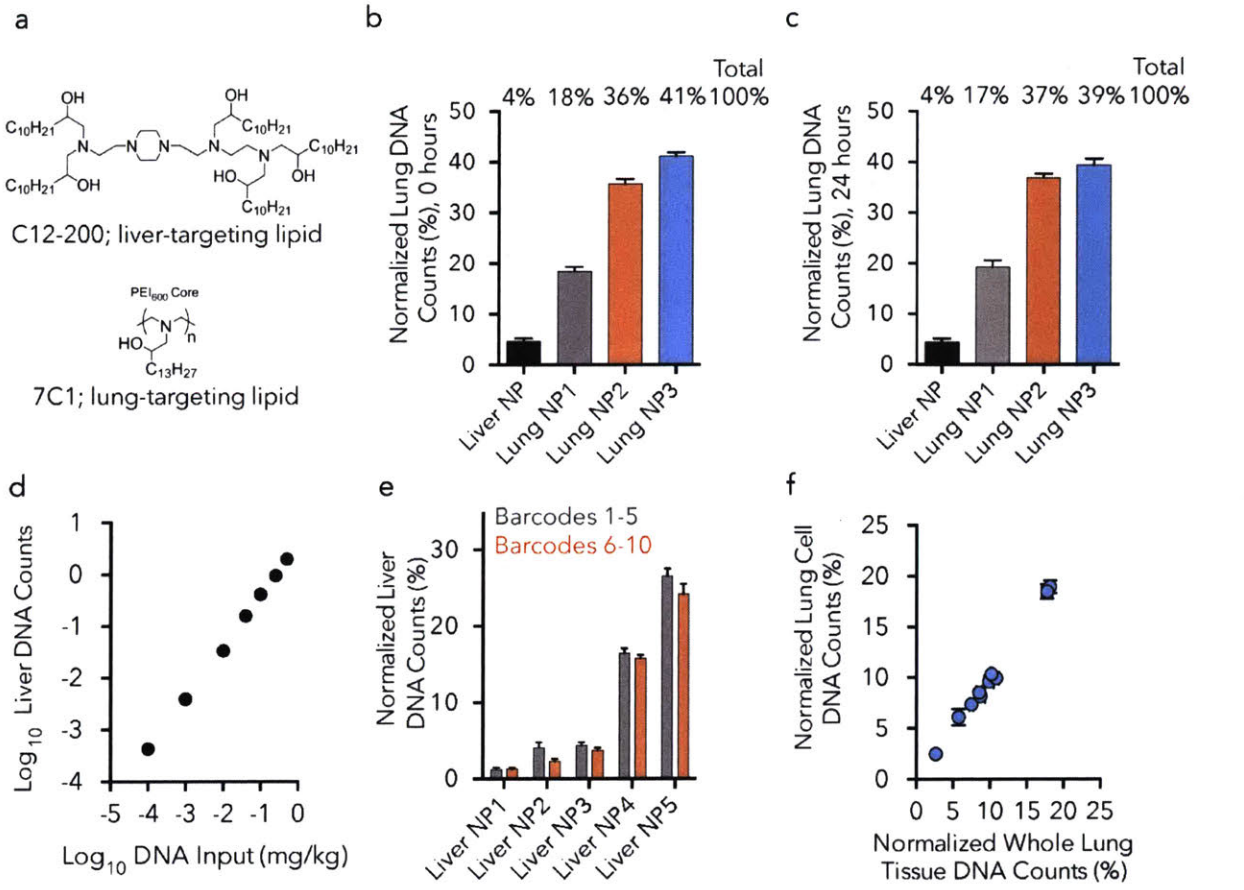

Figure 5-2. Validation of barcoded nanoparticle methodology. (a) NP biodistribution using 7C1 and C12-200, two well validated NPs with known activity in the lung and liver, respectively. **(b)** Normalized DNA barcode counts in the lung 4 hours after the administration of the liver-targeting C12-200, or three different formulations of the lung-targeting 7C1. Normalization technique used for all 'normalized' figures is described in the methods. N=4 mice / group. **(c)** Normalized DNA barcode counts in the lungs 4 hours after administration of the same 4 nanoparticle slution in (b). In this case, the particles were administered the next day, after being allowed to mix for 24 hours. No change in targeting is observed between the 'freshly injected' and '24 hour mixed' particles. N = 4 mice / group. **(d)** DNA barcode counts in the liver 4 hours after administration of an 'in vivo standard curve'. The same C12-200 nanoparticle formulation was made 7 separate times, with 7 different barcodes. These solutions were mixed together at different doses (DNA inputs) to form an 'in vivo standard curve'. DNA readouts align with this DNA input at doses between 0.0001 and 0.5 mg/kg DNA barcode. N = 5 mice / group. **(e)** Normalized DNA barcode counts in liver 4 hours after administration of different DNA sequences. 5 different C12-200 NPs were formulated twice, each with a different barcode. Delivery for each of the 5 NPs did not change with barcode sequence. N = 5 mice / group. **(f)** DNA barcode counts in the lung 4 hours after 10 different 7C1 NPs were injected. Sequencing was performed on either whole lung tissue or lung cells isolated isolated from the same lung by flow cytometry. The delivery of all 10 particles was the same for whole tissue and isolated cells. N = 5 mice / group. For all data presented in Figure 5-2, the detailed NP formulation parameters are listed in Supplementary Figure 5-2, and the data are plotted as average + / - S.T.D.

Barcodes were designed so that exonuclease-mediated degradation would not differentially impact the barcodes based on their sequence. We achieved this by including identical flanking nucleotides (21 base-pair adapters) *on* the 5' and 3' end of each barcode (Table B.5-1). To investigate whether using different barcode sequences would change results, we performed a barcode swapping experiment in which we formulated five distinct C12-200-based LNPs with separate barcodes (barcodes 1-5). We then repeated the same five formulations, but used new barcodes (barcodes 6-10). We then administered all ten nanoparticles together. The relative delivery efficiency of each of the five LNPs to lung or liver remained constant independent of the barcode sequence (**Fig. 5-2e**, **Fig. A.5-1b**). This suggests that the short barcode sequence does not change LNP behavior, and does not appreciably influence the relative efficiency of PCR to amplify slightly different barcode sequences.

Nucleic acid therapeutics must reach affected tissues and access relevant cell types in those tissues. We assessed whether our platform could be used to measure delivery to cells, and not only whole tissue. We barcoded ten distinct 7C1-based nanoparticles and assessed their ability to enter the lung; we selected the lung because we previously established a protocol to isolate live lung cells from mouse tissue.[151] Four hours after injection, half of the lung was processed as a whole tissue, and the other half was digested into a single cell suspension.[151] Live cells were selected by flow cytometry, and barcodes were recovered from cells and whole tissue. The relative delivery efficiency for each of these LNPs was similar in whole lung and flow-sorted lung cells **(Fig. 5-2f)**. The ability to recover oligonucleotides from sorted cells suggests that this assay may be used to assess delivery to cell subtypes isolated from tissue.

5.3 Assessing Structure-Function in a Library of Lipid Nanoparticles

A high-throughput *in vivo* assay can enable systematic studies of how nanoparticle chemical properties impact particle biodistribution. Particle activity can vary with many factors,

including: nanoparticle size, shape, charge, the structure or molar ratio of hydrophilic polymers like poly(ethylene glycol) (PEG), and the molar ratio of lipids including cholesterol.[72] This complexity makes it difficult to systematically study the relationship between nanoparticle chemical structure and *in vivo* activity when a small number of nanoparticles are tested. For example, while PEG-lipids are known to increase LNP circulation,[203] the relationship between the PEG-lipid chemical structure and tissue delivery is less well understood.

To assess the feasibility of a systematic study, we generated a library of thirty distinct C12-200 LNPs. Among the thirty LNPs, we varied three PEG structural parameters: the PEG molecular weight (1 kDa, 2 kDa, or 3 kDa), the mole percentage of PEG in the LNP formulation (0.75% to 4.5%), and the length of the hydrophobic lipid attached to the PEG (C_{14}, C_{16}, C_{18}) **(Fig. 5-3a)**. PEG molecular weight and molar ratio both affect particle shielding, while the lipid length can influence how securely PEG 'anchors' into the LNP.[124] We barcoded all thirty particles, pooled them together, and injected them into mice before isolating the brain, heart, kidney, liver, lung, skeletal muscle, uterus, and pancreas four hours later. We observed a broad range in relative delivery efficiency to different tissues (**Fig. 5-3b**), which was reproducible across mouse replicates. Some tissues behaved similarly to other tissues in their ability to be targeted by certain particles. For example, particles that entered lung efficiently tended to enter the liver well, and were distinct from particles that preferentially entered the heart and other organs **(Fig. 5-3b)**.

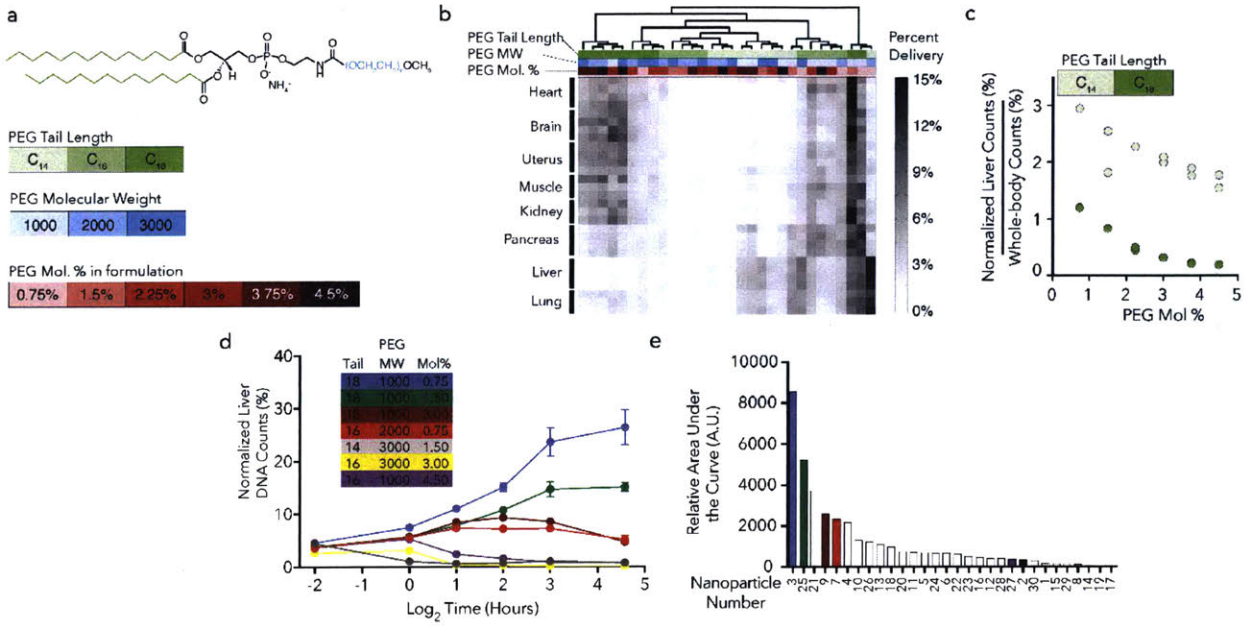

Figure 5-3. Proof of concept of barcoded nanoparticle system in a 30 LNP library. **(a)** Lipid nanoparticles (LNPs) are often formulated with PEG-lipids. The lipid length, PEG MW, and the mole percent of PEG used in the LNP can influence nanoparticle activity. We formulated 30 C12-200 LNPs with different PEGs, varying all three of these parameters. **(b)** Normalized DNA counts, measured four hours after mice were injected with LNPs. Certain tissues 'cluster'; the same tissues tend to be targeted by similar particles. **(c)** Normalized liver counts, divided by the normalized counts for the rest of the tested tissues, as a function of PEG mole percentage. This measure quantifies how delivery to the liver, compared to the rest of the body, changes. Increasing PEG decreased relative delivery to the liver. **(d)** Normalized liver DNA counts for seven nanoparticles 0.25, 1, 2, 4, 8, or 24 hours after injection. The relative distribution of some nanoparticles increased over time, while others decreased. This kinetic analysis was performed with 30 nanoparticles; all data is plotted in Supplementary Figure 5. **(e)** Area under the curve for 30 nanoparticles in the liver. In all cases, data plotted as mean +/- S.T.D., and N = 3 mice / group. In (b), each column is an individual mouse. All formulation details are listed in Supplementary Figure 2.

Because many tissues can be analyzed at once using this method, we studied how nanoparticle delivery to the liver changed relative to the rest of the body. We found that liver delivery efficiency (relative to delivery averaged across all tissues) for each individual LNP increased as C_{14}PEG or C_{18}PEG was reduced (**Fig. 5-3c**). These data, gathered in a single multiplexed study, are consistent with previous studies of liver-targeting LNPs that tested one nanoparticle at a time.[124] The relationship was not observed with C_{16}PEG or nanoparticle diameter (**Fig. A.5-2a,b**). Importantly, these experiments suggest that DNA barcoding can be

used to systematically study how nanoparticle structure influences "whole-body" biodistribution, which could be important in studying on- and off-target effects.

5.4 Pharmacokinetics of Biodistribution

Nanoparticle pharmacokinetics can affect efficacy and off-target effects. To this end, we performed a high throughput pharmacokinetic experiment (**Fig. 5-3d, Fig. A.5-3a**). We chose to measure the relative area under the curve (AUC) because it is an important parameter that approximates how much nucleic acid accumulates in tissue over time. We formulated 30 distinct C12-200 LNPs, and measured biodistribution 0.25, 1, 2, 4, 8, and 24 hours after injection. Interestingly, nanoparticle distribution in the liver varied differentially over time; some nanoparticles became enriched with respect to the pool over time, while others decreased to near-zero values over time (**Fig. 5-3d**). Based on these values, we then calculated AUC for all 30 nanoparticles (**Fig. 5-3e**). We did not observe any simple statistically significant trends between nanoparticle PEG structure and AUC (**Fig. A.5-3b-d**).

5.5 Comparison of Biodistribution and Functionality

Many oligonucleotide therapeutics require intracellular delivery. To assess the ability of our screening approach to uncover particles that functionally deliver nucleic acids, and to eliminate non-functional nanoparticles from consideration, we compared liver biodistribution to functional hepatocyte gene silencing mediated by siRNA (**Fig. 5-4a**). We selected ten of the thirty PEG particles that spanned a broad range of liver delivery as measured by barcode delivery, and formulated them to carry siRNA against Factor VII. Factor VII is an enzyme with a short half-life that is specifically secreted by hepatocytes; its silencing is used to assess functional siRNA delivery to hepatocytes.[18,19,85] We administered each siRNA-carrying nanoparticle individually, and measured Factor VII levels 72 hours later. Particles with low liver delivery were less effective at delivering Factor VII siRNA than particles with higher liver delivery

(Fig. 5-4b). These data suggest that our methodology may be useful as a "first-pass" screen to identify particles for further functional evaluation.

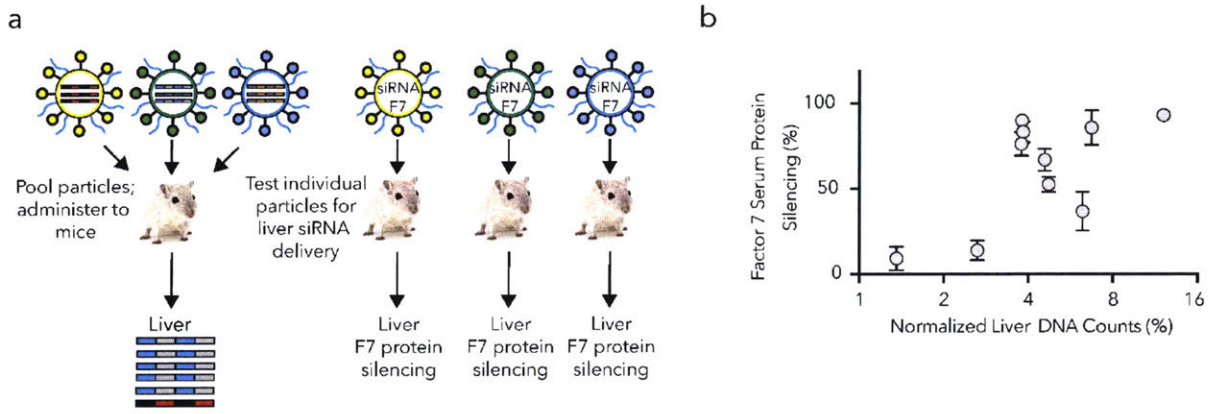

Figure 5-4. Comparing high throughout analysis with individual analysis in vivo. (a) Workflow used to compare high throughput nanoparticle analysis with traditional, individual analysis. 30 nanoparticles with varying PEG characteristics were injected. 10 of the nanoparticles, with a range of liver biodistributions, were analyzed individually by formulating them with siRNA targeting Factor 7, a gene expressed in hepatocytes. Mice were injected with one siRNA containing nanoparticle at a siRNA dose of 0.10 mg/kg, and the resulting Factor 7 protein knockdown was compared to the barcode liver data. **(b)** Factor 7 protein reduction, tested one nanoparticle at a time, plotted against normalized barcode delivery in the liver 15 minutes after intravenous injection, after 30 nanoparticles were tested simultaneously. Data are shown as average + / - S.T.D., and N=3-4 mice /group.

5.6 Discussion and Conclusions

Genetic therapeutics, including aptamers, antisense oligonucleotides, RNAi, and gene editing technologies, function through distinct biological mechanisms.[49,204] However, all genetic therapies are limited by the inability to predict delivery to on- and off-target tissues. Although syntheses of chemically distinct nanoparticles can be high throughput, characterization of nanoparticle behavior *in vivo* is still low throughput.[18,19,80,85,151,192–194] Rapidly screening chemically distinct nanoparticles *in vivo* could accelerate preclinical screening and enable efforts to relate chemical structure to biological function. By incorporating deep sequencing, our approach dramatically increases the number of particles that can be simultaneously measured, as well as improves the sensitivity, specificity, and accuracy of those measurements. Our work,

as well as DNA barcoded particles that were shown to target tumors, demonstrates the power of unbiased *in vivo* approaches.[205] Notably, this platform is distinct from previous reports, which conjugate nucleic acids to the exterior of particles to fluorescently label them, or use them to identify known pathogenic DNA sequences in bodily fluids.[206–209]

We carefully tested our workflow to identify biases that may arise from particle mixing or differences in barcode sequence. DNA barcode readouts varied linearly with the input across 4 orders of magnitude encompassing typical doses of effective nucleic acid therapeutics (0.0001 to 0.5 mg/kg DNA)[72] (**Fig. 5-2d**); the ability to measure a single nanoparticle at a dose as low as 0.0001 mg/kg DNA suggests that dozens, or even hundreds of nanoparticles can be multiplexed in a single experiment. DNA barcode amplification did not vary with barcode sequence (**Fig. 5-2e**). We did not observe any evidence of hybrid particle formation with 7C1 and C12-200 LNPs over 24 hours (**Fig. 5-2b, c**) or when 10 C12-200 based LNPs were tested simultaneously (**Fig. 5-2d**). However, since hybrid particle mixing may occur with other nanoparticles, especially if dozens or hundreds nanoparticles are tested simultaneously, it will be important to control for, and test, particle mixing. Nevertheless, these data demonstrate that the DNA barcoding approach can be used to rapidly study biodistribution and pharmacokinetics. For example, although we did not uncover any structure-function mechanisms or LNPs with new targeting functionality in this study, we did identify a LNP that performed well in many organs, as well as LNPs that distributed inefficiently in all organs (**Fig. 5-3b**).

We designed this system to be useful in many *in vivo* contexts. Because this approach can quantify delivery to cells isolated by flow cytometry (**Fig. 5-2f**), we anticipate that future studies will simultaneously study delivery to multiple cell types in a complex microenvironment. Similarly, we believe this system may be used to study how nanoparticle delivery changes with an animal disease state. Finally, while this system cannot directly differentiate between delivery to, and into, a cell, future work could use this approach to study nanoparticle delivery to

intracellular and subcellular compartments using standard fractionation approaches, with the goal of identifying nanoparticles that evade lysosomes, remain in the cytoplasm, or alternatively enter the nucleus.[210] By associating DNA barcodes with ligands, this may also be used to rapidly identify effective targeting sequences via a process that is akin to phage display.

It is unlikely that this system will work for every drug delivery vehicle; it will be most effective for well-tolerated nanoparticles that are stable in solution before injection. In future studies, it will be important to characterize nanoparticle stability before using this system to study their activity. Even with these constraints, we anticipate that this methodology will facilitate nanoparticle pharmacokinetic studies and will rapidly accelerate the discovery of nanoparticles with wide-ranging therapeutic and research applications.

5.7 Materials and Methods

Oligonucleotide Barcode Amplification and DNA Sequencing. DNA barcodes were 61 nucleotides long, with 3 phosphorothioate bonds at each end (Integrated DNA Technologies) to increase barcode stability and decrease exonuclease degradation. Oligonucleotide sequences and primers are listed in **Table B.5-1**. The "barcode" portion comprised 10 nucleotides in the center of the oligonucleotide. Ten random bases were also included directly 3' of the barcode. The random bases were incorporated to monitor excessive PCR amplification, which was never observed in any experiment (>90% of the randomized sequences were always unique). The 5' and 3' ends of each oligonucleotide contained priming sites for Illumina adapters. Tissues were lysed in 2 mL tubes using 1.4 mm ceramic beads, placed into a tissue-lyser machine that rapidly agitated the tubes. DNA oligonucleotides were isolated from this tissue lysate according to manufacturer instructions (Clarity OTX columns, Phenomenex). Crude oligonucleotide preparations were further purified on Zymo Oligo Clean and Concentrator columns. Each

oligonucleotide pool was amplified by PCR using the following recipe: 5 ul 5X HF Phusion buffer, 0.5 ul 10 mM dNTPs (New England Biolabs), 1 ul oligonucleotide pool, 0.5 ul 5 uM Universal primer, 0.5 ul 5 uM Index primer, 0.5 ul 0.5 uM Index-base primer, 0.25 ul Phusion enzyme (New England Biolabs), 2 ul DMSO, and 14.75 ul H_2O. DNA barcode and primer sequences are described in **Table B.5-1**. Cycling conditions were 98° for 15 seconds, 60° for 15 seconds, and 72° for 30 seconds, repeated 25-30 cycles. PCR products were run by gel electrophoresis on 1.4% TAE agarose, bands were excised, pooled, and purified by Zymo Gel Extraction columns. Agarose bands containing PCR products were pooled only if the Index primers were distinct. The purified products were kept frozen until deep sequencing.

Deep Sequencing. All deep sequencing runs were performed using multiplexed runs on Illumina Miseq machines. PCR product pools were quantitated using the KAPA Library Quantification Kit for NGS. PCR product pools were loaded onto flow cells at 4 nM concentration. Raw counts for all experiments can be found in the supplemental info of Dahlman et al.[211]

Nanoparticle Formulation. All nanoparticle formulation details are listed in **Table B.5-2**. 7C1 lipid was synthesized as previously described[151] and C12-200 lipid was purchased from Wuxi AppTec (Shanghai, China). LNPs were synthesized by mixing a lipid-containing ethanol phase with a nucleic acid-containing aqueous phase at a 1:3 volume ratio in a microfluidic chip as previously described.[87] The ethanol phase was prepared by solubilizing a mixture including some of the following components: lipids 7C1 or C12-200, phospholipid 1,2-distearoyl-sn-glycero-3-phosphocholine (DSPC), cholesterol, and/or lipid-anchored PEG (e.g. C_{14} PEG 2000, C_{18} PEG 1000, and others) (Avanti Polar Lipids, Alabaster, AL). The aqueous phase was prepared in 10 mM citrate buffer with DNA barcode or Factor VII siRNA. The 7C1: nucleic acid and C12-200: nucleic acid weight ratios were 5:1 and 10:1, respectively. Immediately after mixing the ethanol and aqueous phases, the resultant LNPs were dialyzed against 1X PBS

overnight at 4°C. Formulation parameters for the 30 LNP screen were generated using statistical Design of Experiment software JMP (SAS Institute) using the Custom Design feature. In all cases (except for the *in vivo* standard curve in **Figure 5-2d**) we administered 0.04 mg/kg DNA barcode per nanoparticle. This dose was selected because the 'total dose' ranged between 0.16 (e.g., **Figure 5-2b**) mg/kg DNA barcode and 1.2 mg/kg DNA (e.g., **Figure 5-3a**), which are within commonly used doses for 7C1 and C12-200.[85,151]

Nanoparticle Characterization. LNP particle diameter and polydispersity were measured using dynamic light scattering (DLS, ZetaPALS, Brookhaven Instruments) as previously described.[85,151] Nanoparticles were diluted to ~0.001 mg / mL nucleic acid in PBS and analyzed at room temperature. We quantified siRNA or DNA concentration and encapsulation as previously described, and according to manufacturing instructions (Quant-iT RiboGreen RNA assay, Quant-iT OliGreen ssDNA, respectively, Invitrogen).[16] Doses for each nanoparticle and barcode, for each experiment, are listed in **Table B.5-2.**

Tissue/cell Isolation. For experiments in **Figures 2**, as well as **Figure 5-3b** and **Figure 5-3c**, tissues were isolated 4 hours after animals were injected. A 4 hour timepoint was selected because C12-200 and 7C1-based nanoparticles have a half-life of ~10 minutes; at four hours, over 99.9% of the particles would be out of the circulation. In Figure 5-3d, tissues were isolated either 15 minutes, 1 hour, 2 hours, 4 hours, 8 hours, or 24 hours after administration. In all cases, animals were sacrificed, and tissues were snap frozen in liquid nitrogen. To isolate live lung cells in Fig. 5-2f, we used a protocol we previously developed.[151,212] Immediately after sacrificing the mouse, lungs were perfused with 37°C 1X PBS. Lungs were cut into small slices, placed in buffer with Collagenase I, Collagenase XI, and Hyaluronidase, and digested for 30 minutes at 37°C. Whole tissue homogenates were then passed through a 100 um filter to separate cells. Cells were stained to identify live cells (Biolegend Zombie Dyes), and sorted by flow cytometry.

Normalized DNA Counts. For all figures with normalized DNA counts, the following calculations were made: The total number of sequencing reads from a given tissue was added together. The number of sequencing reads with a specific barcode was then calculated. As a simplified example, if a mouse lung generated a total of 10,000 barcode reads, and individual barcodes 1, 2, and 3 had 6,000, 3,000, and 1,000, of those reads respectively, then the percentage delivered in that lung by nanoparticles 1, 2, and 3, were 60%, 30%, and 10%.

Area Under the Curve (AUC) Calculations. The relative AUC for each LNP (units of mass lipid x time / mass liver) was calculated using the trapezoidal rule on a plot of LNP liver concentration vs. time. To translate normalized liver counts for each LNP to liver concentration, we used pharmacokinetic data reported from a previous study[124] in which liver-targeting siRNA-LNPs were formulated with 50% ^{14}C-labelled ionizable lipid, 10% DSPC, 38.5% cholesterol, and 1.5 mol% $C_{16}PEG_{2000}$; following intravenous injection, the liver accumulation of ^{14}C was monitored over time. We created an LNP (#6) with an identical ionizable lipid, DSPC, cholesterol, and $C_{16}PEG_{2000}$ composition to that of the radiolabeled LNP, and assumed that the pharmacokinetic curve of the radiolabelled LNP would make an ideal approximation for LNP #6 in our study. A detailed description of the AUC calculation may be found in Dahlman et al.[211]

Factor VII Analysis. Factor VII siRNA was synthesized and modified to reduce off-target effects and immunostimulation as previously described (provided by Alnylam Pharmaceuticals, Cambridge, MA).[11,18,85] The sense sequence was: 5'-GGAU$_f$C$_f$AU$_f$C$_f$U$_f$C$_f$AAGU$_f$C$_f$U$_f$U$_f$AC$_f$dTdT-3', and antisense was: 5'-GU$_f$AAGAC$_f$U$_f$U$_f$GAGAU$_f$GAU$_f$C$_f$C$_f$dTdT-3' (C$_f$ denotes 2-Fluoro modification to C base, and dT denotes deoxyribonucleic acid). siRNA was administered intravenously at a dose 0.10 mg/kg. After 72 hours, blood was collected via the tail vein and serum was isolated by spinning at 2,000g for 10 minutes at 4°C. Factor VII was quantified according to manufacturer instructions (Biophen FVII, Aniara Corporation), as described

previously.[18,19,85] Factor VII levels were compared to mice injected with PBS; Factor VII expression in PBS treated mice was treated as '100%' Factor VII expression.

Animal Experiments. The MIT Institutional Animal Care and Use Committee approved all animal experiments. Seven to 10 week old, female C57BL/6 mice between 17 and 21 grams were used in these experiments (Charles River Labs). Randomization of sample groups was not necessary, since mouse replicates were administered the same pool of nanoparticles, except in **Fig. 5-4b**, where mice were randomly assigned different siRNA formulations. Results from experiments shown in **Fig. 5-2** were very consistent among cohorts of 4 or 5 animals, and as a result, later experiments shown in **Fig. 5-3 and 5-4** were performed using cohorts of 3-4 animals.

Data Blinding. In all experiments, preparation of deep sequencing libraries was performed in a manner blinded to nanoparticle administration and tissue harvest.

Data Analysis. Python scripts were written to count barcodes from Illumina fastq files. Additional python scripts were used to plot and analyze all data. Ordinary least squares linear regression with two-sided p-values was performed using scipy.linregress, as this test requires minimal assumptions about the data. Code is available upon request.

5.8 Acknowledgements

JED was funded by MIT Presidential, NDSEG, and NSF GRFP graduate fellowships. YX, TES, and CCD were funded by the MIT Undergraduate Research Opportunities Program (UROP). YX and experiments were funded by the Kathy and Curt Marble Cancer Research Fund / Koch Institute Frontier Grant, awarded to ETW and DGA, and NIH grant DP5-OD017865, awarded to

ETW. We thank the Animal Imaging and Preclinical Testing and Flow Cytometry Cores at the Koch Institute at MIT.

Chapter 6

A Mouse Model for Analysis of Vectored mRNA Expression *in vivo* with Single Cell Resolution

The work presented in this chapter is in preparation for publication:

Kauffman, K.J.*; Oberli, M.A.*; Dorkin, J.R.; Hurtado, J.E.; Bhadini, S.; Wyckoff, J.; Langer, R.; Jaklenec, A.; Anderson, D.G. "A Mouse Model for the Analysis of Vectored mRNA Expression with Single-Cell Resolution." *In preparation.*

6.1 Introduction

Messenger RNA (mRNA) therapeutics have the potential to address unmet medical needs by inducing specific intracellular protein expression *in vivo*. mRNA-based therapies have entered clinical trials for vaccine and protein replacement applications and are being studied pre-clinically in other areas such as genome editing.[22,213] However, successful delivery of mRNA into the target tissue and the cytoplasm of the target cell type remains challenging. Various vectors – including lipid nanoparticles, polymeric nanoparticles, and protamine-based complexes – have been utilized to encapsulate and deliver mRNA payloads intracellularly.[7,141] To evaluate the transfection ability, biodistribution, and pharmacokinetics of these delivery vectors *in vivo*, mRNAs coding for reporter genes (e.g. bioluminescent luciferases, fluorescent proteins, β-galactosidase, and others) are often used to optimize the system before therapeutic mRNA is attempted.[214] Additionally, for most vectored mRNA delivery applications, it is useful to identify not only the targeted tissue but also the targeted cell populations within that tissue. For example, cancer immunotherapies would ideally express mRNA encoding antigen in dendritic cells of the lymphatic system;[26,181] conversely, protein replacement therapy for cystic fibrosis would target expression of mRNA encoding CFTR in lung epithelial cells.[172,215].

Firefly luciferase (Luc) mRNA is a commonly-used reporter mRNA in the literature for *in vivo* studies and has been used to show mRNA transfection in the liver,[140,149] spleen,[52,175] pancreas,[149] lung,[175,178] bone marrow,[175] lymph nodes,[174,175] muscle,[146,152] and xenograft tumors.[116] Upon activation by a nontoxic and stable substrate, Luc emits light at tissue-penetrating wavelengths which can be imaged *in vivo,* [216] making Luc useful for surveying the entire animal and identifying mRNA translation in bulk tissues. Thus, this *in vivo* bioluminescence imaging (BLI) technique is a powerful tool to localize protein expression and guide the researcher to the most appropriate tissue for further *in vivo* analysis with fluorescent markers.[217] However, the desired single cell resolution cannot be achieved with Luc using

conventional techniques such as flow cytometry or microscopy – which require a strong fluorescent signal – without the use of engineered luciferase-fluorescent protein conjugates[74,218,219] or additional disruptive antibody staining steps requiring membrane permeabilization.[220,221] In principle, mRNAs encoding fluorescent proteins can allow for facile single-cell analysis via microscopy or flow cytometry. However, current commercially-available GFP and tdTomato mRNAs delivered to wildtype mice using previously-reported formulations did not induce sufficient protein expression to be visualized *in vivo,* despite having strong GFP and tdTomato signal when delivered to cells *in vitro* **(Fig. A.6-1-A.6-3)**. Thus, there is a need for a mouse model which can sensitively and rapidly identify mRNA-transfected cell populations *in vivo* to optimize mRNA delivery vectors for diverse cellular targets and clinical applications.

We hypothesized that *in vivo* delivery of mRNA could be more easily visualized in a genetically-modified mouse with a loxP-flanked STOP cassette preventing transcription of a CAG promoter-driven tdTomato protein in all cells, such as the Ai14 reporter mouse **(Fig. 6-1a)**.[222] In this model, cells which are successfully transfected with mRNA encoding Cre recombinase (Cre) would excise the loxP-flanked STOP cassette and result in permanent tdTomato transcription and subsequent strong, amplified tdTomato expression. To validate this model, we delivered Cre mRNA with two distinct delivery vectors to Ai14 mice and analyzed the resultant tdTomato expression using whole-organ imaging, fluorescent microscopy, and flow cytometry **(Fig. 6-1b).** In this report, we use this Ai14/Cre mRNA mouse model to describe vectored mRNA transfection *in vivo* with single-cell resolution at low mRNA doses.

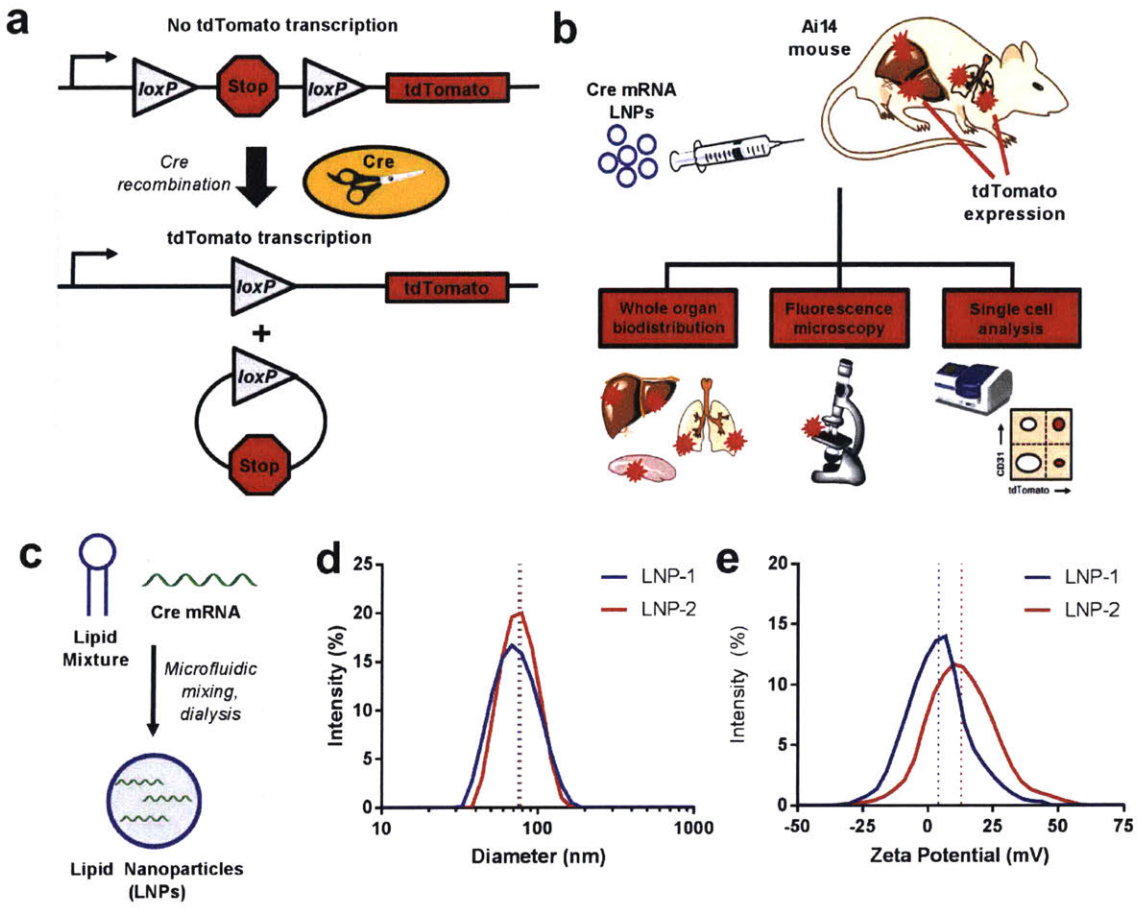

Figure 6-1. Ai14/Cre mRNA mouse model description and lipid nanoparticle characterization. (a) Diagram of *loxP*-flanked STOP cassette upstream of tdTomato with and without Cre recombination, **(b)** Workflow for investigation of mRNA expression biodistribution using Cre mRNA LNPs in Ai14 mice, **(c)** Schematic of LNP formulation process (more detailed description in **Fig. A.6-4**), **(d)** Diameter distribution for LNP-1 and LNP-2, **(e)** Zeta potential distribution for LNP-1 and LNP-2.

6.2 Validation of the Ai14/Cre mRNA Model *in vivo*

We first investigated whether vectored mRNA encoding for GFP or tdTomato could result in sufficient GFP or tdTomato signal for whole-organ imaging. An optimized[149] lipid nanoparticle (LNP) formulation **(Fig. 6-1c,d)** capable of achieving high levels of Luc mRNA expression predominately in the liver following intravenous administration to mice (LNP-1) has been previously reported.[140] The composition of LNP-1 is shown in **Fig. A.6-4**. We formulated LNP-1 with commercially-available GFP or tdTomato mRNA and administered i.v. to wildtype

C57BL/6 mice at 0.3 mg/kg. The GFP or tdTomato fluorescence of the liver and two additional organs (spleen, lungs) was measured 24 hr, the approximate half-life of these fluorescent proteins **(Fig. 6-1a).**[223] We found no detectable GFP or tdTomato signal from LNP-1-administered wildtype mice at this dose using GFP or tdTomato mRNAs, meaning that an alternative method of measuring mRNA translation in whole organs is needed for LNP-1.

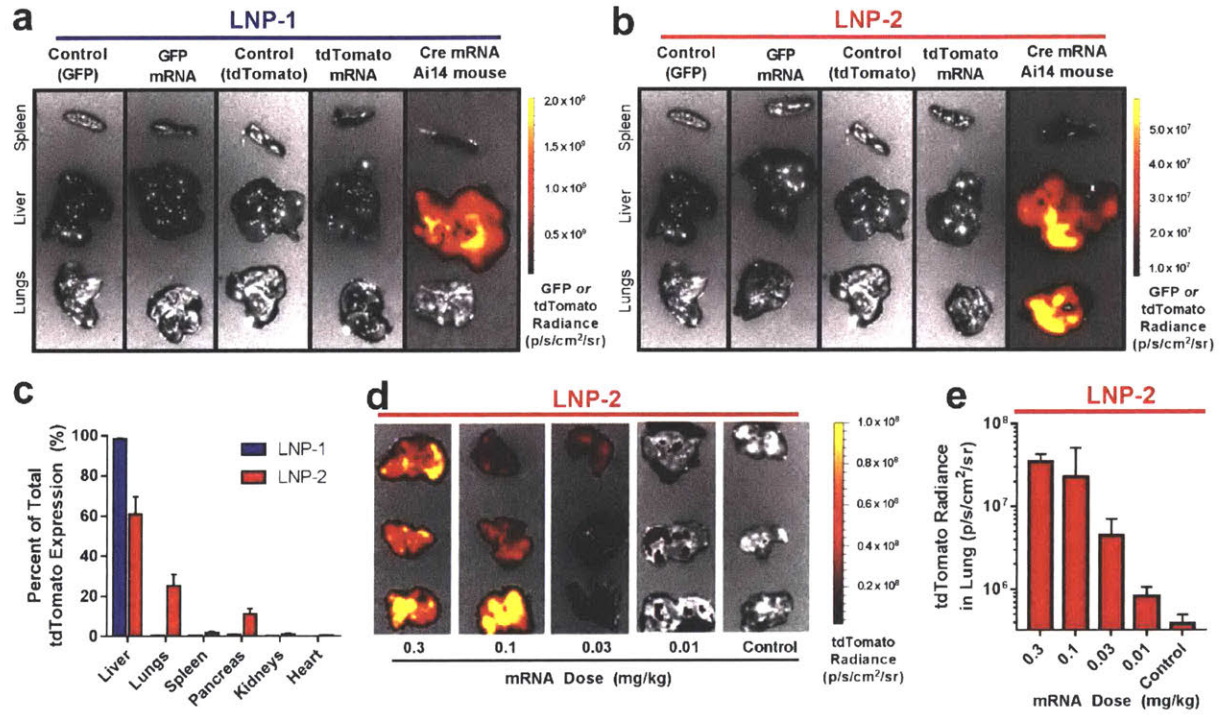

Figure 6-2. Whole organ fluorescence for the Ai14/Cre mRNA mouse model. (a,b) Representative (*n* = 3, 1 pictured) GFP or tdTomato expression in three organs for LNP-1 or LNP-2 injected mice under IVIS imaging. LNPs with GFP and tdTomato mRNA were administered to C57BL/6 mice (24 hr), and LNPs with Cre mRNA were administered to Ai14 mice (48 hr). Control mice are PBS-treated C57BL/6 mice. **(c)** Biodistribution of tdTomato fluorescence for LNP-1 and LNP-2 in Ai14 mice, **(d)** tdTomato expression in the lungs for LNP-2 in Ai14 mice at various doses under IVIS imaging, **(e)** Quantification of (d). Data in (c) and (e) are presented as mean + standard deviation, *n* = 3.

We next tested the ability of the hypothesized Ai14/Cre mRNA model to produce measurable tdTomato expression in whole organs. We formulated Cre mRNA into LNP-1 and administered i.v. to Ai14 mice at 0.3 mg/kg. At 48 hr post-injection (to provide additional time for

the Cre recombination and transcription steps), there was tdTomato expression in the liver which was orders-of-magnitude higher than background tissue autofluorescence **(Fig. 6-1a)**, demonstrating that vectored Cre mRNA could generate tdTomato signal in Ai14 mice as proposed. Furthermore, the liver biodistribution of tdTomato expression was comparable to that of previously-published[140] Luc expression **(Fig. A.6-5)** for LNP-1, suggesting that the Ai14/Cre mRNA model can successfully describe the whole organ expression of protein from vectored mRNA.

6.3 Characterization of a New Formulation with Whole Organ Imaging

Recently, a publication by Kranz et al.[175] reported that Luc-encoding mRNA-LNPs could be redirected to the lungs by increasing the zeta potential of the LNP. To this end, we sought to formulate a new, more positively-charged version of our LNP (LNP-2) and examine its tissue delivery properties **(Fig. 6-1e, A.6-4)**. As hypothesized, i.v. administration of LNP-2 encapsulating Cre mRNA to Ai14 mice resulted in significant tdTomato expression in the lungs **(Fig. 6-2b,c)**, consistent with the related formulation and data generated described by Kranz et al. with Luc mRNA[175] As previously observed with LNP-1, no observable whole-organ fluorescence was found in C57BL/6 mice administered LNP-2 formulated with GFP or tdTomato mRNA at a 0.3 mg/kg (approximately 5 μg) dose **(Fig. 6-2b)**. To test the sensitivity of our Ai14/Cre mRNA model, we performed a dose-response experiment with LNP-2 in the lungs and detected tdTomato expression by IVIS at mRNA doses as low as 0.01 mg/kg (approximately 200 ng) **(Fig. 6-2d,e)** Importantly, tdTomato expression was dose-dependent, suggesting that tdTomato expression can be used both as a proxy for vectored mRNA transfection efficacy and to potentially estimate the percentage of transfected cells in a given tissue.

6.4 Two Photon Microscopy for Ai14/Cre mRNA Model

One potential advantage of the Ai14/Cre mRNA model over traditional Luc reporter models is the ability to rapidly perform fluorescent microscopy to probe the cellular structure of tdTomato-expressing tissues and flow cytometry to identify tdTomato-expressing cell populations. Whereas Luc would require additional secondary antibody staining (which is also more disruptive for intracellular proteins like Luc due to the need to permeabilize the cellular membrane), tdTomato-expressing tissues and cells from Ai14 mice can be immediately analyzed. We chose to first perform two-photon excitation microscopy because it uses freshly isolated tissue and requires no potentially-damaging fixation or lengthy antibody staining steps.[224] This technique was used to study the liver, spleen, and lung tissue architecture of LNP-1 and LNP-2 administered Ai14 mice **(Fig. 6-3)**, revealing tdTomato expression in liver cells (**Fig. 6-3a**), spleen cells (**Fig. 6-3b**), and cells lining both exterior (**Fig. 6-3c**) and interior (**Fig. 6-3d**) blood vessels of the lung.

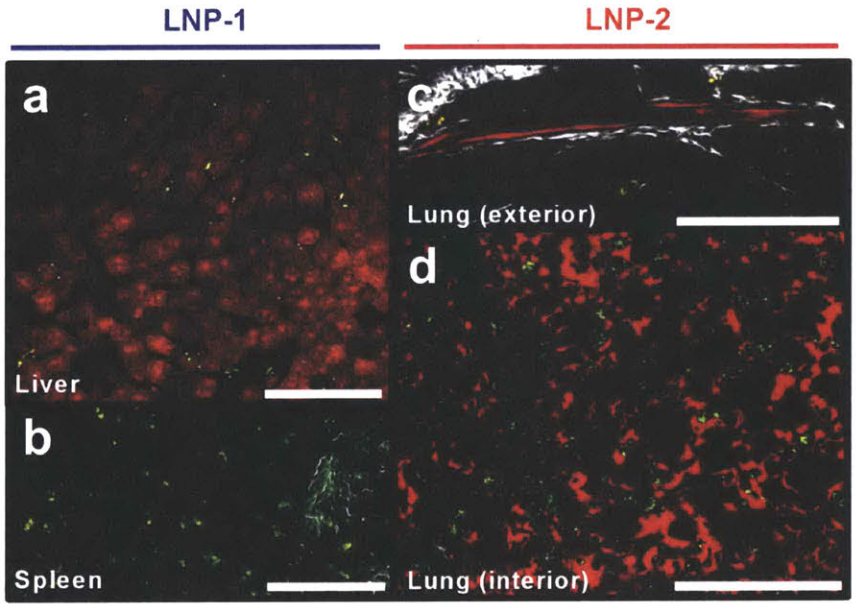

Figure 6-3. Two-photon excitation microscopy of tissues for the Ai14/Cre mRNA mouse model. (a) Liver cells treated with LNP-1, **(b)** Spleen cells treated with LNP-1, **(c)** Blood vessel on the exterior of the

lung treated with LNP-2, **(d)** Interior of the lung treated with LNP-2. Scale bar = 100 μm in all pictures. In all pictures, gray = collagen I (Em. 425/30 nm), green = tissue autofluorescence (Em. 525/45 nm), red = tdTomato (Em. 607/70 nm).

Microscopy experiments for LNP-1 injected Ai14 mice revealed tdTomato expression in liver cells (**Fig. 6-3a**). We postulate these tdTomato+ cells to be hepatocytes, as their morphology is cuboidal[225] and previous siRNA formulations made with LNPs similar to LNP-1 were found to silence expression of a hepatocyte-specific protein *in vivo*.[80] The spleen (**Fig. 6-3b**) has a high degree of autofluorescence due to the abundance of phagocytic cells which endocytose autofluorescent debris and dead cells, but tdTomato+ cells are still clearly visible. For LNP-2 administered Ai14 mice, we observed tdTomato+ cells which lined exterior blood vessels of the lungs (**Fig. 6-3c**) and tdTomato+ cells in the interior of the lungs in the blood vessels surrounding the alveoli (**Fig. 6-3d**). To more conclusively identify these transfected lung and spleen cell populations, flow cytometry was next performed.

6.5 Flow Cytometry for Ai14/Cre mRNA Model

We then investigated the ability of lung cells isolated from the LNP-2 administered Ai14 mice to undergo flow cytometry. As was observed for whole-organ imaging, flow cytometry analysis could not detect GFP or tdTomato fluorescence above background for wildtype mice administered LNP-2 formulated with GFP or tdTomato mRNA **(Fig. 6-4a)**. However, strong tdTomato signal was observed in CD31+ (endothelial) cells of the lung for Ai14 mice administered LNP-2 formulated with Cre mRNA **(Fig. 6-4a)**. A 2D plot of CD31 vs. tdTomato for all lung cells confirmed that tdTomato-positive cells were nearly exclusively CD31+ (endothelial) lung cells **(Fig. 6-4b)**, with over 75% of isolated CD31+ lung cells expressing tdTomato at the highest tested dose (0.3 mg/kg) **(Fig. 6-4c)**. At the lowest dose tested (0.01 mg/kg), our

Ai14/Cre mRNA model could still clearly identify a tdTomato+ population comprising only 0.4% of all CD31+ lung cells.

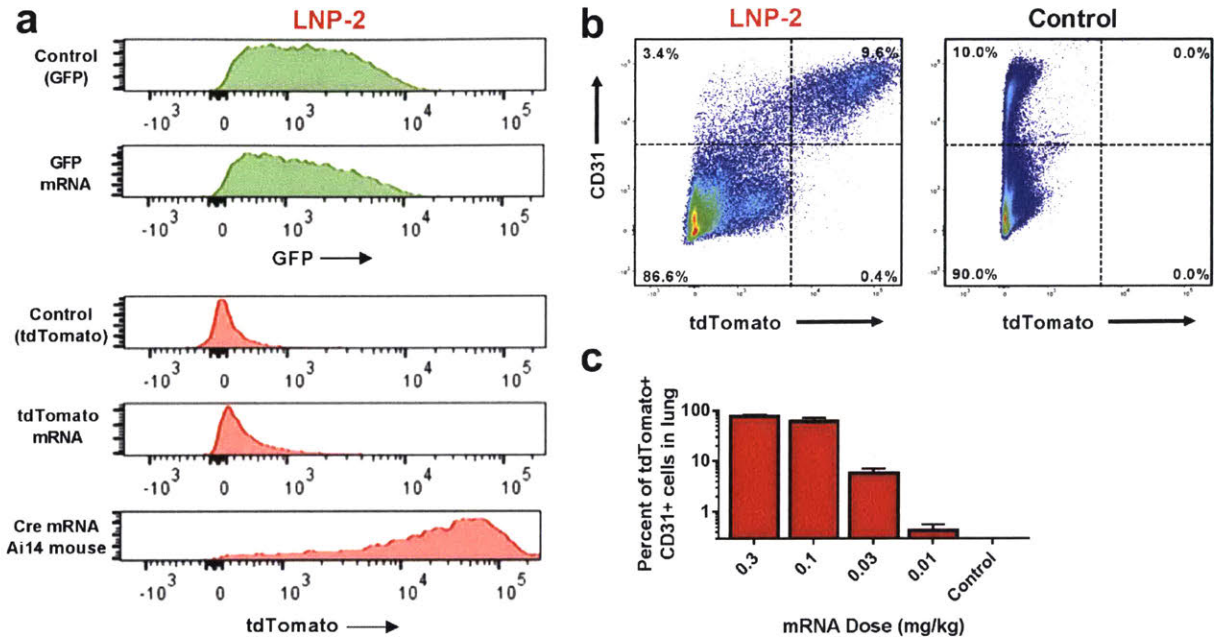

Figure 6-4. Single cell analysis of lung cells from the Ai14/Cre mRNA mouse model. (a) Representative (n = 3, 1 pictured) histograms of GFP or tdTomato signal for CD31+ (endothelial) lung cells in LNP-2 administered mice determined by flow cytometry. LNPs with GFP and tdTomato mRNA were administered to C57BL/6 mice (24 hr), and LNPs with Cre mRNA were administered to Ai14 mice (48 hr). Control mice are PBS-treated C57BL/6 mice. **(b)** Representative FACS plot of lung CD31 vs. tdTomato for LNP-2 (left) and control (right) injected mice, **(c)** Percent of lung CD31+ cells that are tdTomato+ at multiple doses in LNP-2 injected Ai14 mice, presented as mean + standard deviation, n = 3.

Kranz et al. previously reported that mRNA-LNPs could be redirected to the lungs by increasing their cationic character but did not identify which cell types were transfected.[175] For the first time, we identify endothelial cells as the primary transfected lung cell population when mice are administered with LNP-2, a newly described more cationic version of LNP-1, using two methods of detection **(Fig. 6-3, 6-4)**. The observation of endothelial cell targeting by cationic LNPs matches reports of previous lung-targeting siRNA-based cationic formulations which

silenced protein expression in lung endothelial cells but not epithelial or immune cell populations in the lung.[151,183] The ability to selectively transfect lung endothelial cells with therapeutic mRNAs is important for many clinical applications, including pulmonary hypertension[179] and cancer.[180]

We next aimed to compare the efficacy of two mRNA delivery vectors in a more complex population of cells; furthermore, we sought to identify rarer transfected cell populations which would challenge the sensitivity of the Ai14/Cre mRNA model for visualization. We chose to study the immune cell population of the spleen since LNP-1 and LNP-2 were both identified to weakly transfect spleen cells **(Fig. 6-2a,b)**, and the spleen contains a variety of therapeutically-important immune cells involved in both the innate and adaptive immune responses.[177] Whereas a majority of lung CD31+ cells expressed tdTomato for LNP-2 treated mice, CD45+ spleen cells expressing tdTomato for LNP-1 treated mice are much less common **(Fig. 6-5a)** and only observable in the Cre/Ai14 mouse model.

Flow cytometry analysis of Ai14 mice administered with LNP-1 and LNP-2 identified a wide variety of tdTomato+ spleen immune cells **(Fig. 6-5b)**. Notably, LNP-1 resulted in greater proportions of all measured tdTomato+ splenic CD45+ populations compared to LNP-2, matching the observation that whole spleen tdTomato fluorescence is significantly greater for LNP-1 than LNP-2 **(Fig. 6-2a, 6-2b, A.6-6)**. Compared to other CD45+ cells, both LNP-1 and LNP-2 transfected a greater proportion of macrophages (CD11b+, F4/80+) than any other cell type. Although macrophages made up less than 1% of CD45+ cells, they accounted for approximately 25% of the total tdTomato+ CD45+ cells in the spleen **(Fig. 6-5c).**

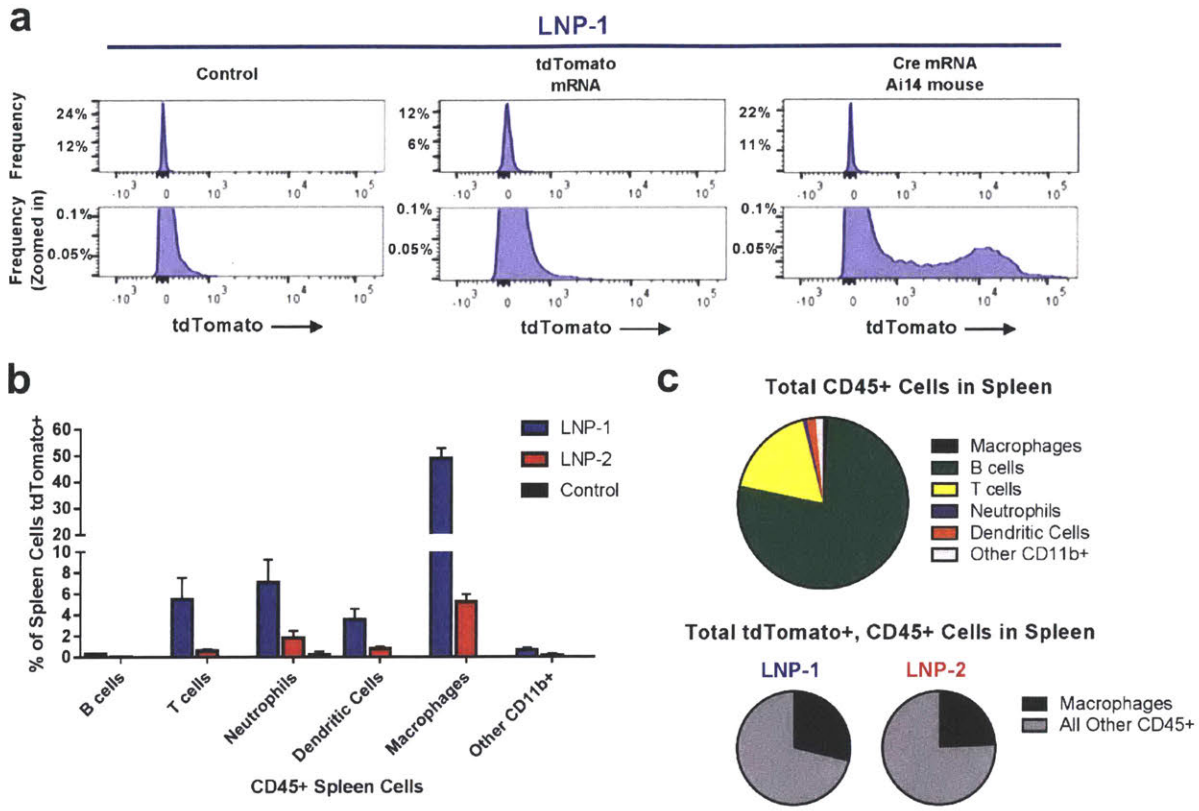

Figure 6-5. Single cell analysis of spleen cells from the Ai14/Cre mRNA mouse model. (a) Representative (n = 3, 1 pictured) histograms of tdTomato signal for CD45+ (immune) spleen cells in LNP-1 administered mice determined by flow cytometry. The y-axis on histograms in the bottom row is zoomed-in to highlight tdTomato signal. LNPs with GFP and tdTomato mRNA were administered to C57BL/6 mice, and LNPs with Cre mRNA were administered to Ai14 mice. Control mice are PBS-treated C57BL/6 mice. **(b)** Percent of CD45+ spleen cells that are tdTomato+ in LNP-1 or LNP-2 injected Ai14 mice, presented as mean + standard deviation, n = 3, **(c)** Distribution of CD45+ splenic cells (top) and tdTomato+ CD45+ splenic cells (bottom), presented as mean, n = 3.

siRNA-formulated lipid nanoparticles similar in composition to LNP-1 had been previously found to silence protein predominately in hepatocytes with only weak silencing in splenic myeloid cells.[80] However, no further transfected splenic cell types were identified with siRNA and the ability of LNP-1-type formulations to transfect splenic cells with mRNA has not yet been investigated. In the present study with mRNA-formulated LNP-1 vectors in the Ai14/Cre mRNA model, we discovered many additional splenic cell types with clearly identifiable mRNA-induced tdTomato+ populations. Excitingly, LNP-1 promoted mRNA expression in many

cell types important for mRNA immunotherapies,[26,177] including lymphocytes and antigen-presenting cells **(Fig. 6-5)** with approximately 4% of splenic dendritic cells and over half of macrophages transfected, making LNP-1 an attractive candidate for future studies with mRNA-based vaccines or immuno-modulators.

The discovery of these transfected cell types *in vivo* would not have been possible or would have required significantly more labor with vectored siRNA. It has been common practice to determine if siRNA vectors were efficacious in particular cell types by designing siRNA against proteins only expressed in those cells (e.g. Factor VII for hepatocytes,[19,80,85] Tie2 for endothelial cells[151,183]); mRNA offers no such analog since any cell with the proper ribosomal machinery should in principle be capable of translation. Many delivery vectors originally designed for siRNA delivery have been re-engineered for mRNA delivery.[141] The identification of many new cell populations successfully transfected by mRNA vectors like LNP-1 and LNP-2 suggests that, unless the mRNA vs. siRNA payload dramatically affects vector transfection ability, siRNA vectors may have been transfecting more cell types than originally thought and limited in efficacy only by siRNA potency.

6.6 Discussion

Many potential mRNA therapies could benefit from formulations capable of providing selective delivery to the required tissue and cell type *in vivo*. Different mRNA imaging methods provide for different levels of sensitivity. One of the most common reporters for surveying *in vivo* mRNA activity is Luc mRNA, which when translated into protein and activated by substrate emits measurable light. However, identification of transfected cell populations by Luc is challenging, as immunohistochemistry or flow cytometry would require incubation with secondary anti-Luc fluorescent-tagged antibodies which must permeabilize and potentially disrupt the cellular membrane. To the best of our knowledge, as of this writing no report has

measured Luc mRNA transfection *in vivo* using these techniques. Instead, alternate approaches have been taken: for example, two independent reports confirmed the transfection of splenic CD11c+ cells with an mRNA vector by comparing the Luc expression between wildtype and genetically modified CD11c-depleted mice;[175,226] however, this generalized approach would require a different knockout mouse for every potential transfected cell type of interest, which researchers would also need to know *a priori.*

Alternatively, some publications have used fluorophore-labelled RNAs *in vivo* to study the biodistribution and cellular localization of vectored nucleic acids.[86,178,183,227] However, tissue and cellular transfection of the mRNA itself does not always correlate well to translation of the desired protein.[178] Furthermore, this method cannot distinguish between fluorophore-labelled mRNA adhered to the surface of cells, those which are trapped in cellular compartments such as endosomes, and those which have successfully transfected into the cytoplasm. Because knowing the biodistribution of mRNA and vector materials is indeed important for understanding both toxicity and pharmacokinetics, the use of fluorophore-labelled mRNA vectors in concert with the Ai14/Cre mRNA model would give a more complete description of the *in vivo* behavior of mRNA delivery vectors.

In this report, we present a mouse model to determine the location of mRNA expression *in vivo* with single cell resolution using commercially available reagents and mice. Using previously-reported and novel lipid nanoparticle vectors, we deliver mRNA encoding for Cre protein to Ai14 mice, which express tdTomato upon Cre recombination **(Fig. 6-1)**. When the same lipid nanoparticles were formulated with mRNAs encoding fluorescent protein (GFP and tdTomato) and administered to wildtype mice, no fluorescence was observed above background *in vivo* for whole organs or individual cell populations **(Fig. 6-2, 6-4, 6-5)** which highlights the significantly improved sensitivity of the Cre/Ai14 model. It should be noted that the GFP, tdTomato, and Cre mRNAs used in these experiments are commercially-available and differed

only in their coding regions; they had identical 5' caps, UTR sequences, polyA tail lengths, and base modifications, all of which are known to strongly influence the potency of the mRNA.[22] We found one report in the literature of measuring expression from GFP mRNA *in vivo* with flow cytometry,[175] but the GFP mRNA was delivered at far higher doses than we demonstrate (1 mg/kg vs. as low as 0.01 mg/kg) and the GFP mRNA was also highly optimized and synthesized in-house.[228] Because both the Ai14 mice and the Cre mRNA are readily commercially available, the Ai14/Cre mRNA model would permit researchers without access to often proprietary mRNA optimization algorithms to screen mRNA vectors *in vivo* for the first time at far lower doses and with less potent delivery materials.

While it has significant advantages, the Ai14/Cre mRNA model does have limitations compared to traditional Luc models. Genetically-engineered Ai14 mice are more expensive to purchase than standard C57BL/6 or other mouse strains, and Luc mRNA remains a fast (luminescence visible minutes after substrate injection) and robust (low signal-to-noise ratio) method to screen mRNA expression in tissues *in vivo*. Luc mRNA also can be non-invasive, making it appropriate for longitudinal studies to measure protein expression over time. Additionally, whereas Luc expression (the output) in a given tissue should be directly proportional to the quantity of transfected mRNA (the input), the Ai14/Cre mRNA model is a binary, "on/off" system where the successful transfection of one Cre mRNA would have the same tdTomato expression as many Cre mRNAs. Thus, we envision the Ai14/Cre mRNA system to be used not as a replacement of Luc models but rather primarily for identifying transfected cell populations *in vivo* and discovering low-expressing tissues or rare cell types too weak to be visualized with Luc; we also envision the system to be used for determining these hits at lower doses, longer timepoints, and with less overall efficacious vectors.

The binary nature of the Ai14/Cre mRNA mouse model is also advantageous in particular applications, such as understanding of the limitations of vectored mRNA delivery; with

LNP-2, for example, tdTomato expression saturates around a dose of 0.1 to 0.3 mg/kg in the lungs (**Fig. 6-2e, 6-4b)**, suggesting that a certain number of endothelial cells might be incapable of transfection regardless of dose escalation. Additionally, a binary readout in which only one Cre protein (from delivered Cre mRNA) must transfect the nucleus to express tdTomato is highly analogous to genome editing applications such as the CRISPR/Cas system in which one Cas9 protein (from delivered Cas9 mRNA) must transfect the nucleus to edit a gene. Thus, we anticipate the Ai14/Cre mRNA mouse model to be highly useful for researchers performing mechanistic analyses of *in vivo* mRNA delivery and for those studying *in vivo* genome editing with nuclease-encoding mRNAs. A recent publication further demonstrated the utility of reporter mice similar to Ai14 mice for CRISPR applications by co-delivering Cas9 mRNA and sgRNA against loxP, thus cutting out the STOP cassette and inducing tdTomato in transfected cells.[229]

6.7 Conclusions

In conclusion, we have demonstrated the use of a mouse model in which mRNA expression can be identified with single cell resolution *in vivo*. Due to the increased sensitivity of the Ai14/Cre mRNA model over traditional reporter mRNAs (i.e. luciferase, GFP or tdTomato), we discovered that a previously-reported lipid nanoparticle mRNA formulation is capable of transfecting splenic lymphocytes and antigen-presenting cells, and we designed a new mRNA formulation capable of transfecting lung endothelial cells. We propose that this described Ai14/Cre mRNA mouse model be used together with traditional luciferase models in future experiments to screen and optimize mRNA delivery vectors for therapeutic applications, including protein replacement therapies, genomic engineering, and mRNA vaccines.

6.8 Materials and Methods

Messenger RNA (mRNA). Commercially-available mRNA encoding NLS-Cre recombinase (Cre) and enhanced green fluorescent protein (GFP) were purchased from TriLink Biotechnologies (San Diego, CA). mRNA encoding tdTomato was custom synthesized by TriLink according to the same specifications as Cre and GFP. All mRNAs were 100% modified with pseudouridine and 5-methylcytidine, capped with Cap 0, and polyadenylated.

Lipid Nanoparticle Formulation. The ethanol phase contained a mixture of cKK-E12 (prepared as previously described,[80] courtesy of Shire Pharmaceuticals, Lexington, MA), 1,2-dioleoyl-*sn*-glycero-3-phosphoethanolamine (DOPE, Avanti Polar Lipids, Alabaster, AL), 1,2-dioleoyl-3-trimethylammonium-propane (DOTAP, Avanti), cholesterol (Sigma), and/or 1,2-dimyristoyl-*sn*-glycero-3-phosphoethanolamine-N-[methoxy(polyethylene glycol)-2000] (C14 PEG 2000, Avanti) in differing molar ratios (**Table B.6-1**) for LNP-1 and LNP-2. The aqueous phase contained mRNA in 10 mM citrate buffer (pH 3). Syringe pumps were used to mix the ethanol and aqueous phases together at a 1:3 volume ratio in a microfluidic chip device as previously described.[87] The resulting LNPs were dialyzed against 1x PBS in a 20,000 MWCO cassette at 4°C for 2 h.

Lipid Nanoparticle Characterization. To calculate the mRNA encapsulation efficiency, a modified Quant-iT RiboGreen RNA assay (Invitrogen) was performed as previously described.[16] The diameter (measured by intensity) and polydispersity of the LNPs were measured using dynamic light scattering (ZetaPALS, Brookhaven Instruments). Zeta potential was measured using the same instrument in a 0.1x PBS solution.

Animal Experiments. Animal studies were approved by the M.I.T. Institutional Animal Care and Use Committee and were consistent with local, state, and federal regulations as applicable. Female B6.Cg-*Gt(ROSA)26Sor*$^{tm14(CAG-tdTomato)Hze}$/J (Ai14) mice and control C57BL/6 mice were

purchased from Jackson Laboratory (Bar Harbor, ME). Mice (18-22 g) were intravenously injected with LNPs via the tail vein at a dose of 0.3 mg/kg unless otherwise noted for dose-response experiments. For GFP and tdTomato mRNA experiments, *in vivo* measurements were taken at 24 hr post-injection (according to the half-life of the proteins). For Cre mRNA experiments, measurements were taken at 48 hr post-injection. Mice were euthanized by carbon dioxide asphyxiation.

Whole Organ Imaging. To measure whole organ fluorescence, organs were collected and measured using an IVIS imaging system (PerkinElmer, Waltham, MA) and quantified using LivingImage software (PerkinElmer).

Two-Photon Excitation Microscopy. Imaging was performed on an Olympus FV-1000MPE (Olympus Americas, Walthum MA) using a 25X, N.A. 1.05 water objective. Excitation was achieved using a DeepSee Tai-sapphire femtosecond pulse laser (Spectro-Physics, Santa Clara, CA.) at 840 nm. The emitted fluorescence was collected by PMTs with emission filters of 425/30 nm for collagen 1, 525/45 nm for tissue autofluorescence, and 607/70 nm for tdTomato. Collagen 1 was excited by second harmonic generation and emits as polarized light at half the excitation wavelength. All images were processed using ImageJ.

Flow Cytometry. Spleen single cell suspensions were prepared as previously described.[230] To prepare lung single cell suspensions, lungs were digested in a mixture of collagenase I (450 U), collagenase XI (125 U), and DNase I (2 U) in 1 mL at 37 °C for 1 hr. The digest was passed through a 70 μm filter. Following centrifugation and removal of supernatant, cells were treated with red blood cell (RBC) lysis buffer for 10 min at 4 °C and then passed throw a 40 μm filter.

Once single cell suspensions were generated, cells were stained with a mixture of anti-mouse antibodies at a 1:300 dilution in flow buffer (PBS containing 0.5% BSA and 2 mM EDTA). The antibodies included TCR-β (clone H57-597), CD19 (clone 6D5), CD11b (clone M1/70), Ly-6G

(clone 1A8), CD45 (clone 30-F11), F4/80 (clone BM8), CD11c (clone N418), CD31 (clone 390), and EpCAM (clone G8.8) Antibodies were purchased from Biolegend (San Diego, CA), and data was collected using a BD LSR II cytometer (BD Biosciences). Data was analyzed with FlowJo software (Ashland, OR).

Splenic cell populations were identified as follows: 1) T cells: CD45+, CD11b-, TCR-β+, 2) B cells: CD45+, CD11b-, CD19+, 3) Neutrophils: CD45+, CD11b+, Ly-6G+, 4) Macrophages: CD45+, CD11b+, F4/80+, 5) Dendritic cells: CD45+, CD11b+, CD11c+, 6) Other myeloid cells: CD45+, CD11b+, Ly-6G-, F4/80-, CD11c-. Lung cell populations were identified as follows: 1) Endothelial cells: CD31+, 2) Epithelial cells: EpCAM+, 3) Immune cells: CD45+.

***In vitro* Experiments.** HeLa cells (ATCC, Manassas, VA) were cultured in high glucose Dulbecco's Modified Eagle's Medium (ThermoFisher) supplemented with 10% fetal bovine serum. Cells were maintained at 37 °C and 5% CO_2. Cells were plated at 20,000 cells/well in a clear-bottom, black-walled 96-well plate. After 24 hr, the media in each well was replaced with 150 µL of media containing GFP or tdTomato mRNA-LNPs or mRNA-Stemfect complexes. The mRNA transfection reagent Stemfect (Stemgent, Lexington, MA) was used according to the manufacturer's protocol. After another 24 hr, the fluorescence was measured. Fluorescence microscopy was performed with an EVOS FL cell imaging system (ThermoFisher). To quantify the fluorescence, cells were lysed with 50 uL of Cell Lytic M for 10 min at 37°C at 400 rpm. 150 uL of PBS was added to each well and fluorescence was measured with a Tecan Infinite m200 Pro microplate reader.

Statistics. To compare two groups, a Student's *t*-test was performed assuming a Gaussian distribution with unequal variances. Statistical significance was defined with an alpha level of 0.05. All statistical analysis was performed using GraphPad Prism 7 software (La Jolla, CA).

6.9 Acknowledgements

This work was supported by Shire Pharmaceuticals (Lexington, MA), the Koch Institute Marble Center for Cancer Medicine, and the Cancer Center Support (core) Grant P30-CA14051. We thank the Animal Imaging and Preclinical Testing Core, Microscopy, and Flow Cytometry Core at the Koch Institute at MIT.

Chapter 7

Conclusions

7.1 Thesis Summary

The unifying theme of this Thesis is the optimization of mRNA lipid nanoparticles in regard to formulation efficacy, immunogenicity, and target organ/cell type transfection. We conceived of a method to optimize lipid nanoparticles for mRNA delivery and then studied their immunogenicity. We also used new materials to rationally modulate the potency and biodistribution of these formulations. Finally, we generated two separate, novel *in vivo* models to screen vectored mRNA and ascertain both their biodistribution and transfected cell populations. It is the hope that this work will contribute to the development of mRNA therapeutics by increasing their efficacy and accelerating the discovery of delivery vectors which transfect desired tissues and cell types.

7.2 Future Perspectives for mRNA Delivery

To conclude this Thesis, I describe four areas of topical interest for future work involving mRNA therapeutics and their delivery.

7.2.1 mRNA Optimization

From the field of siRNA delivery, we learned that the chemical structure of the ionizable lipid can have profound effects on LNP potency but also that siRNAs themselves can be rigorously optimized though chemical modifications.[46,49] Over 100 experimentally validated chemical modifications to the sugar, phosphate, or base components have been recorded for siRNA,[231] but far fewer modifications have been tested for mRNA in the literature. We ourselves investigated the effect of one such base modification on mRNA function (pseudouridine),[230] but there are dozens of other viable base modifications for mRNA which may have differing behavior *in vivo*.[130,141,146] Moreover, the generation of novel synthetic nucleosides may lead to

even more stabilized and potent mRNAs in coming years, but there are challenges: modified mRNA must still recognized enough by cellular machinery to translate into protein and synthetic nucleotide triphosphates must be incorporated into the mRNA by polymerases. High throughput screenings of different combinations of mRNA modifications have recently shown promise in quantifying modified mRNA potency *in vitro*,[147] but as always, caution should be taken before applying these limited conclusions *in vivo*.

In addition to base modifications, there are many other avenues for optimizing the mRNA sequence itself. Codon optimization has been performed with success to improve mRNA translation and half-life, e.g. using only the most GC-rich codons in the open reading frame.[59] The 5' cap on the mRNA also offers considerable opportunities for modulating mRNA behavior; recent work has begun to study the effects of novel, synthetic 5' caps on mRNA stability and potency.[232] Other work has reported how the 5' cap and the poly(A) tail regulate mRNA translation in a synergistic fashion.[56] Another crucial yet significantly underreported aspect of the mRNA is its untranslated regions (UTRs), which flank the open reading frame. Literature data[57,58] and preliminary work in our lab have indicated the importance of both the 5' and 3' UTR sequence for mRNA potency, and some publications have reported screening various combinations of UTRs to find the most efficacious ones.[59] As of this writing, UTR sequences are not commonly reported in the mRNA literature, which significantly hampers independent reproducibility of results and the mRNA delivery field as a whole.

An additional unexplored aspect in the field of modified mRNAs is precisely how these modified mRNAs improve translation *in vivo*. Although at a basic level we understand that certain modifications impart resistance to nucleases or reduce inhibitory immune responses,[54] more fundamental biology/computational research is needed to understand modified mRNAs at a mechanistic level, e.g. how ribosomes differently translate modified mRNAs, how modifications influence mRNA secondary structure and loading into delivery vehicles, how

modified mRNAs degrade differently than unmodified mRNAs, etc. With so many variables to independently tune (5' cap, 3' tail, UTRs, codon optimization, base modifications) which likely are interdependent, Design of Experiment is advised to be used to reduce the number of experiments to a manageable level. Additionally, advances in high throughput mRNA synthesis will undoubtedly accelerate the optimization of mRNAs for therapeutic applications.

7.2.2 Immunogenicity and Safety

Early clinical trials of siRNA therapeutics encountered toxicity issues resulting from both the nucleic acid and its delivery vehicle.[233,234] As has been previously discussed, mRNA and its delivery vehicles can be immunogenic as well. We have explored the extracellular innate immune response to mRNAs and others have performed preliminary work understanding the intracellular innate immune response to mRNA,[10,54] but a potential adaptive immune response to mRNA and its delivery vehicles needs to be studied. For long-term mRNA therapies that provide functional copies of a non-functional protein, there should be additional concerns that antibodies might be generated against the non-native proteins coded by the mRNA and render them less efficacious. Encouragingly, a recent study has provided evidence that mRNA can be dosed repeatedly over the course of several weeks without loss of efficacy or the formation of antibodies against the coded protein,[235] but more work is needed to assess if these results hold in different conditions or at longer timepoints.

Ongoing work in our lab and others' is attempting to reduce the toxicity of lipid delivery materials by incorporating biodegradable and/or bioreducible linkages into the lipid tails,[84,86,236] but it is not yet clear how strongly these moieties reduce short- or long-term toxicity of the LNP as a whole. Degradable polymer mRNA delivery vehicles may prove to be less toxic than those using lipids, but the tradeoffs between toxicity and efficacy must be considered. The therapeutic indication will likely influence how tolerable certain levels of immunogenicity and toxicity will be. For therapies requiring a limited number of applications such as vaccines or genome editing,

these safety concerns will be less important than those requiring repeated, long-term dosing like protein replacement therapies.

7.2.3 Alternative Routes of Administration

We have performed preliminary work on subcutaneous and intramuscular mRNA-LNP delivery and outlined the rationale in previous chapters for non-intravenous injections, but other routes of administration are also being explored for mRNA therapeutics to both improve tolerability and potentially target non-liver cells. Inhalable formulations post-nebulization could potentially target lung epithelial cells, making this an appealing route to deliver functional CFTR-encoding mRNA for cystic fibrosis therapy.[172] Several issues must first be addressed for inhalable mRNA nanoparticles, including the orders-of-magnitude larger dosing requirements for nebulization and particle/mRNA stability after aerosolization; in addition, therapeutics for cystic fibrosis in particular must overcome mucosal barriers and avoid alveolar macrophages.[215] Intratracheal,[100] intrathecal,[237] and intraperitoneal[53,152] routes of administration of mRNA vectors have all been explored in the literature to target non-liver cells, but their clinical translatability remains to be seen.

In the realm of LNPs, it is probable that different routes of administration will require alternately-optimized LNP parameters based on how important serum stability, particle diffusion, particle size, particle charge, and other factors are in different environments. The mRNA itself may be able to be optimized based on the cell type in which it is being expressed. One potential example is for applications requiring secretion of translated protein, such as some protein replacement therapies or antibody-encoding mRNAs: there is evidence that different signal peptides in the mRNA sequence (which are responsible for protein secretion) may be poorly recognized by heterologous cells.[22] As such, it should be investigated if signal peptides can be

better optimized to increase secretion of the desired protein for these new routes of administration which target an array of different tissues.

7.2.4 Genome Editing

Genome engineering is a particularly exciting field which can benefit from mRNA delivery. CRISPR/Cas9 is a genome editing tool in which Cas9 nuclease (guided to a particular site on DNA by sgRNAs) makes a precise double strand break which can then be repaired through endogenous DNA repair mechanisms, sometimes via homology-directed repair when DNA donor template is provided.[204] This technique holds great therapeutic promise for genetic disorders as it can be used to permanently correct defective genes, but it also requires effective and safe delivery of CRISPR/Cas9 biomacromolecule components (Cas9 protein, sgRNA, optionally DNA donor template).[238] Historically, viral vectors have been used to deliver these materials, but delivery of Cas9 protein via mRNA is attractive for two main reasons. First, the large size of Cas9 makes it difficult to load into adeno-associated viral (AAV) vectors (which typically have a size limit of ~4.7 kb); second, transient expression of Cas9 nuclease from mRNA delivery could lead to fewer off-target effects than permanently integrated Cas9.

Our group recently reported a combination viral/non-viral CRISPR/Cas9 *in vivo* approach, in which Cas9 mRNA LNPs were co-delivered with AAV containing sgRNA and donor template.[239] It would be of great interest to co-deliver two (sgRNA + Cas9 mRNA) or all three CRISPR/Cas9 (sgRNA + Cas9 mRNA + donor template) components non-virally using a single LNP, but this approach presents multiple challenges. From a characterization level, quantifying the loading of each nucleic acid into the LNP would be difficult, as many fluorescence-based RNA detection assays cannot distinguish between different types of nucleic acid. Also, the ideal relative ratios of each encapsulated component is likely not 1:1:1; for example, a recently published study found efficacious gene editing *in vivo* at a 4:1 Cas9 mRNA:sgRNA wt. ratio,[229] but it is unclear

how much optimization was performed to arrive at this ratio. The timing of each component's delivery may also be important, as Cas9 mRNA would require some amount of time to translate into functional nuclease and sgRNA must survive long enough intracellularly to bind Cas9. Lastly, donor template DNA delivered via LNP must transfect the nucleus to undergo homology-directed repair; perhaps high doses of DNA template delivered via LNP may result in an extremely low but sufficient nucleus concentration for genome editing, or nuclear localization signals[240] can be incorporated into the DNA template.

Appendix A

Supplementary Figures

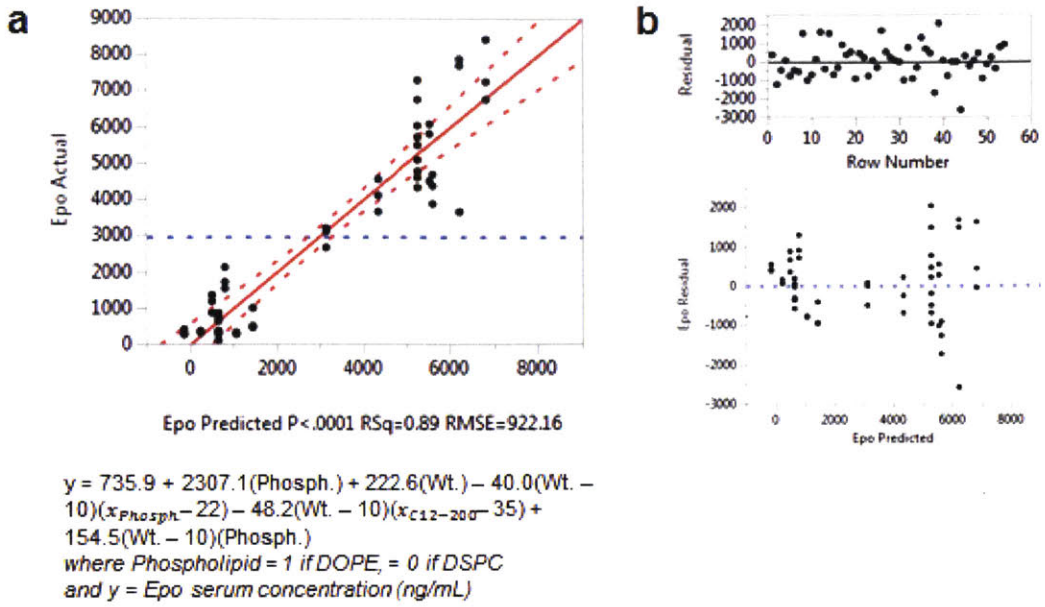

Figure A.2-1. Statistical information for the least-squares model to predict EPO serum concentration from Library B. (**a**) Actual by predicted plot for EPO serum concentration *(n = 1* each point). (**b**) Residual plots by row number and predicted, showing randomly dispersed residuals and thus a good-fitting model.

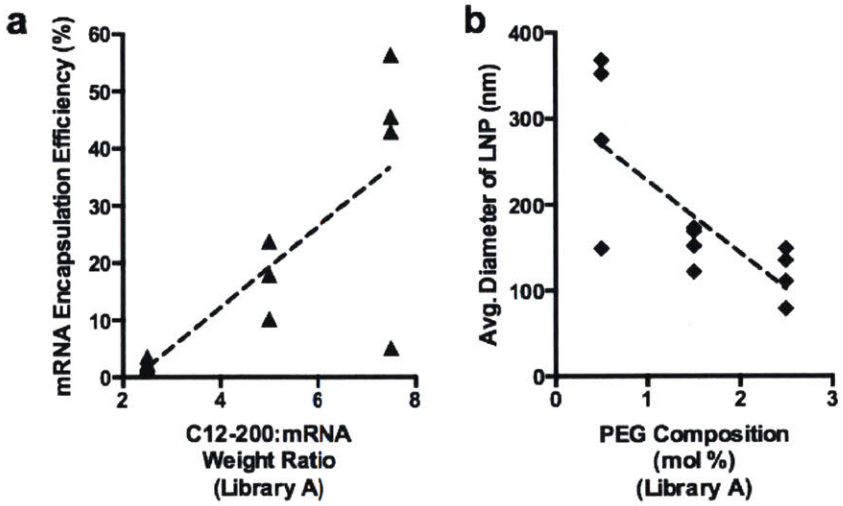

Figure A.2-2. Statistically significant orthogonal trends from Library A. (**a**) A statistically significant ($p < 0.05$) trend of increasing mRNA encapsulation efficiency was observed with increasing C12-200:mRNA weight ratio for Library A formulations, independent of the other formulation parameters *(n = 1* each point*)*. (**b**) A statistically significant ($p < 0.05$) trend of decreasing LNP size was observed with increasing molar PEG composition for Library A formulations, independent of the other formulation parameters (*n = 1* each point).

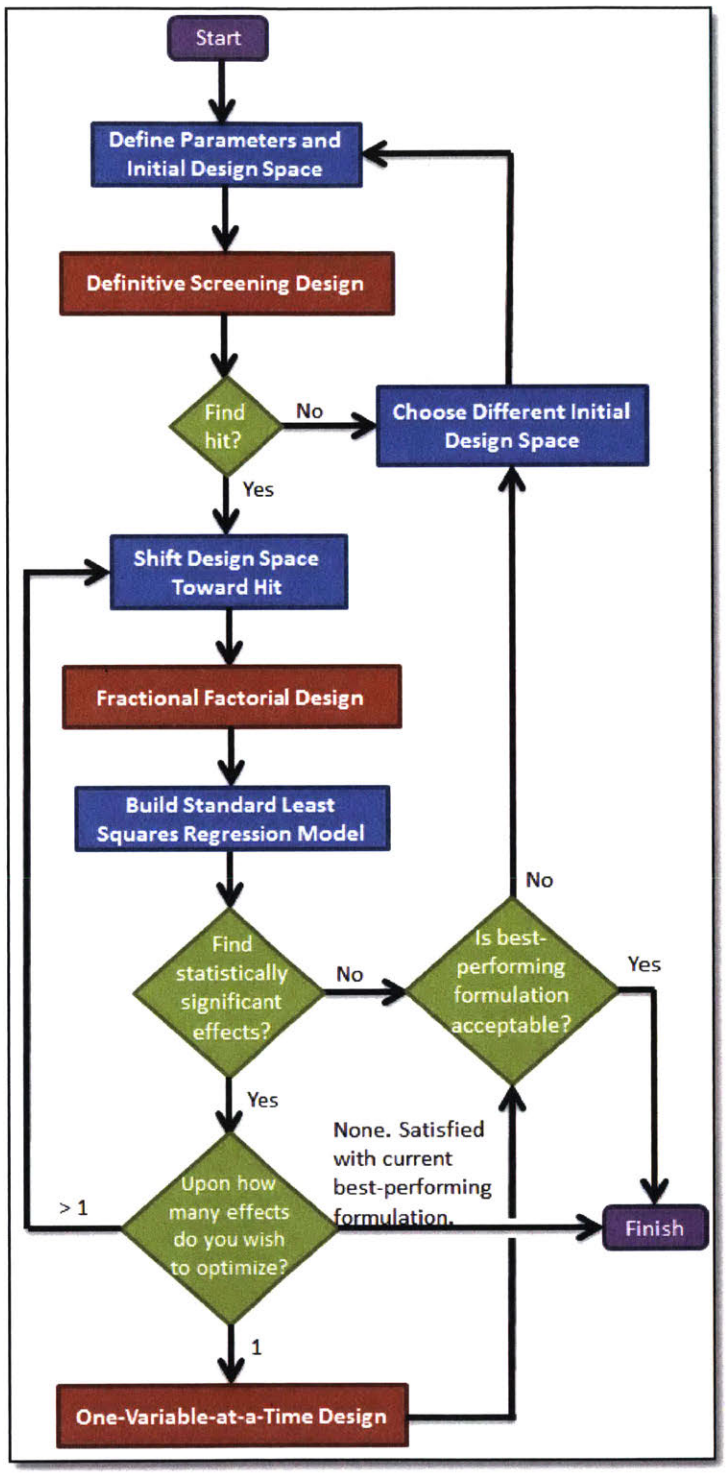

Figure A.2-3. Flowchart of DOE methodology. A general methodology is presented for the optimization of nanoparticle formulations *in vivo*.

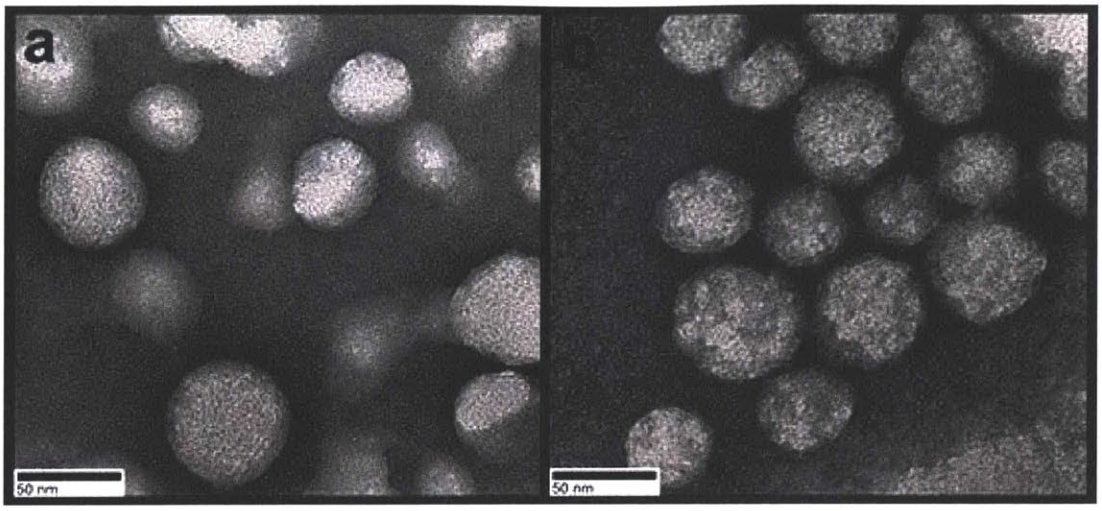

Figure A.2-4. Transmission Electron Microscope (TEM) images of LNP formulations. (**a**) TEM image of the original mRNA-loaded LNP formulation. (**b**) TEM image of the optimized mRNA-loaded LNP formulation C-35.

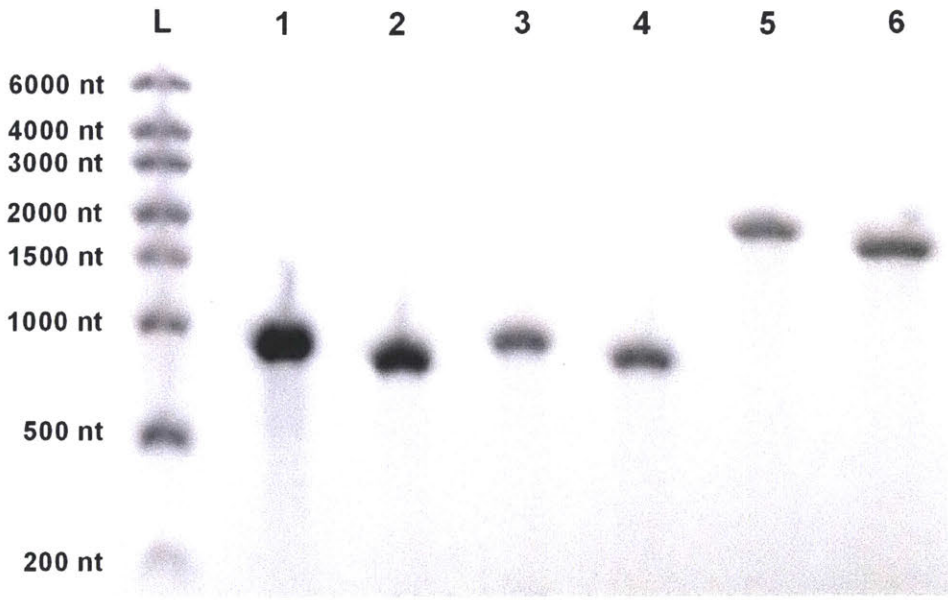

Figure A.3-1. Electrophoresis on 1% agarose gel with all six mRNAs used in the study. L = ladder, 1 = unmodified scramble mRNA, 2 = PseudoU scramble mRNA, 3 = unmodified EPO mRNA, 4 = PseudoU EPO mRNA, 5 = unmodified Luc mRNA, 6 = PseudoU Luc mRNA.

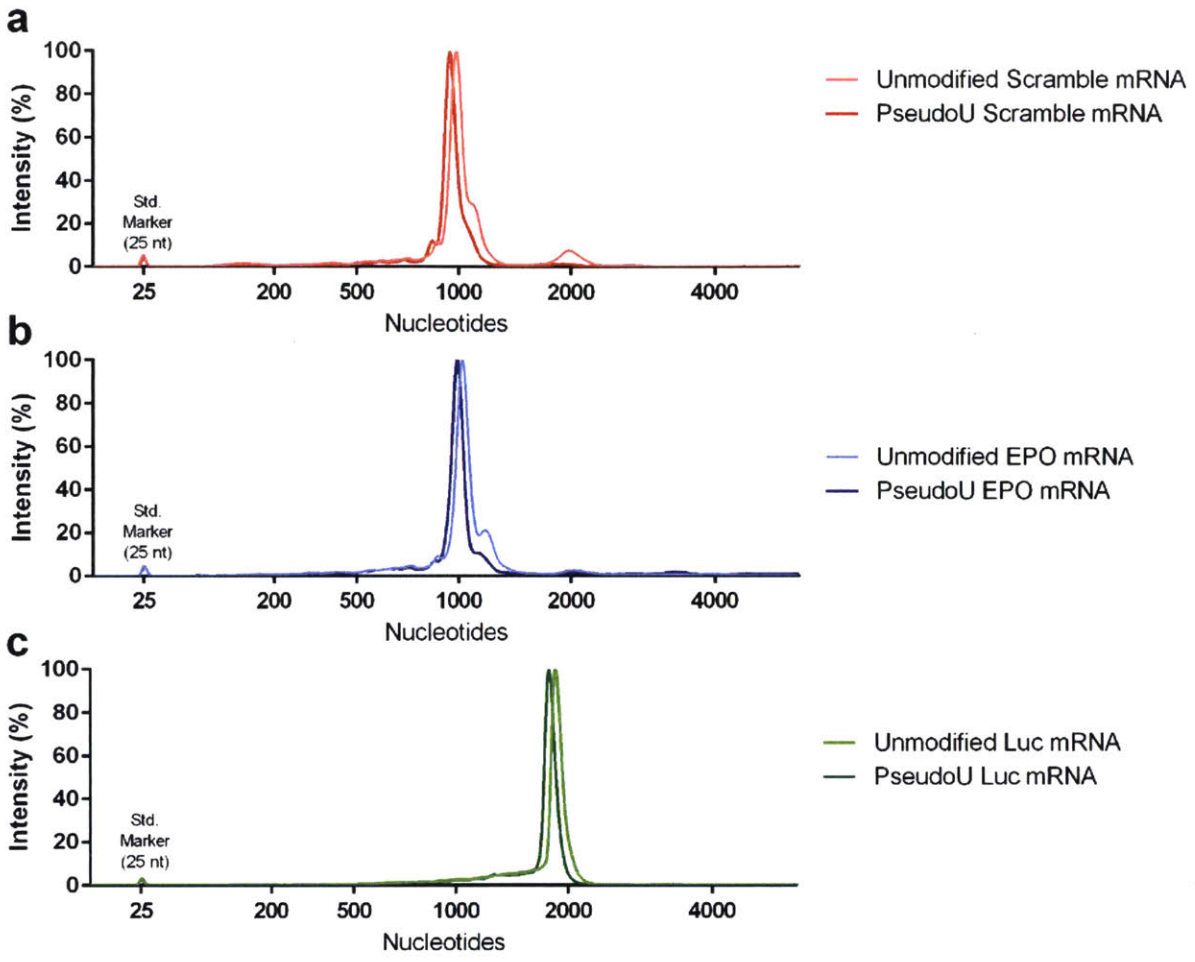

Figure A.3-2. Electrophoresis size fractionation performed by an Agilent Bioanalyzer on all six mRNAs used in the study. (a) Unmodified and PseudoU scramble mRNA. Small peak (7%) at 1975 nt for unmodified scramble mRNA is double the expected length and is likely duplexed mRNA. (b) Unmodified and PseudoU EPO mRNA. (c) Unmodified and PseudoU Luc mRNA.

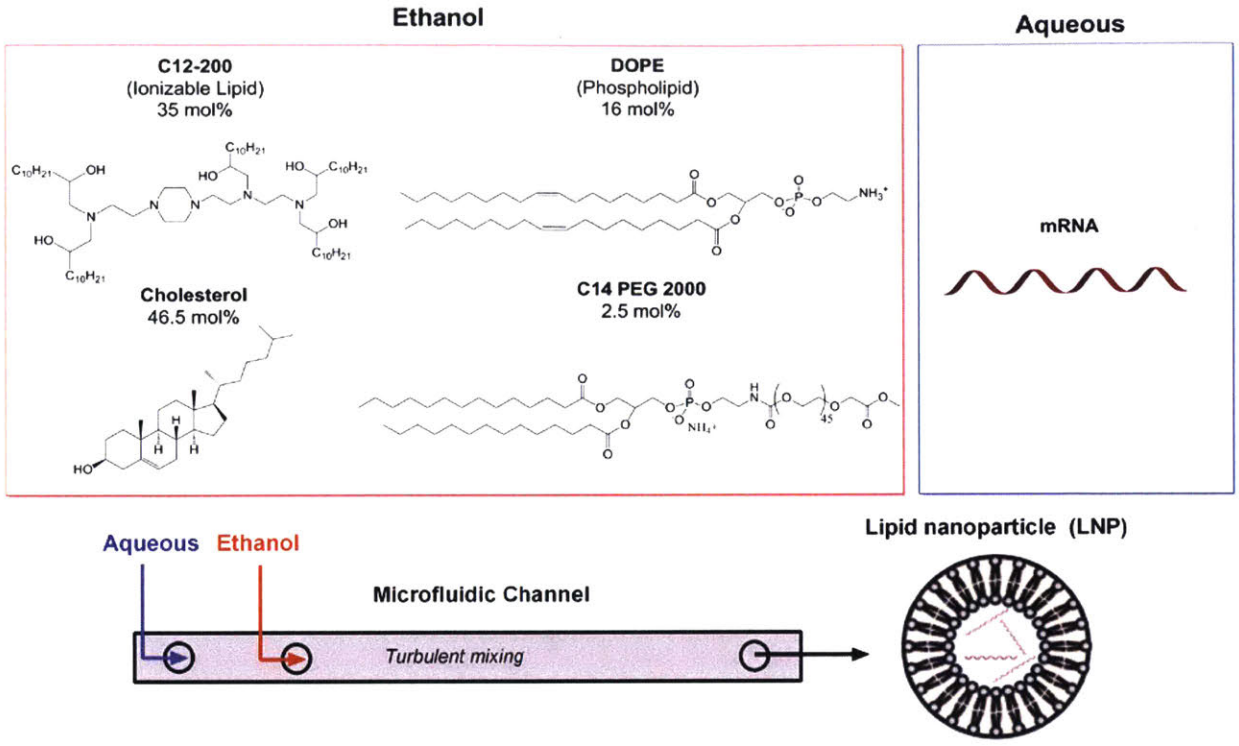

Figure A.3-3. Formulation process to make mRNA-loaded C12-200 lipid nanoparticles. An ethanolic lipid solution is mixed with an aqueous mRNA solution in a microfluidic chip to yield LNPs.

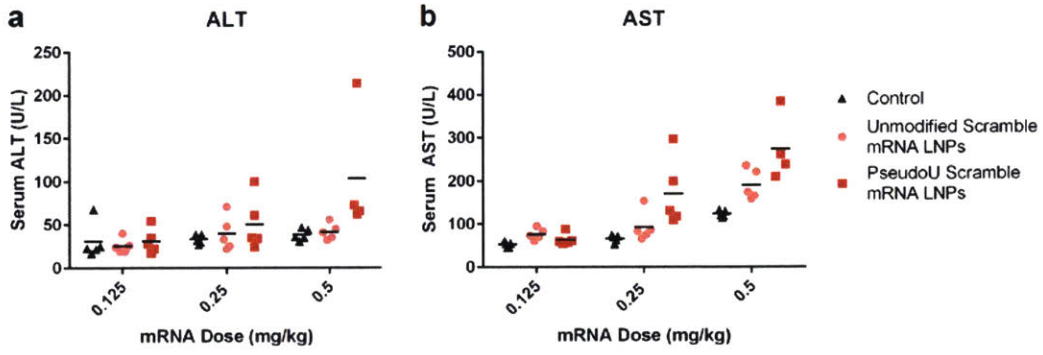

Figure A.3-4. Serum liver enzyme levels 6 hr post-i.v. injection of mRNA-LNPs. (**a**) Alanine aminotransferase (ALT) concentration. (**b**) Aspartate aminotransferase (AST) concentration.

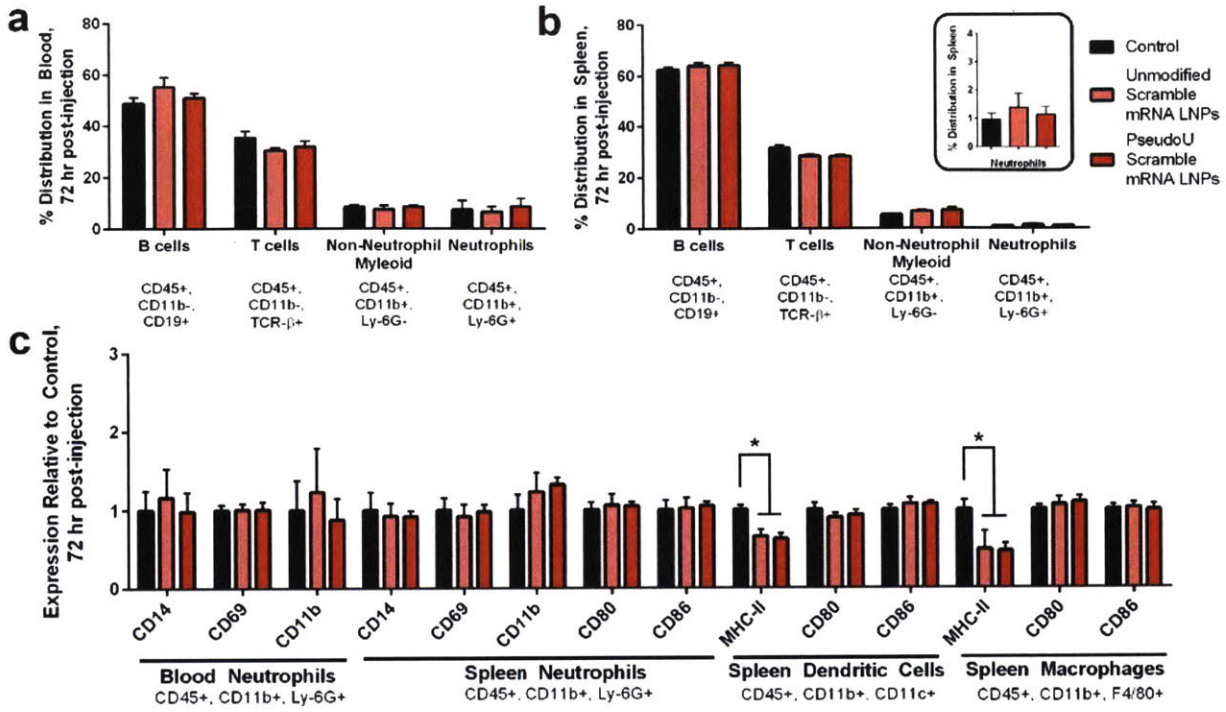

Figure A.3-5: Neutrophilia and activation not observed with mRNA-LNPs at 72 hr post-i.v. injection. (**a**) Immune cell (CD45+) distribution in the blood as measured by FACS. (**b**) Immune cell (CD45+) distribution in the spleen as measured by FACS. (**c**) Activation of neutrophils in the blood and spleen, and activation of dendritic cells and macrophages in the spleen as measured by FACS. Significantly lower MHC-II expression is observed in splenic dendritic cells and macrophages after mRNA-LNP treatment 72 hr post-injection, but no marker expression is increased over control. All data presented as mean +/- std. dev. (n = 4).

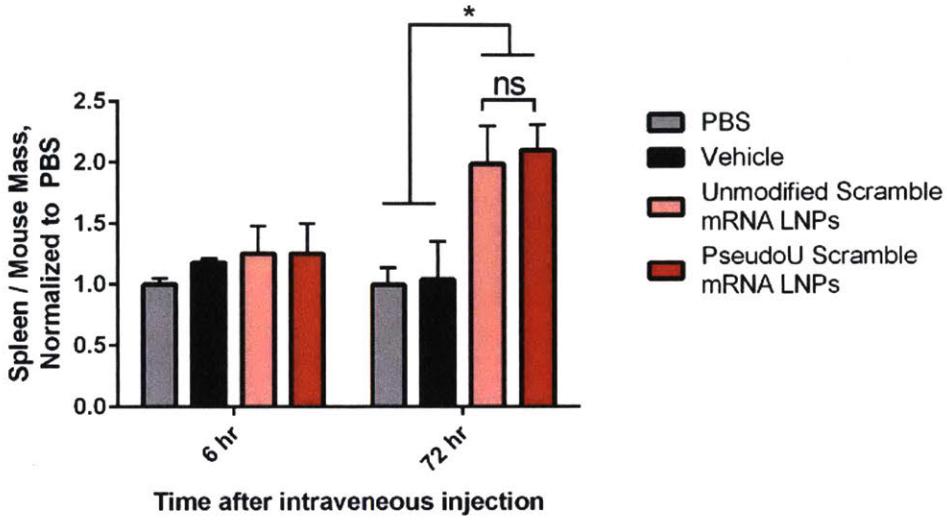

Figure A.3-6: Spleen mass at 72 hr post-injection with mRNA-LNPs. Asterisk represents statistical significance. Data presented as mean +/- std. dev. (n = 4).

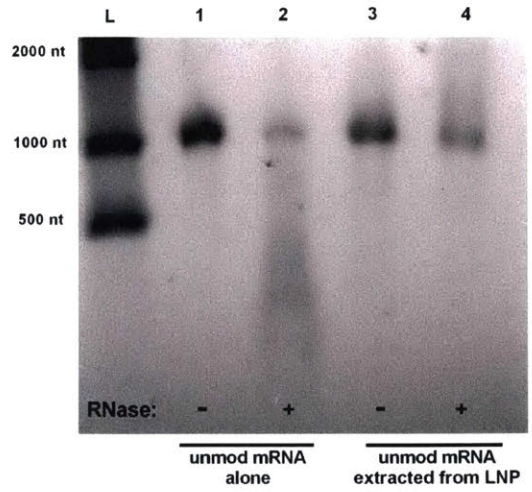

Figure A.3-7. LNPs protect encapsulated unmodified mRNA from degradation by exposure to RNase. L = ladder, 1 = unmod EPO mRNA, 2 = unmod EPO mRNA treated with RNase, 3 = unmod EPO mRNA extracted from LNP, 4 = unmod EPO mRNA extracted from LNP treated with RNase.

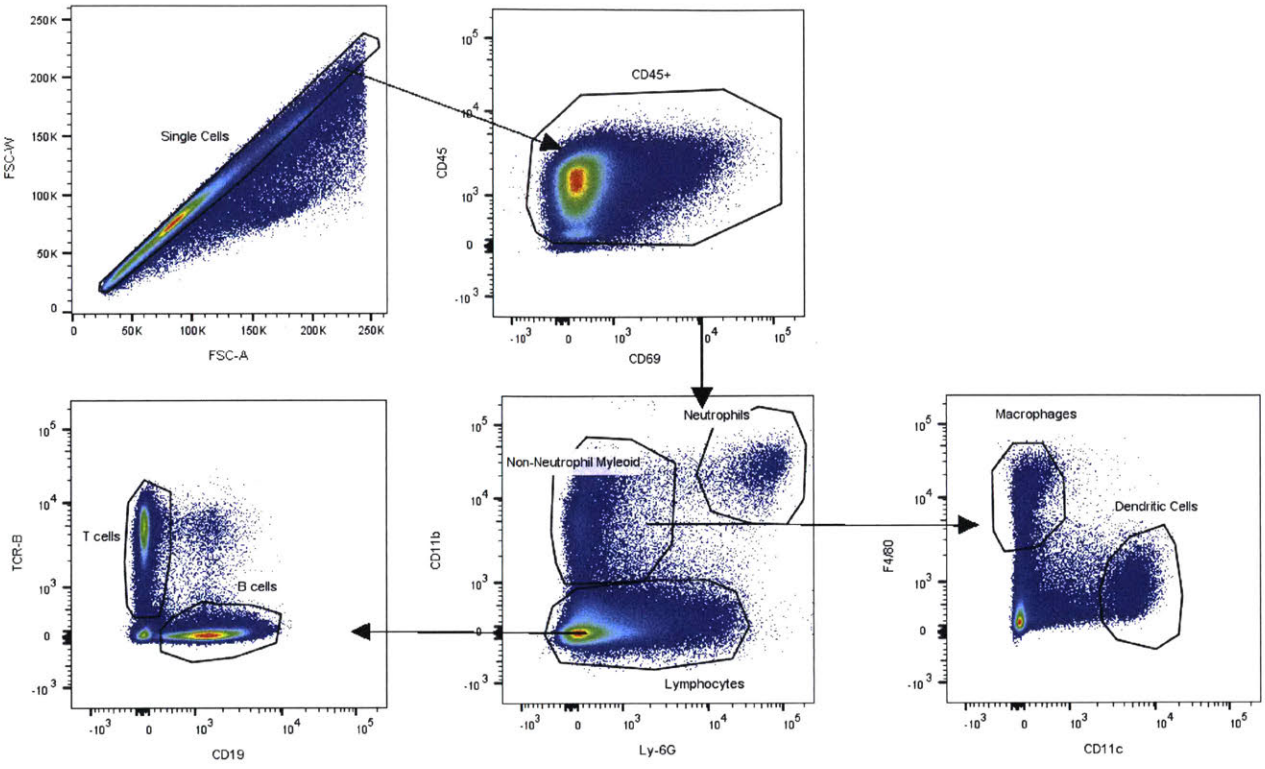

Figure A.3-8. Gating strategy to distinguish cell types. Representative spleen is shown. Single cells were identified as falling along the diagonal of FSC-A vs. FSC-W. Neutrophils were identified as $CD45^+$, $CD11b^+$, $Ly\text{-}6G^+$. Lymphocytes were identified as $CD45^+$, $CD11b^-$, $Ly\text{-}6G^-$ and were further differentiated into T cells ($TCR\text{-}\beta^+$, $CD19^-$) and B cells ($TCR\text{-}\beta^-$, $CD19^+$). Non-neutrophil myeloid were identified as $CD45^+$, $CD11b^+$, $Ly\text{-}6G^-$ and for spleens were further differentiated into macrophages ($F4/80^+$, $CD11c^-$) and dendritic cells (DCs, $F4/80^-$, $CD11c^+$).

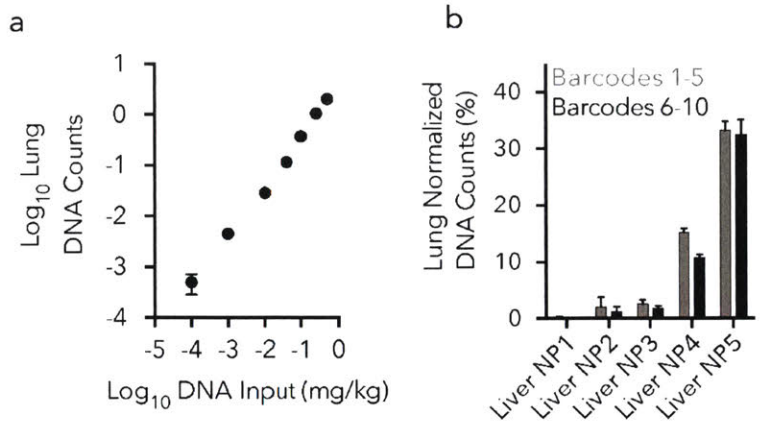

Figure A.5-1. DNA barcoded nanoparticle biodistribution provides a linear output. (a) DNA barcode counts in the liver 4 hours after the administration of an 'in vivo standard curve'. The same C12-200 nanoparticle formulation was made 7 separate times, with 7 different barcodes. These solutions were mixed together at different doses (inputs) to form an 'in vivo standard curve'. DNA readouts align with this DNA input at doses between 0.0001 and 0.5 mg/kg DNA barcode. N = 5 mice / group. **(b)** Normalized DNA barcode counts in lung 4 hours after administration of different DNA sequences. 5 different C12-200 NPs were formulated twice, each with a different barcode. N = 5 mice / group. In all cases, the data are plotted as average + / - standard deviation.

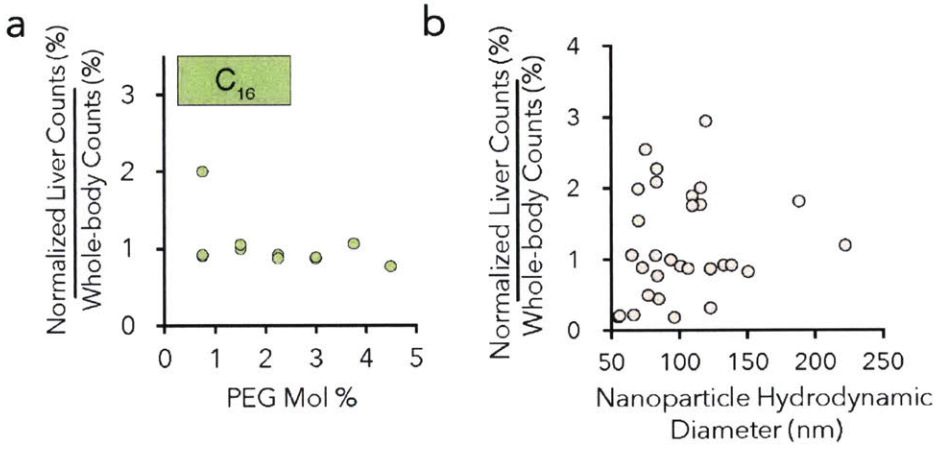

Figure A.5-2. Liver delivery as a function of LNP properties (a) Normalized liver counts, divided by the normalized counts for the rest of the tested tissues, as a function of PEG mole percentage. This measure quantifies how delivery to the liver, compared to the rest of the body, changes. **(b)** Normalized liver counts, divided by the normalized counts for the rest of the tested tissues, as a function of nanoparticle diameter.

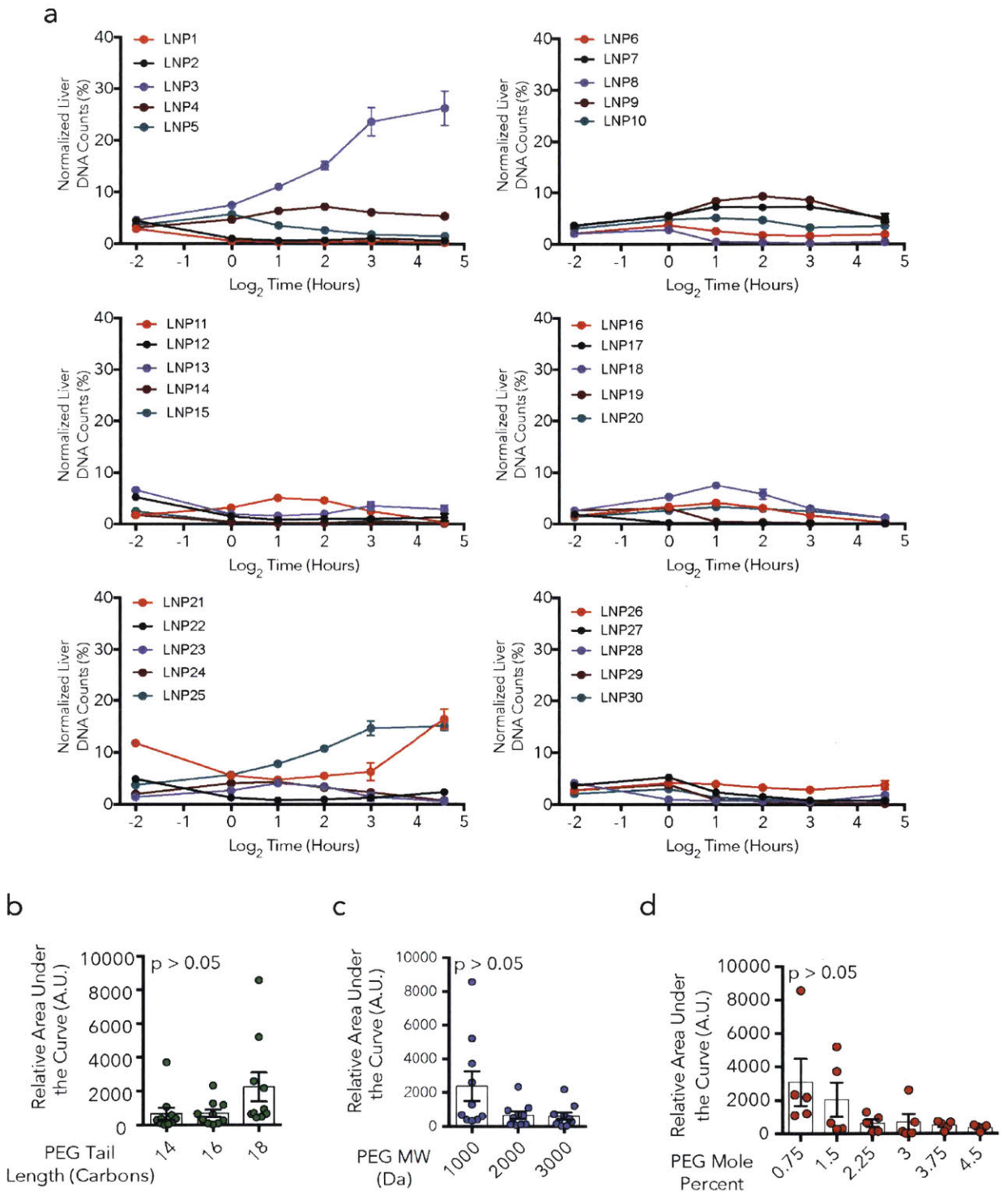

Figure A.5-3. Pharmacokinetics of 30 LNP library in the liver. (a) Normalized liver DNA counts for thirty nanoparticles between 0.25 and 24 hours after injection. **(b-d)** Area under the curve for 30 nanoparticles in the liver, as a function of PEG lipid length, PEG molecular weight, or mole % PEG, respectively.

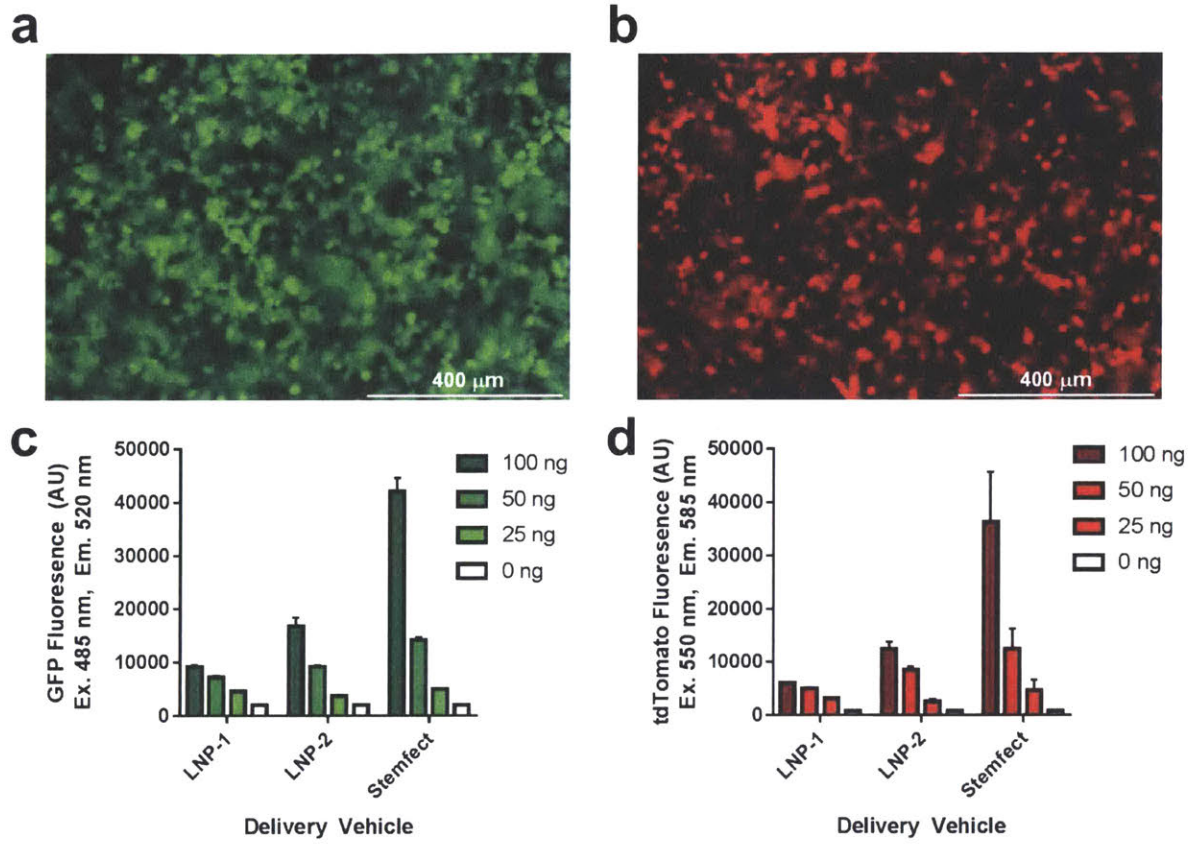

Figure A.6-1. ***In vitro*** **transfection of GFP and tdTomato-encoding mRNAs. (a)** Fluorescent microscopy with GFP light cube (Ex. 470 nm, Em. 510 nm) of HeLa cells treated with 100 ng of GFP mRNA + Stemfect, **(b)** Fluorescent micrscopy with RFP light cube (Ex. 531 nm, Em. 593 nm) of HeLa cells treated with 100 ng of tdTomato mRNA + Stemfect, **(c)** Quantification of GFP fluoresence of HeLa cells treated with GFP mRNA LNP-1, LNP-2, or Stemfect, **(d)** Quantification of tdTomato fluoresence of HeLa cells treated with tdTomato mRNA LNP-1, LNP-2, or Stemfect. Data in (c) and (d) presented as mean + standard deviation, $n = 4$.

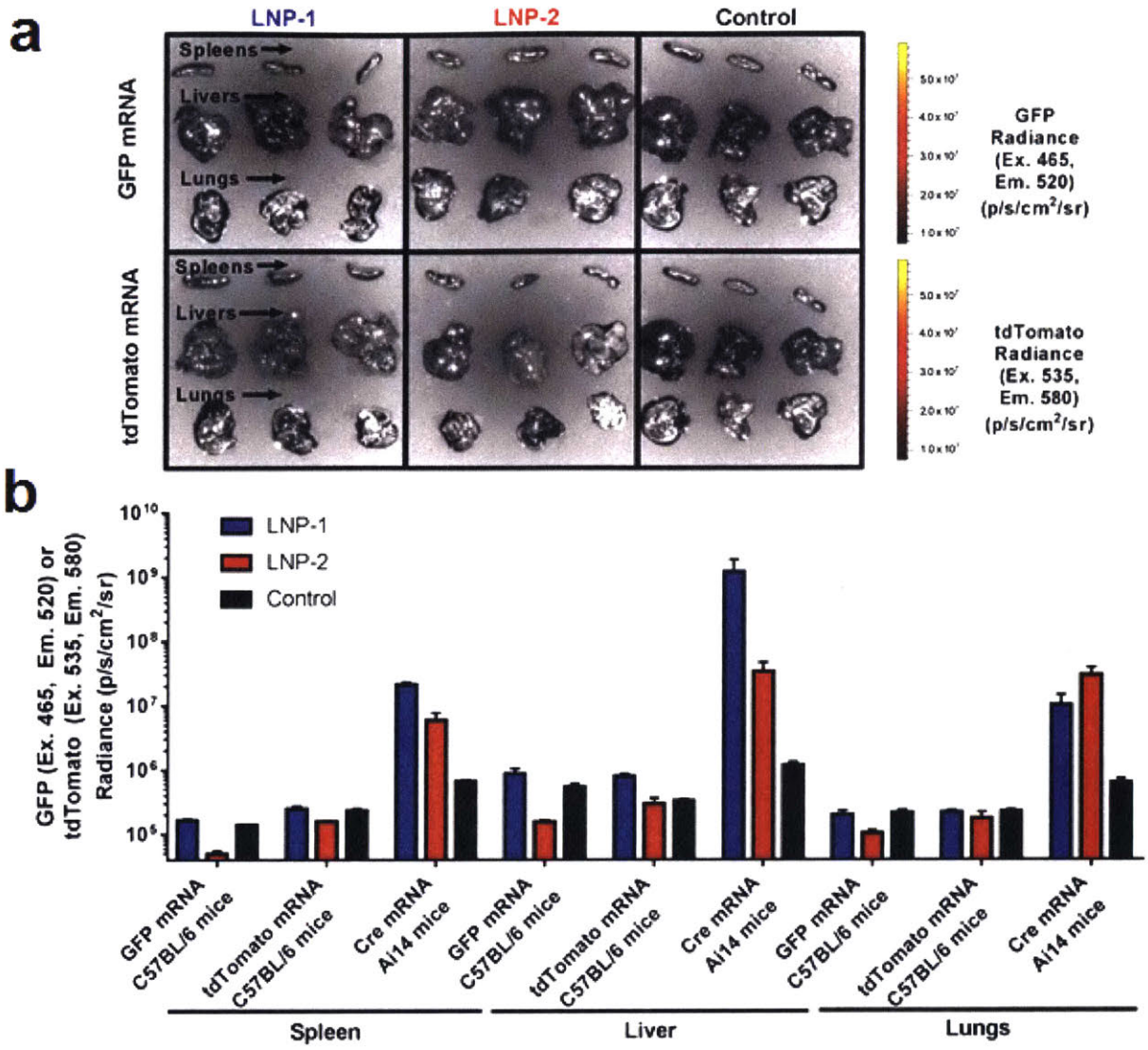

Figure A.6-2. Whole organ fluorescence of GFP and tdTomato encoding mRNAs. (a) Whole organ fluorescence of spleens, livers, and lungs for C57BL/6 mice treated with GFP mRNA LNPs (top row) or tdTomato mRNA LNPs (bottom row) as determined by IVIS. **(b)** Quantification of fluorescence for (a) along with Ai14/Cre mRNA mouse model for comparison (quantification of Fig. 6-2a,b); data presented as mean + standard deviation, $n = 3$.

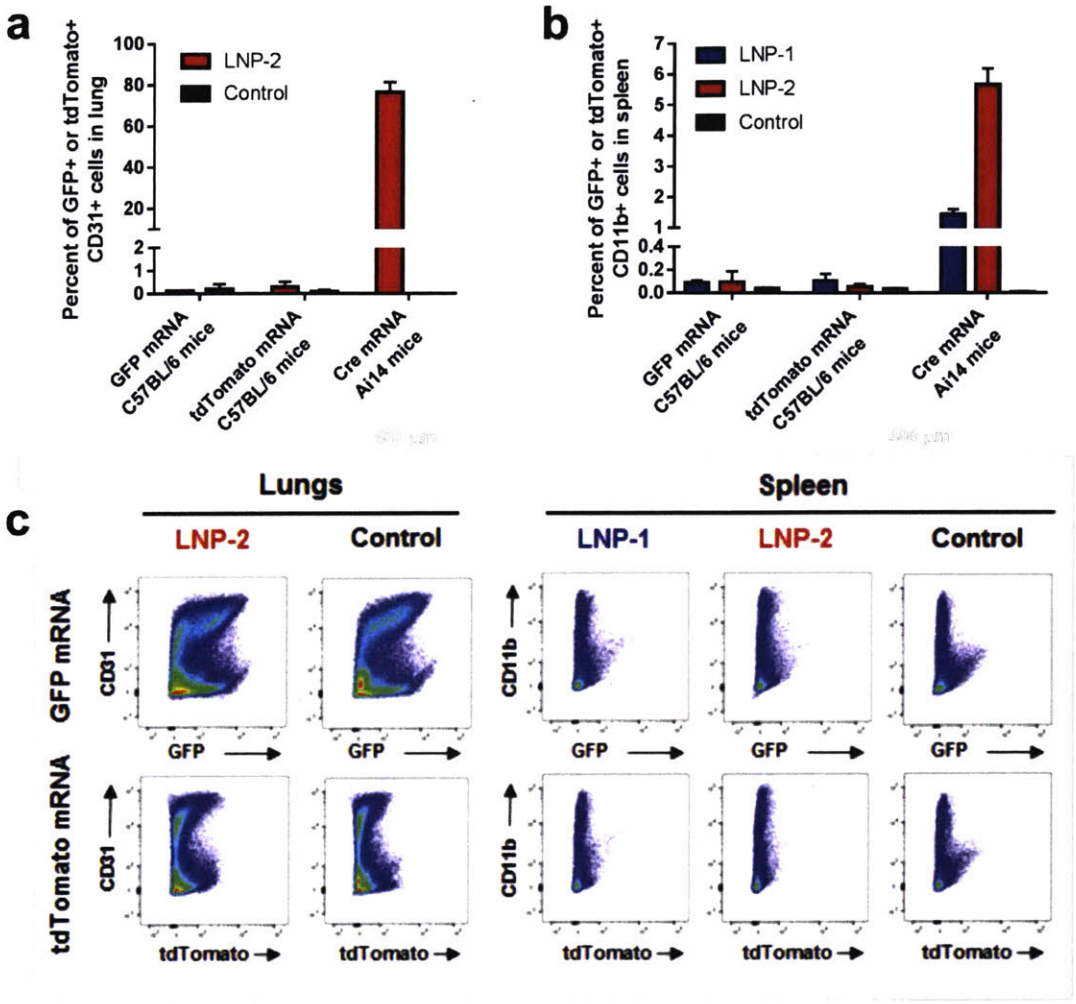

Figure A.6-3. Single cell analysis of GFP and tdTomato-encoding mRNAs by flow cytometry. (a) Percent of GFP+ or tdTomato+ lung CD31+ cells by flow cytometry with GFP/tdTomato mRNA in C57BL/6 mice or Cre mRNA in Ai14 mice for comparison; data presented as mean + standard deviation, n = 3, **(b)** Percent of GFP+ or tdTomato+ spleen CD45+ cells by flow cytometry with GFP/tdTomato mRNA in C57BL/6 mice or Cre mRNA in Ai14 mice for comparison, **(c)** Flow cytometry plots of lung (left) and spleen (right) for GFP or tdTomato mRNA LNP-treated C57BL/6 mice.

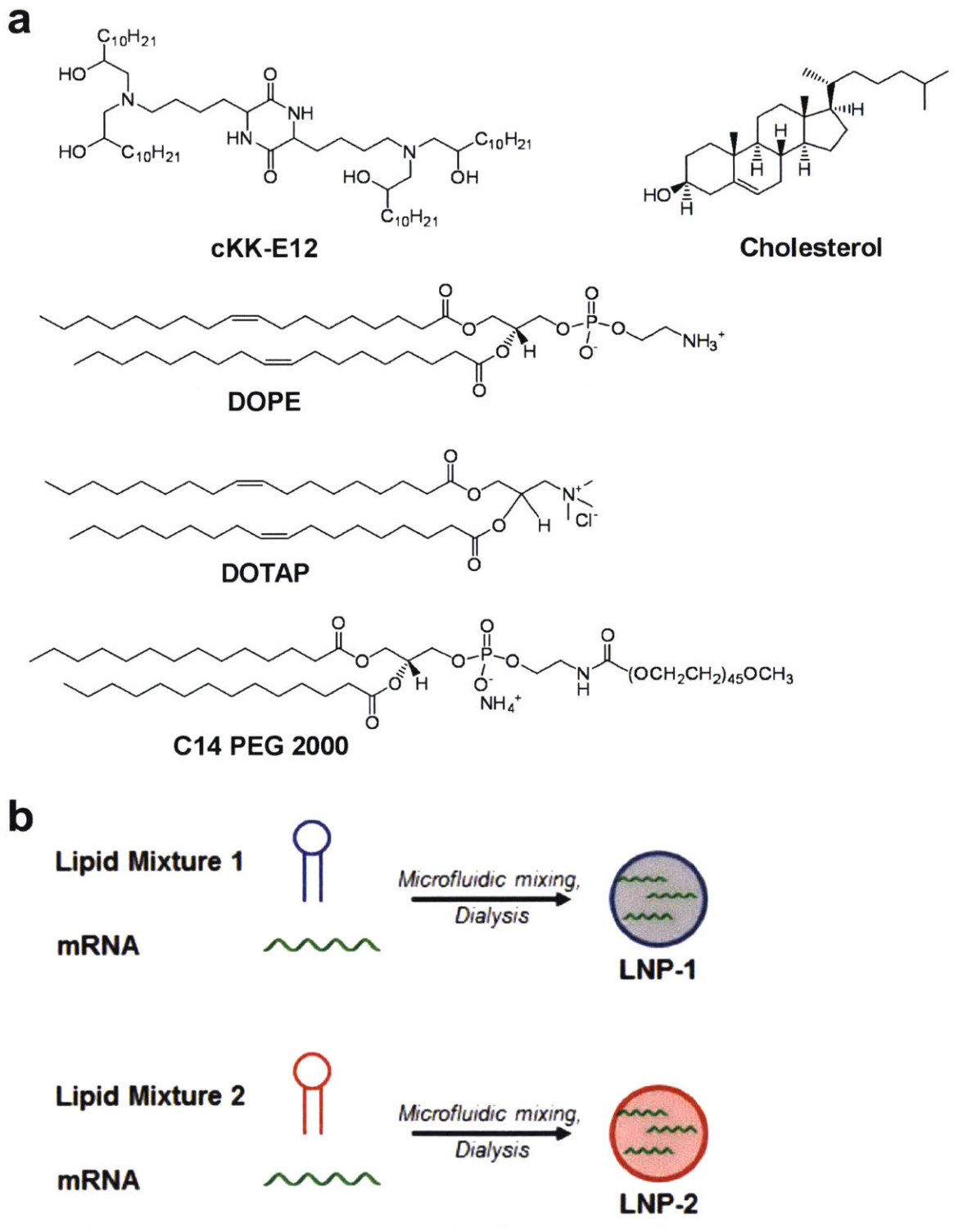

Figure A.6-4. Formulation of LNPs. (a) Chemical structures of lipids used to make LNP-1 and LNP-2 (compositions found in **Table B.6-1**), **(b)** Process for LNP formulation.

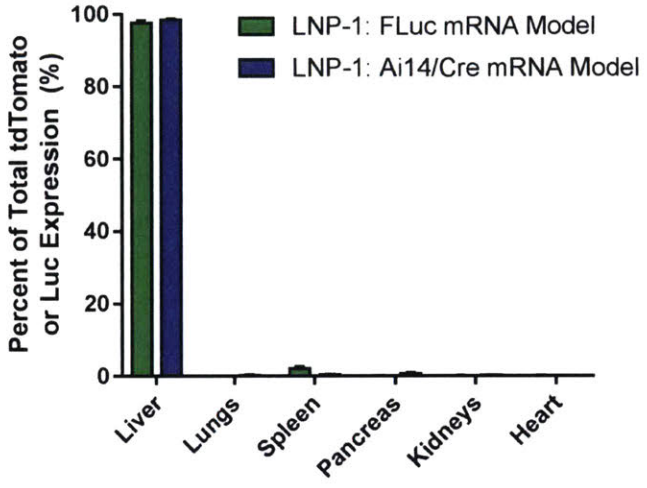

Figure A.6-5. Comparison of biodistribution between Luc and Ai14/Cre mRNA models for LNP-1., LNP-1 formulated with Luc mRNA was administered to C57BL/6 mice and was previously published in Fenton et al.[140] LNP-1 formulated with Cre mRNA was administered to Ai14 mice. Data presented as mean + standard deviation, $n = 3$.

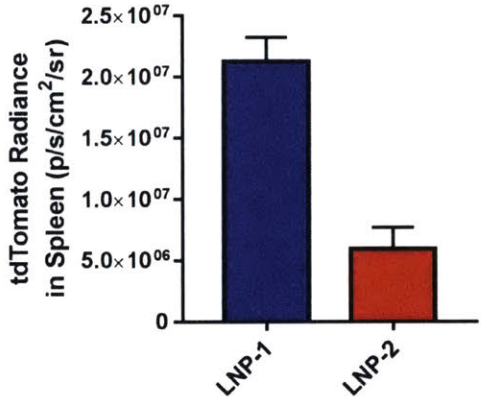

Figure A.6-6. Total spleen tdTomato fluorescence in Ai14 mice following Cre mRNA-LNP administration, data presented as mean + standard deviation, $n = 3$.

Appendix B

Supplementary Tables

Table B.2-1. Parameters and characterization of all Chapter 2 LNP formulations

Code	C12-200:mRNA Weight Ratio	Phosph.	Molar Composition (%)				EE (%)	Size (nm)	PDI	Serum EPO (ng/mL)
			C12-200	Phosph.	Chol.	PEG				
PBS	n/a	n/a	n/a	n/a	n/a	n/a	n/a	n/a	n/a	0.018 ± 0.002
Original	5	DSPC	50	10	38.5	1.5	24	152	0.102	962 ± 141
A-01	7.5	DOPE	60	4	33.5	2.5	5	111	0.182	169 ± 14
A-02	7.5	DOPE	40	16	42.5	1.5	56	122	0.121	6445 ± 1237
A-03	2.5	DOPC	60	16	31.5	2.5	4	135	0.341	176 ± 21
A-04	2.5	DSPC	60	4	34.5	1.5	1	169	0.217	72 ± 4
A-05	2.5	DOPE	60	10	29.5	0.5	2	275	0.173	86 ± 5
A-06	5	DOPC	40	4	55.5	0.5	18	352	0.200	297 ± 18
A-07	5	DSPE	50	10	38.5	1.5	*	*	*	*
A-08	2.5	DOPE	40	4	53.5	2.5	2	149	0.341	238 ± 20
A-09	7.5	DSPC	40	10	47.5	2.5	46	79	0.177	2072 ± 302
A-10	7.5	DSPC	60	16	23.5	0.5	43	149	0.212	443 ± 104
A-11	2.5	DSPC	40	16	43.5	0.5	2	368	0.430	86 ± 2
A-12	5	DSPE	60	16	21.5	2.5	*	*	*	*
A-13	5	DOPC	50	10	38.5	1.5	10	173	0.151	595 ± 225
A-14	7.5	DSPE	50	4	45.5	0.5	*	*	*	*
B-15	7.5	DSPC	30	22	45.5	2.5	59	95	0.336	326 ± 85
B-16	12.5	DOPE	40	22	35	3	30	117	0.195	4307 ± 403
B-17	10	DOPE	40	28	29.5	2.5	42	113	0.168	5937 ± 1272
B-18	10	DSPC	40	22	35.5	2.5	55	88	0.245	753 ± 88
B-19	7.5	DSPC	35	28	34	3	46	89	0.228	285 ± 14
B-20	7.5	DOPE	30	16	51.5	2.5	24	109	0.284	2989 ± 307
B-21	10	DSPC	35	16	45.5	3.5	40	77	0.196	348 ± 262
B-22	12.5	DOPE	30	28	38.5	3.5	42	87	0.182	6400 ± 2405
B-23	7.5	DOPE	40	28	28.5	3.5	32	85	0.208	5464 ± 843
B-24	7.5	DOPE	35	22	40	3	39	96	0.154	4084 ± 452
B-25	12.5	DSPC	35	28	34.5	2.5	58	109	0.303	316 ± 58
B-26	12.5	DOPE	35	16	46.5	2.5	44	89	0.174	7485 ± 854
B-27	12.5	DSPC	30	22	44.5	3.5	57	74	0.328	648 ± 311
B-28	10	DOPE	35	22	39.5	3.5	35	93	0.205	5960 ± 834
B-29	10	DOPE	30	16	51	3	38	77	0.198	4792 ± 620
B-30	10	DSPC	30	28	39	3	60	86	0.287	293 ± 13
B-31	12.5	DSPC	40	16	41	3	45	65	0.396	1795 ± 298
B-32	7.5	DSPC	40	16	40.5	3.5	39	64	0.295	1126 ± 260
C-33	5	DOPE	35	16	46.5	2.5	33	106	0.216	3134 ± 502
C-34	7.5	DOPE	35	16	46.5	2.5	40	106	0.159	4504 ± 586
C-35	10	DOPE	35	16	46.5	2.5	43	102	0.158	7065 ± 513
C-36	15	DOPE	35	16	46.5	2.5	48	102	0.147	7548 ± 208
C-37	20	DOPE	35	16	46.5	2.5	53	98	0.177	7268 ± 366
C-38	25	DOPE	35	16	46.5	2.5	52	109	0.151	6179 ± 361

PBS = phosphate buffered saline, EE = Encapsulation Efficiency, PDI = polydispersity index, phospholipid abbreviations: DS = 1,2-distearyol-*sn*-glycero- (saturated tail), DO = 1,2-dioleoyl-*sn*-glycero- (Δ9-cis unsaturated tail), PC = 3-phosphocholine (primary amine head group), PE = 3-phosphoethanolamine (quaternary amine head group), Serum EPO reported as mean ± SD (n = 3) 6 hr after 15 μg total mRNA intravenous injection into mice, * indicates that LNP could not be synthesized due to insolubility of DSPE in ethanol at all concentrations tested

Table B.2-2. Statistical information for the Standard Least Squares regression model used to analyze EPO production in Library B.

Summary of Fit	
R^2	0.887
Adjusted R^2	0.875
Root Mean Square Error	922.2
Mean	2961.6
n	54

ANOVA Results			
Source	Degrees of Freedom	Sum of Squares	Mean Square
Model	5	319139752	63827950
Error	48	40818601	850387
Total	53	359958353	
F-Test Results			
	F Ratio	Prob > F	
ANOVA	75.06	< 0.0001	

Parameter Estimates				
Term in Model	**Estimate**	**Std. Error**	**t Ratio**	**Prob > |t|**
Intercept	735.9	627.4	1.17	0.2466
Phospholipid[DOPE]	2307.1	125.5	18.38	< 0.0001
Wt. Ratio	222.6	61.5	3.62	0.0007
(Wt. Ratio - 10) x ($x_{Phospholipid}$ - 22)	-40.0	12.6	-3.16	0.0027
(Wt. Ratio - 10) x ($x_{C12\text{-}200}$- 35)	-48.2	15.2	-3.18	0.0026
(Wt. Ratio - 10) x (Phospholipid[DOPE])	154.5	61.5	2.51	0.0154

Effect Tests			
Effect	**Sum of Squares**	**F Ratio**	**Prob > F**
Phospholipid	287429131	338	< 0.0001
Wt. Ratio	11145582	13.1	0.0007
(Wt. Ratio) x ($x_{Phospholipid}$)	8512352	10.0	0.0027
(Wt. Ratio) x ($x_{C12\text{-}200}$)	8582877	10.1	0.0026
(Wt. Ratio) x (Phospholipid)	5369261	6.31	0.0154

Table B.2-3. Parameters and characterization of LNPs made with luciferase mRNA

Code	C12-200:mRNA Weight Ratio	Phosph.	Molar Composition (%)				EE (%)	Size (nm)	PDI	Total Flux (p/s) x 10^9
			C12-200	Phosph.	Chol.	PEG				
Original, Luc	5	DSPC	50	10	38.5	1.5	27	113	0.147	0.99 ± 0.44
C-35, Luc	10	DOPE	35	16	46.5	2.5	48	82	0.221	3.21 ± 1.18

EE = Encapsulation Efficiency, PDI = polydispersity index, phospholipid abbreviations: DS = 1,2-distearyol-*sn*-glycero- (saturated tail), DO = 1,2-dioleoyl-*sn*-glycero- (Δ9-cis unsaturated tail), PC = 3-phosphocholine (primary amine head group), PE = 3-phosphoethanolamine (quaternary amine head group), Total flux from luminesence reported as mean ± SD (n = 3) after 6 hr after intravenous injection of 15 μg total mRNA

Table B.2-4. Parameters and characterization of LNPs made with FVII siRNA.

Code	C12-200:siRNA Weight Ratio	Phosph.	Molar Composition (%)				EE (%)	Size (nm)	PDI	Serum FVII (%)
			C12-200	Phosph.	Chol.	PEG				
PBS	n/a	n/a	n/a	n/a	n/a	n/a	n/a	n/a	n/a	100 ± 18
Original, siFVII	5	DSPC	50	10	38.5	1.5	59	65	0.150	0.1 mg/kg: 10 ± 3 0.03 mg/kg: 43 ± 12 0.01 mg/kg: 79 ± 9
C-35, siFVII	10	DOPE	35	16	46.5	2.5	58	109	0.288	0.1 mg/kg: 7 ± 1 0.03 mg/kg: 48 ± 5 0.01 mg/kg: 76 ± 9

PBS = phosphate buffered saline, EE = Encapsulation Efficiency, PDI = polydispersity index, phospholipid abbreviations: DS = 1,2-distearyol-*sn*-glycero- (saturated tail), DO = 1,2-dioleoyl-*sn*-glycero- (Δ9-cis unsaturated tail), PC = 3-phosphocholine (primary amine head group), PE = 3-phosphoethanolamine (quaternary amine head group), FVII (Factor VII) expression reported as mean ± SD (n = 3) after 72 hr after intravenous injection of indicated total dose of siRNA.

Table B.3-1. Representative yields for in vitro transcription (IVT) of PseudoU-modified scramble mRNA. Yields of PseudoU-modified scramble mRNA are given with respect to unmodified scramble mRNA at each step after purification (i.e. unmodified mRNA yield was set to 100%)

Step #	mRNA	PseudoU mRNA Yield
1	Post-IVT (uncapped, untailed)	42%
2	Post-capping (untailed)	46%
3	Post-tailing (whole mRNA)	40%

Table B.5-1. DNA barcodes and PCR-based barcode amplification. (a) Up to 30 different nanoparticles were analyzed in the same mouse using the following thirty sequences. The barcodes were subdivided into 'universal' sites, which were the same for all sequences, and unique barcodes, which varied with each sequence. The random sequence was inserted to monitor potentially excessive PCR amplification. **(b)** PCR primers used to amplify the DNA sequences. The three primers were added together in a PCR reaction. The Index base was added at 1/10th the concentration of the Universal Reverse and Index Final Forward Primers. The PCR conditions are outlined in detail in the Methods Section. The * refers to a phosphorothioate-modifed linkage, and N's represent random nucleotides.

a

	Universal Site 1, 'Barcode Sequence', Random Sequence, Universal Site 2
Barcode 1	A*G*A*CGTGTGCTCTTCCGATCT GAGGGTACTT NNNNNNNNNN AGATCGGAAGAGCGTCG*T*G*T
Barcode 2	A*G*A*CGTGTGCTCTTCCGATCT GACAATTGCC NNNNNNNNNN AGATCGGAAGAGCGTCG*T*G*T
Barcode 3	A*G*A*CGTGTGCTCTTCCGATCT TAACGCACCT NNNNNNNNNN AGATCGGAAGAGCGTCG*T*G*T
Barcode 4	A*G*A*CGTGTGCTCTTCCGATCT ATGATCGTCG NNNNNNNNNN AGATCGGAAGAGCGTCG*T*G*T
Barcode 5	A*G*A*CGTGTGCTCTTCCGATCT TGTCTCCCAT NNNNNNNNNN AGATCGGAAGAGCGTCG*T*G*T
Barcode 6	A*G*A*CGTGTGCTCTTCCGATCT GGAGAAACAG NNNNNNNNNN AGATCGGAAGAGCGTCG*T*G*T
Barcode 7	A*G*A*CGTGTGCTCTTCCGATCT CGTACAAACG NNNNNNNNNN AGATCGGAAGAGCGTCG*T*G*T
Barcode 8	A*G*A*CGTGTGCTCTTCCGATCT GATTTGTGGG NNNNNNNNNN AGATCGGAAGAGCGTCG*T*G*T
Barcode 9	A*G*A*CGTGTGCTCTTCCGATCT TTGCAGCCTT NNNNNNNNNN AGATCGGAAGAGCGTCG*T*G*T
Barcode 10	A*G*A*CGTGTGCTCTTCCGATCT GAATGCTGAC NNNNNNNNNN AGATCGGAAGAGCGTCG*T*G*T
Barcode 11	A*G*A*CGTGTGCTCTTCCGATCT ATCCATGAGG NNNNNNNNNN AGATCGGAAGAGCGTCG*T*G*T
Barcode 12	A*G*A*CGTGTGCTCTTCCGATCT TTCCACGATG NNNNNNNNNN AGATCGGAAGAGCGTCG*T*G*T
Barcode 13	A*G*A*CGTGTGCTCTTCCGATCT GCTGGGAATT NNNNNNNNNN AGATCGGAAGAGCGTCG*T*G*T
Barcode 14	A*G*A*CGTGTGCTCTTCCGATCT CAAAACGACG NNNNNNNNNN AGATCGGAAGAGCGTCG*T*G*T
Barcode 15	A*G*A*CGTGTGCTCTTCCGATCT TCTCGCCTTT NNNNNNNNNN AGATCGGAAGAGCGTCG*T*G*T
Barcode 16	A*G*A*CGTGTGCTCTTCCGATCT CAGATCAGAG NNNNNNNNNN AGATCGGAAGAGCGTCG*T*G*T
Barcode 17	A*G*A*CGTGTGCTCTTCCGATCT GACACGTTCT NNNNNNNNNN AGATCGGAAGAGCGTCG*T*G*T
Barcode 18	A*G*A*CGTGTGCTCTTCCGATCT GCTAAGGTCT NNNNNNNNNN AGATCGGAAGAGCGTCG*T*G*T
Barcode 19	A*G*A*CGTGTGCTCTTCCGATCT TGTTCGACCT NNNNNNNNNN AGATCGGAAGAGCGTCG*T*G*T
Barcode 20	A*G*A*CGTGTGCTCTTCCGATCT CCCAAAGACA NNNNNNNNNN AGATCGGAAGAGCGTCG*T*G*T
Barcode 21	A*G*A*CGTGTGCTCTTCCGATCT CAGGTAGGAA NNNNNNNNNN AGATCGGAAGAGCGTCG*T*G*T
Barcode 22	A*G*A*CGTGTGCTCTTCCGATCT CATTATCGCG NNNNNNNNNN AGATCGGAAGAGCGTCG*T*G*T
Barcode 23	A*G*A*CGTGTGCTCTTCCGATCT CAGAGACTGA NNNNNNNNNN AGATCGGAAGAGCGTCG*T*G*T
Barcode 24	A*G*A*CGTGTGCTCTTCCGATCT TGACATGCAC NNNNNNNNNN AGATCGGAAGAGCGTCG*T*G*T
Barcode 25	A*G*A*CGTGTGCTCTTCCGATCT TGTTGGTTCC NNNNNNNNNN AGATCGGAAGAGCGTCG*T*G*T
Barcode 26	A*G*A*CGTGTGCTCTTCCGATCT CTCTCTGAAC NNNNNNNNNN AGATCGGAAGAGCGTCG*T*G*T
Barcode 27	A*G*A*CGTGTGCTCTTCCGATCT CACTAGCCAA NNNNNNNNNN AGATCGGAAGAGCGTCG*T*G*T
Barcode 28	A*G*A*CGTGTGCTCTTCCGATCT TGACTTTGCC NNNNNNNNNN AGATCGGAAGAGCGTCG*T*G*T
Barcode 29	A*G*A*CGTGTGCTCTTCCGATCT TTCAGCGAAG NNNNNNNNNN AGATCGGAAGAGCGTCG*T*G*T
Barcode 30	A*G*A*CGTGTGCTCTTCCGATCT ACAGGCATAC NNNNNNNNNN AGATCGGAAGAGCGTCG*T*G*T

b

Binds to universal site 1
Binds to universal site 2
Index for Illumina Sequencing

Universal Reverse Primer	AATGATACGGCGACCACCGAGATCTACACTCTTTCCCTACACGACGCTCTTCCGATCT
Index Base Forward Primer	TGACTGGAGTTCAGACGTGTGCTCTTCCGATCT
Index Final Forward Primer	CAAGCAGAAGACGGCATACGAGATGGCAGATAGTGACTGGAGTTCAGACGTGTG

Table B.5-2. Formulation details for all nanoparticles in Chapter 5. Nanoparticle formulations 2, 3, 7, 9, 13, 19, 20, 21, 25, and 27 were used in the Factor 7 siRNA experiment in Figure 5-4b.

Figure 2b, Figure 2c. Dose is 0.04 mg/kg for each barcode.

Name in Figure	Lipid	PEG	Lipid Mol %	PEG Mol %	Cholesterol Mol %	DSPC Mol %
Liver LNP	C12-200	C14 PEG2000	50	1.5	38.5	10
Lung LNP1	7C1	C14 PEG2000	70	30	0	0
Lung LNP2	7C1	C14 PEG2000	80	0	20	0
Lung LNP3	7C1	C14 PEG2000	70	20	10	0

Figure 2d, Supplementary Figure 3a

Name in Figure	Lipid	PEG	Lipid Mol %	PEG Mol %	Cholesterol Mol %	DSPC Mol %
All Data Points	C12-200	C14 PEG2000	50	1.5	38.5	10

Figure 2e, Supplementary Figure 3b. Dose is 0.04 mg/kg for each barcode.

Name in Figure	Lipid	PEG	Lipid Mol %	PEG Mol %	Cholesterol Mol %	DSPC Mol %
Liver NP1	C12-200	C14 PEG2000	50	1.5	38.5	10
Liver NP2	C12-200	C14 PEG2000	50	1.5	38.5	10
Liver NP3	C12-200	C14 PEG2000	50	1.5	38.5	10
Liver NP4	C12-200	C14 PEG2000	50	1.5	38.5	10
Liver NP5	C12-200	C14 PEG2000	50	1.5	38.5	10

Figure 2f. Dose is 0.04 mg/kg for each barcode.

Lipid	PEG	Lipid Mol %	PEG Mol %	Cholesterol Mol %	DSPC Mol %
7C1	C14 PEG2000	50	0	50	0
7C1	C14 PEG2000	50	25	25	0
7C1	C14 PEG2000	65	15	20	0
7C1	C14 PEG2000	65	35	0	0
7C1	C14 PEG2000	70	30	0	0
7C1	C14 PEG2000	70	20	10	0
7C1	C14 PEG2000	75	25	0	0
7C1	C14 PEG2000	80	20	0	0
7C1	C14 PEG2000	80	15	5	0
7C1	C14 PEG2000	90	10	0	0

Figure 3, Supplementary Figure 4, Supplementary Figure 5. Dose is 0.04 mg/kg for each barcode.

Barcode	Lipid	PEG Tail	PEG MW (Da)	PEG Mol%	Lipid Mol %	DSPC mol%	Chol. mol%	PEG mol%
1	C12-200	14	3000	2.25	50	10	37.75	2.25
2	C12-200	14	3000	1.50	50	10	38.50	1.50
3	C12-200	18	1000	0.75	50	10	39.25	0.75
4	C12-200	18	3000	0.75	50	10	39.25	0.75
5	C12-200	16	1000	3.00	50	10	37.00	3.00
6	C12-200	16	2000	1.50	50	10	38.50	1.50
7	C12-200	16	2000	0.75	50	10	39.25	0.75
8	C12-200	16	2000	3.75	50	10	36.25	3.75
9	C12-200	18	1000	3.00	50	10	37.00	3.00
10	C12-200	16	1000	2.25	50	10	37.75	2.25
11	C12-200	18	2000	3.75	50	10	36.25	3.75
12	C12-200	14	1000	4.50	50	10	35.50	4.50
13	C12-200	14	2000	0.75	50	10	39.25	0.75
14	C12-200	14	2000	4.50	50	10	35.50	4.50
15	C12-200	14	2000	3.00	50	10	37.00	3.00
16	C12-200	18	3000	4.50	50	10	35.50	4.50
17	C12-200	14	3000	3.00	50	10	37.00	3.00
18	C12-200	18	2000	2.25	50	10	37.75	2.25
19	C12-200	16	3000	3.00	50	10	37.00	3.00
20	C12-200	18	3000	3.75	50	10	36.25	3.75
21	C12-200	14	1000	1.50	50	10	38.50	1.50
22	C12-200	14	1000	3.75	50	10	36.25	3.75
23	C12-200	18	2000	4.50	50	10	35.50	4.50
24	C12-200	18	3000	2.25	50	10	37.75	2.25
25	C12-200	18	1000	1.50	50	10	38.50	1.50
26	C12-200	16	3000	0.75	50	10	39.25	0.75
27	C12-200	16	1000	4.50	50	10	35.50	4.50
28	C12-200	14	1000	3.75	50	10	36.25	3.75
29	C12-200	16	2000	2.25	50	10	37.75	2.25
30	C12-200	16	3000	1.50	50	10	38.50	1.50

Table B.6-1. Formulation parameters for LNPs in Chapter 6.

	LNP-1	**LNP-2**
cKK-E12 mol%	35	30
DOPE mol%	16	0
DOTAP mol%	0	39
Cholesterol mol%	46.5	30
C14 PEG 2000 mol%	2.5	1
cKK-E12:mRNA weight ratio	10:1	7.5:1

Appendix C

References

1. Carlberg, C. & Molnár, F. in *Mechanisms of Gene Regulation* 3–15 (2014).

2. Holoch, D. & Moazed, D. RNA-mediated epigenetic regulation of gene expression. *Nat. Rev. Genet.* **16,** 71–84 (2015).

3. Cox, D. B. T., Platt, R. J. & Zhang, F. Therapeutic genome editing: prospects and challenges. *Nat. Med.* **21,** 121–131 (2015).

4. Naldini, L. Gene therapy returns to centre stage. *Nature* **526,** 351–360 (2015).

5. Weissman, D. & Karikó, K. mRNA: Fulfilling the Promise of Gene Therapy. *Mol. Ther.* **23,** 1416–1417 (2015).

6. Ozcan, G., Ozpolat, B., Coleman, R. L., Sood, A. K. & Lopez-Berestein, G. Preclinical and clinical development of siRNA-based therapeutics. *Adv. Drug Deliv. Rev.* **87,** 108–119 (2015).

7. Yin, H. *et al.* Non-viral vectors for gene-based therapy. *Nat. Rev. Genet.* **15,** 541–555 (2014).

8. Hillaireau, H. & Couvreur, P. Nanocarriers' entry into the cell: relevance to drug delivery. *Cell. Mol. Life Sci.* **66,** 2873–96 (2009).

9. Whitehead, K. A., Langer, R. & Anderson, D. G. Knocking down barriers: advances in siRNA delivery. *Nat. Rev. Drug Discov.* **8,** 129–138 (2009).

10. Karikó, K., Buckstein, M., Ni, H. & Weissman, D. Suppression of RNA recognition by Toll-like receptors: The impact of nucleoside modification and the evolutionary origin of RNA. *Immunity* **23,** 165–175 (2005).

11. Whitehead, K. A., Dahlman, J. E., Langer, R. S. & Anderson, D. G. Silencing or Stimulation? siRNA Delivery and the Immune System. *Annu. Rev. Chem. Biomol. Eng.* **2,** 77–96 (2011).

12. Luo, D. & Saltzman, W. M. Synthetic DNA delivery systems. *Nat. Biotechnol.* **18,** 33–37 (2000).

13. Scheicher, B., Schachner-Nedherer, a.-L. & Zimmer, a. Protamine–oligonucleotide-nanoparticles: Recent advances in drug delivery and drug targeting. *Eur. J. Pharm. Sci.* **75,** 54–59 (2015).

14. Bettinger, T., Carlisle, R. C., Read, M. L., Ogris, M. & Seymour, L. W. Peptide-mediated RNA delivery: a novel approach for enhanced transfection of primary and post-mitotic cells. *Nucleic Acids Res.* **29,** 3882–3891 (2001).

15. Green, J. J., Langer, R. & Anderson, D. G. A Combinatorial Polymer Library Approach Yields Insight into Nonviral Gene Delivery. *Acc. Chem. Res.* **41,** 749–759 (2008).

16. Heyes, J., Palmer, L., Bremner, K. & MacLachlan, I. Cationic lipid saturation influences intracellular delivery of encapsulated nucleic acids. *J. Control. Release* **107,** 276–287 (2005).

17. Fire, A. *et al.* Potent and specific genetic interference by double-stranded RNA in Caenorhabditis elegans. *Nature* **391,** 806–811 (1998).

18. Akinc, A. *et al.* A combinatorial library of lipid-like materials for delivery of RNAi therapeutics. *Nat. Biotechnol.* **26,** 561–569 (2008).

19. Semple, S. C. *et al.* Rational design of cationic lipids for siRNA delivery. *Nat. Biotechnol.* **28,** 172–176 (2010).

20. McIvor, R. S. Therapeutic delivery of mRNA: the medium is the message. *Mol. Ther.* **19,** 822–823 (2011).

21. Weissman, D. mRNA transcript therapy. *Expert Rev. Vaccines* **14,** 265–281 (2015).

22. Sahin, U., Karikó, K. & Türeci, Ö. mRNA-based therapeutics — developing a new class of drugs. *Nat. Rev. Drug Discov.* **13,** 759–780 (2014).

23. Vallazza, B. *et al.* Recombinant messenger RNA technology and its application in cancer immunotherapy, transcript replacement therapies, pluripotent stem cell induction, and beyond. *Wiley Interdiscip. Rev. RNA* **6,** 471–499 (2015).

24. Hacein-Bey-Abina, S. *et al.* A serious adverse event after successful gene therapy for X-linked severe combined immunodeficiency. *N. Engl. J. Med.* **348,** 255–256 (2003).

25. Kreiter, S., Diken, M. & Sahin, U. in *Cancer Immunotherapy Meets Oncology* (ed. Britten, C. M.) 21–27 (2014).

26. Pollard, C., De Koker, S., Saelens, X., Vanham, G. & Grooten, J. Challenges and advances towards the rational design of mRNA vaccines. *Trends Mol. Med.* **19,** 705–713 (2013).

27. Weiss, R., Scheiblhofer, S., Roesler, E., Weinberger, E. & Thalhamer, J. mRNA vaccination as a safe approach for specific protection from type I allergy. *Expert Rev. Vaccines* **11,** 55–67 (2012).

28. Wang, H. *et al.* One-step generation of mice carrying mutations in multiple genes by CRISPR/cas-mediated genome engineering. *Cell* **153,** 910–918 (2013).

29. Bernal, J. a. RNA-based tools for nuclear reprogramming and lineage-conversion: Towards clinical applications. *J. Cardiovasc. Transl. Res.* **6,** 956–968 (2013).

30. Kotterman, M. a & Schaffer, D. V. Engineering adeno-associated viruses for clinical gene therapy. *Nat. Rev. Genet.* **15,** 445–451 (2014).

31. Giacca, M. & Zacchigna, S. Virus-mediated gene delivery for human gene therapy. *J. Control. Release* **161,** 377–388 (2012).

32. Lorenz, C. *et al.* Protein expression from exogenous mRNA: Uptake by receptor-mediated endocytosis and trafficking via the lysosomal pathway. *RNA Biol.* **8,** 627–636 (2011).

33. Zhao, Y. *et al.* High-efficiency transfection of primary human and mouse T lymphocytes using RNA electroporation. *Mol. Ther.* **13,** 151–159 (2006).

34. Piggott, J. M., Sheahan, B. J., Soden, D. M., O'Sullivan, G. C. & Atkins, G. J. Electroporation of RNA stimulates immunity to an encoded reporter gene in mice. *Mol. Med. Rep.* **2,** 753–756 (2009).

35. Ainger, K. *et al.* Transport and localization of exogenous myelin basic protein mRNA microinjected into oligodendrocytes. *J. Cell Biol.* **123,** 431–441 (1993).

36. Mehier-Humbert, S. & Guy, R. H. Physical methods for gene transfer: Improving the kinetics of gene delivery into cells. *Adv. Drug Deliv. Rev.* **57,** 733–753 (2005).

37. Vassilev, V. B., Gil, L. H. V. G. & Donis, R. O. Microparticle-mediated RNA immunization against bovine viral diarrhea virus. *Vaccine* **19,** 2012–2019 (2001).

38. Phua, K. K. L., Leong, K. W. & Nair, S. K. Transfection efficiency and transgene expression kinetics of mRNA delivered in naked and nanoparticle format. *J. Control. Release* **166,** 227–233 (2013).

39. Wolff, J. a *et al.* Direct gene transfer into mouse muscle in vivo. *Science* **247,** 1465–1468 (1990).

40. Van Lint, S. *et al.* Preclinical evaluation of TriMix and antigen mRNA-based antitumor therapy. *Cancer Res.* **72,** 1661–1671 (2012).

41. Soutschek, J. *et al.* Therapeutic silencing of an endogenous gene by systemic administration of modified siRNAs. *Nature* **432,** 173–8 (2004).

42. Wolfrum, C. *et al.* Mechanisms and optimization of in vivo delivery of lipophilic siRNAs. *Nat. Biotechnol.* **25,** 1149–57 (2007).

43. Rensen, P. C. *et al.* Determination of the upper size limit for uptake and processing of ligands by the asialoglycoprotein receptor on hepatocytes in vitro and in vivo. *J. Biol. Chem.* **276,** 37577–84 (2001).

44. Drickamer, K. Selective Sugar Binding to the Carbohydrate Recognition Domains of the Rat Hepatic and Macrophage Asialoglycoprotein Receptors. *J. Biol. Chem.* **271,** 6686–6693 (1996).

45. Mamidyala, S. K. *et al.* Glycomimetic ligands for the human asialoglycoprotein receptor. *J. Am. Chem. Soc.* **134,** 1978–81 (2012).

46. K. Nair, J. *et al.* Multivalent N-Acetylgalactosamine-Conjugated siRNA Localizes in Hepatocytes and Elicits Robust RNAi-mediated Gene Silencing. *J. Am. Chem. Soc.* **136,** 16948–16961 (2014).

47. Matsuda, S. *et al.* siRNA Conjugates Carrying Sequentially Assembled Trivalent N-Acetylgalactosamine Linked Through Nucleosides Elicit Robust Gene Silencing In Vivo in Hepatocytes. *ACS Chem. Biol.* **10,** 1181–1187 (2015).

48. Rand, T. a., Petersen, S., Du, F. & Wang, X. Argonaute2 cleaves the anti-guide strand of siRNA during RISC activation. *Cell* **123,** 621–629 (2005).

49. Deleavey, G. F. & Damha, M. J. Designing chemically modified oligonucleotides for targeted gene silencing. *Chem. Biol.* **19,** 937–54 (2012).

50. Calabretta, a., Kupfer, P. a. & Leumann, C. J. The effect of RNA base lesions on mRNA translation. *Nucleic Acids Res.* 1–8 (2015).

51. Wang, X. *et al.* N6-methyladenosine Modulates Messenger RNA Translation Efficiency.

Cell **161,** 1388–1399 (2015).

52. Karikó, K. *et al.* Incorporation of pseudouridine into mRNA yields superior nonimmunogenic vector with increased translational capacity and biological stability. *Mol. Ther.* **16,** 1833–1840 (2008).

53. Karikó, K., Muramatsu, H., Keller, J. M. & Weissman, D. Increased erythropoiesis in mice injected with submicrogram quantities of pseudouridine-containing mRNA encoding erythropoietin. *Mol. Ther.* **20,** 948–953 (2012).

54. Anderson, B. R. *et al.* Incorporation of pseudouridine into mRNA enhances translation by diminishing PKR activation. *Nucleic Acids Res.* **38,** 5884–5892 (2010).

55. Wilusz, C. J., Wormington, M. & Peltz, S. W. The cap-to-tail guide to mRNA turnover. *Nat. Rev. Mol. Cell Biol.* **2,** 237–246 (2001).

56. Gallie, D. R. The cap and poly(A) tail function synergistically to regulate mRNA translational efficiency. *Genes Dev.* **5,** 2108–2116 (1991).

57. Jackson, R. J. Cytoplasmic regulation of mRNA function: The importance of the 3' untranslated region. *Cell* **74,** 9–14 (1993).

58. Wilkie, G. S., Dickson, K. S. & Gray, N. K. Regulation of mRNA translation by 5'- and 3'-UTR-binding factors. *Trends Biochem. Sci.* **28,** 182–188 (2003).

59. Thess, A. *et al.* Sequence-engineered mRNA without chemical nucleoside modifications enables an effective protein therapy in large animals. *Mol. Ther.* 1–9 (2015).

60. Mauro, V. P. & Chappell, S. a. A critical analysis of codon optimization in human therapeutics. *Trends Mol. Med.* **20,** 604–613 (2014).

61. Amos, H. Protamine Enhancement of RNA Uptake by Cultured Chick Cells. *Biochem. Biophys. Res. Commun.* **5,** 1–4 (1961).

62. Choi, Y. S. *et al.* The systemic delivery of siRNAs by a cell penetrating peptide, low molecular weight protamine. *Biomaterials* **31,** 1429–1443 (2010).

63. Kallen, K. J. *et al.* A novel, disruptive vaccination technology: Self-adjuvanted RNActive vaccines. *Hum. Vaccines Immunother.* **9,** 2263–2276 (2013).

64. Fotin-Mleczek, M. *et al.* Messenger RNA-based vaccines with dual activity induce balanced TLR-7 dependent adaptive immune responses and provide antitumor activity. *J. Immunother.* **34,** 1–15 (2011).

65. Scheel, B. *et al.* Toll-like receptor-dependent activation of several human blood cell types by protamine-condensed mRNA. *Eur. J. Immunol.* **35,** 1557–1566 (2005).

66. Schell, B. *et al.* Immunostimulating capacities of stabilized RNA molecules. *Eur. J. Immunol.* **34,** 537–547 (2004).

67. Heil, F. *et al.* Species-specific recognition of single-stranded RNA via toll-like receptor 7 and 8. *Science* **303,** 1526–1529 (2004).

68. Petsch, B. *et al.* Protective efficacy of in vitro synthesized, specific mRNA vaccines

against influenza A virus infection. *Nat. Biotechnol.* **30,** 1210–6 (2012).

69. Weide, B. *et al.* Direct injection of protamine-protected mRNA: results of a phase 1/2 vaccination trial in metastatic melanoma patients. *J. Immunother.* **32,** 498–507 (2009).

70. Sebastian, M. *et al.* Phase Ib study evaluating a self-adjuvanted mRNA cancer vaccine (RNActive®) combined with local radiation as consolidation and maintenance treatment for patients with stage IV non-small cell lung cancer. *BMC Cancer* **14,** 748 (2014).

71. Kübler, H. *et al.* Self-adjuvanted mRNA vaccination in advanced prostate cancer patients: a first-in-man phase I/IIa study. *J. Immunother. Cancer* **3,** 26 (2015).

72. Kanasty, R., Dorkin, J. R., Vegas, A. & Anderson, D. Delivery materials for siRNA therapeutics. *Nat. Mater.* **12,** 967–977 (2013).

73. Midoux, P. & Pichon, C. Lipid-based mRNA vaccine delivery systems. *Expert Rev. Vaccines* **14,** 221–234 (2015).

74. Kormann, M. S. D. *et al.* Expression of therapeutic proteins after delivery of chemically modified mRNA in mice. *Nat. Biotechnol.* **29,** 154–157 (2011).

75. Rejman, J., Tavernier, G., Bavarsad, N., Demeester, J. & De Smedt, S. C. MRNA transfection of cervical carcinoma and mesenchymal stem cells mediated by cationic carriers. *J. Control. Release* **147,** 385–391 (2010).

76. Pollard, C. *et al.* Type I IFN Counteracts the Induction of Antigen-Specific Immune Responses by Lipid-Based Delivery of mRNA Vaccines. *Mol. Ther.* **21,** 251–259 (2012).

77. Akinc, A. *et al.* Targeted delivery of RNAi therapeutics with endogenous and exogenous ligand-based mechanisms. *Mol. Ther.* **18,** 1357–64 (2010).

78. Sahay, G. *et al.* Efficiency of siRNA delivery by lipid nanoparticles is limited by endocytic recycling. *Nat. Biotechnol.* **31,** 653–658 (2013).

79. Wittrup, A. *et al.* Visualizing lipid-formulated siRNA release from endosomes and target gene knockdown. *Nat. Biotechnol.* 1–9 (2015).

80. Dong, Y. *et al.* Lipopeptide nanoparticles for potent and selective siRNA delivery in rodents and nonhuman primates. *Proc. Natl. Acad. Sci.* **111,** 3955–3960 (2014).

81. Zimmermann, T. S. *et al.* RNAi-mediated gene silencing in non-human primates. *Nature* **441,** 111–4 (2006).

82. Geall, a. J. *et al.* Nonviral delivery of self-amplifying RNA vaccines. *Proc. Natl. Acad. Sci.* **109,** 14604–14609 (2012).

83. Jayaraman, M. *et al.* Maximizing the potency of siRNA lipid nanoparticles for hepatic gene silencing in vivo. *Angew. Chem. Int. Ed. Engl.* **51,** 8529–8533 (2012).

84. Maier, M. a *et al.* Biodegradable lipids enabling rapidly eliminated lipid nanoparticles for systemic delivery of RNAi therapeutics. *Mol. Ther.* **21,** 1570–1578 (2013).

85. Love, K. T. *et al.* Lipid-like materials for low-dose, in vivo gene silencing. *Proc. Natl. Acad. Sci. U. S. A.* **107,** 1864–1869 (2010).

86. Whitehead, K. a *et al.* Degradable lipid nanoparticles with predictable in vivo siRNA delivery activity. *Nat. Commun.* **5,** 4277 (2014).

87. Chen, D. *et al.* Rapid discovery of potent siRNA-containing lipid nanoparticles enabled by controlled microfluidic formulation. *J. Am. Chem. Soc.* **134,** 6948–6951 (2012).

88. Brito, L. a *et al.* A cationic nanoemulsion for the delivery of next generation RNA vaccines. *Mol. Ther.* **22,** 2118–2129 (2014).

89. Bogers, W. M. *et al.* Potent Immune Responses in Rhesus Macaques Induced by Nonviral Delivery of a Self-amplifying RNA Vaccine Expressing HIV Type 1 Envelope With a Cationic Nanoemulsion. *J. Infect. Dis.* **211,** 947–955 (2014).

90. Kanasty, R. L., Whitehead, K. a, Vegas, A. J. & Anderson, D. G. Action and Reaction: The Biological Response to siRNA and Its Delivery Vehicles. *Mol. Ther.* **20,** 513–24 (2012).

91. Mundargi, R. C., Babu, V. R., Rangaswamy, V., Patel, P. & Aminabhavi, T. M. Nano/micro technologies for delivering macromolecular therapeutics using poly(d,l-lactide-co-glycolide) and its derivatives. *J. Control. Release* **125,** 193–209 (2008).

92. Lungwitz, U., Breunig, M., Blunk, T. & Göpferich, a. Polyethylenimine-based non-viral gene delivery systems. *Eur. J. Pharm. Biopharm.* **60,** 247–266 (2005).

93. Günther, M. *et al.* Polyethylenimines for RNAi-mediated gene targeting in vivo and siRNA delivery to the lung. *Eur. J. Pharm. Biopharm.* **77,** 438–49 (2011).

94. Lv, H., Zhang, S., Wang, B., Cui, S. & Yan, J. Toxicity of cationic lipids and cationic polymers in gene delivery. *J. Control. Release* **114,** 100–109 (2006).

95. Agarwal, S., Zhang, Y., Maji, S. & Greiner, A. PDMAEMA based gene delivery materials. *Mater. Today* **15,** 388–393 (2012).

96. Üzgün, S. *et al.* PEGylation improves nanoparticle formation and transfection efficiency of messenger RNA. *Pharm. Res.* **28,** 2223–2232 (2011).

97. Kim, S. W. Polylysine copolymers for gene delivery. *Cold Spring Harb. Protoc.* **7,** 433–438 (2012).

98. Mao, S., Sun, W. & Kissel, T. Chitosan-based formulations for delivery of DNA and siRNA. *Adv. Drug Deliv. Rev.* **62,** 12–27 (2010).

99. Nafee, N., Taetz, S., Schneider, M., Schaefer, U. F. & Lehr, C. M. Chitosan-coated PLGA nanoparticles for DNA/RNA delivery: effect of the formulation parameters on complexation and transfection of antisense oligonucleotides. *Nanomedicine Nanotechnology, Biol. Med.* **3,** 173–183 (2007).

100. Mahiny, A. J. *et al.* In vivo genome editing using nuclease-encoding mRNA corrects SP-B deficiency. *Nat. Biotechnol.* 2–6 (2015).

101. Lynn, D. M. & Langer, R. Degradable Poly (beta-amino esters): Synthesis , Characterization , and Self-Assembly with Plasmid DNA. *J Am Chem Soc* **122,** 10761–10768 (2000).

102. Anderson, D. G., Lynn, D. M. & Langer, R. Semi-automated synthesis and screening of a large library of degradable cationic polymers for gene delivery. *Angew. Chem. Int. Ed. Engl.* **42,** 3153–8 (2003).

103. Anderson, D. G., Akinc, A., Hossain, N. & Langer, R. Structure/property studies of polymeric gene delivery using a library of poly(beta-amino esters). *Mol. Ther.* **11,** 426–34 (2005).

104. Zugates, G. T. *et al.* Rapid Optimization of Gene Delivery by Parallel End-modification of Poly(β-amino ester)s. *Mol. Ther.* **15,** 1306–1312 (2007).

105. Eltoukhy, A. a, Chen, D., Alabi, C. a, Langer, R. & Anderson, D. G. Degradable Terpolymers with Alkyl Side Chains Demonstrate Enhanced Gene Delivery Potency and Nanoparticle Stability. *Adv. Mater.* **25,** 1487–1493 (2013).

106. Su, X., Fricke, J., Kavanagh, D., Irvine, D. J. & Chase, C. In vitro and in vivo mRNA delivery using lipid-enveloped pH- responsive polymer nanoparticles. *Mol Pharm* **8,** 774–787 (2011).

107. Dorbnik, J., Saudek, V., Vlasak, J. & Kalal, J. Polyaspartamide - a potential drug carrier. *J. Polym. Sci. Polym. Symp.* **66,** 65–74 (1979).

108. Kim, H. J. *et al.* PEG-detachable cationic polyaspartamide derivatives bearing stearoyl moieties for systemic siRNA delivery toward subcutaneous BxPC3 pancreatic tumor. *J. Drug Target.* **20,** 33–42 (2012).

109. Miyata, K. *et al.* Polyplexes from poly(aspartamide) bearing 1,2-diaminoethane side chains induce pH-selective, endosomal membrane destabilization with amplified transfection and negligible cytotoxicity. *J. Am. Chem. Soc.* **130,** 16287–16294 (2008).

110. Zhang, M., Liu, M., Xue, Y., Huang, S. & Zhuo, R. Polyaspartamide-Based Oligo-ethylenimine Brushes with High Buffer Capacity and Low Cytotoxicity for Highly Efficient Gene Delivery Polyaspartamide-Based Oligo-ethylenimine Brushes with High Buffer Capacity and Low Cytotoxicity for Highly Efficient Gene De. *Bioconjug. Chem.* 440–446 (2009).

111. Baba, M., Itaka, K., Kondo, K., Yamasoba, T. & Kataoka, K. Treatment of neurological disorders by introducing mRNA in vivo using polyplex nanomicelles. *J. Control. Release* **201,** 41–48 (2015).

112. Uchida, H. *et al.* Modulated Protonation of Side Chain Aminoethylene Repeats in. *J. Am. Chem. Soc.* **136,** 12396–12405 (2014).

113. Uchida, H. *et al.* Odd-even effect of repeating aminoethylene units in the side chain of N-substituted polyaspartamides on gene transfection profiles. *J. Am. Chem. Soc.* **133,** 15524–15532 (2011).

114. Li, S. D. & Huang, L. Surface-modified LPD nanoparticles for tumor targeting. *Ann. N. Y. Acad. Sci.* **1082,** 1–8 (2006).

115. Li, S.-D., Chen, Y.-C., Hackett, M. J. & Huang, L. Tumor-targeted delivery of siRNA by self-assembled nanoparticles. *Mol. Ther.* **16,** 163–169 (2008).

116. Wang, Y. *et al.* Systemic Delivery of Modified mRNA Encoding Herpes Simplex Virus 1

Thymidine Kinase for Targeted Cancer Gene Therapy. *Mol. Ther.* **21,** 1–10 (2012).

117. Palamà, I. E., Cortese, B., D'Amone, S. & Gigli, G. mRNA delivery using non-viral PCL nanoparticles. *Biomater. Sci.* **3,** 144–151 (2015).

118. Leuschner, F. & Dutta, P. Therapeutic siRNA silencing in inflammatory monocytes in mice. *Nat. Biotechnol.* **29,** 1–9 (2011).

119. Novobrantseva, T. I. *et al.* Systemic RNAi-mediated Gene Silencing in Nonhuman Primate and Rodent Myeloid Cells. *Mol. Ther. Nucleic Acids* **1,** e4 (2012).

120. Speicher, T. *et al.* Knockdown and knockout of β1-integrin in hepatocytes impairs liver regeneration through inhibition of growth factor signalling. *Nat. Commun.* **5,** 3862 (2014).

121. Zuhorn, I. S. *et al.* Nonbilayer phase of lipoplex-membrane mixture determines endosomal escape of genetic cargo and transfection efficiency. *Mol. Ther.* **11,** 801–810 (2005).

122. Allen, T. M. & Cullis, P. R. Liposomal drug delivery systems: from concept to clinical applications. *Adv. Drug Deliv. Rev.* **65,** 36–48 (2013).

123. Lu, J. J., Langer, R. & Chen, J. A Novel Mechanism Is Involved in Cationic Lipid-Mediated Functional siRNA Delivery. *Mol. Pharm.* **6,** 763–771 (2009).

124. Mui, B. L. *et al.* Influence of Polyethylene Glycol Lipid Desorption Rates on Pharmacokinetics and Pharmacodynamics of siRNA Lipid Nanoparticles. *Mol. Ther. Nucleic Acids* **2,** e139 (2013).

125. Akinc, A. *et al.* Development of Lipidoid–siRNA Formulations for Systemic Delivery to the Liver. *Mol. Ther.* **17,** 872–879 (2009).

126. Belliveau, N. M. *et al.* Microfluidic Synthesis of Highly Potent Limit-size Lipid Nanoparticles for In Vivo Delivery of siRNA. *Mol. Ther. Nucleic Acids* **1,** e37 (2012).

127. Montgomery, D. C. *Design and Analysis of Experiments.* (John Wiley & Sons, 2008).

128. Gooding, O. W. Process optimization using combinatorial design principles: Parallel synthesis and design of experiment methods. *Curr. Opin. Chem. Biol.* **8,** 297–304 (2004).

129. Whitehead, K. A. *et al.* In Vitro-In Vivo Translation of Lipid Nanoparticles for Hepatocellular siRNA Delivery. *ACS Nano* **6,** 6922–6929 (2012).

130. Zangi, L. *et al.* Modified mRNA directs the fate of heart progenitor cells and induces vascular regeneration after myocardial infarction. *Nat. Biotechnol.* **31,** 898–907 (2013).

131. Rao, R. S., Kumar, C. G., Prakasham, R. S. & Hobbs, P. J. The Taguchi methodology as a statistical tool for biotechnological applications: a critical appraisal. *Biotechnol. J.* **3,** 510–523 (2008).

132. Jones, B. & Nachtsheim, C. J. A Class of Three-Level Designs for Definitive Screening in the Presence of Second-Order Effects. *J. Qual. Technol.* **43,** 1–15 (2011).

133. Leung, A. K. K. *et al.* Lipid Nanoparticles Containing siRNA Synthesized by Microfluidic Mixing Exhibit an Electron-Dense Nanostructured Core. *J. Phys. Chem. C* **116,** 18440–

18450 (2012).

134. Garbuzenko, O., Barenholz, Y. & Priev, A. Effect of grafted PEG on liposome size and on compressibility and packing of lipid bilayer. *Chem. Phys. Lipids* **135,** 117–129 (2005).

135. Harvey, R. D. *et al.* Stabilization of distearoylphosphatidylcholine lamellar phases in propylene glycol using cholesterol. *Mol. Pharm.* **10,** 4408–4417 (2013).

136. Farhood, H., Serbina, N. & Huang, L. The role of dioleoyl phosphatidylethanolamine in cationic liposome mediated gene transfer. *Biochim. Biophys. Acta* **1235,** 289–295 (1995).

137. Fasbender, A. *et al.* Effect of co-lipids in enhancing cationic lipid-mediated gene transfer in vitro and in vivo. *Gene Ther.* **4,** 716–725 (1997).

138. Kundu, A. K. *et al.* Development and Optimization of Nanosomal Formulations for siRNA Delivery to the Liver. *Eur. J. Pharm. Biopharm.* **80,** 257–267 (2012).

139. Albanese, A., Tang, P. S. & Chan, W. C. W. The Effect of Nanoparticle Size, Shape, and Surface Chemistry on Biological Systems. *Annu. Rev. Biomed. Eng.* **14,** 1–16 (2012).

140. Fenton, O. S. *et al.* Bioinspired Alkenyl Amino Alcohol Ionizable Lipid Materials for Highly Potent In Vivo mRNA Delivery. *Adv. Mater.* **28,** 2939–2943 (2016).

141. Kauffman, K. J., Webber, M. J. & Anderson, D. G. Materials for Non-viral intracellular delivery of messenger RNA therapeutics. *J. Control. Release* **240,** 227–234 (2016).

142. Karikó, K., Ni, H., Capodici, J., Lamphier, M. & Weissman, D. mRNA Is an Endogenous Ligand for Toll-like Receptor 3. *J. Biol. Chem.* **279,** 12542–12550 (2004).

143. Hornung, V. *et al.* 5'-Triphosphate RNA Is the Ligand for RIG-I. *Science (80-.).* **314,** 994–997 (2006).

144. Loomis, K. H., Kirschman, J. L., Bhosle, S., Bellamkonda, R. V. & Santangelo, P. J. Strategies for modulating innate immune activation and protein production of in vitro transcribed mRNAs. *J. Mater. Chem. B* **4,** 1619–1632 (2016).

145. Warren, L. *et al.* Highly efficient reprogramming to pluripotency and directed differentiation of human cells with synthetic modified mRNA. *Cell Stem Cell* **7,** 618–630 (2010).

146. Andries, O. *et al.* N1-methylpseudouridine-incorporated mRNA outperforms pseudouridine-incorporated mRNA by providing enhanced protein expression and reduced immunogenicity in mammalian cell lines and mice. *J. Control. Release* **217,** 337–344 (2015).

147. Li, B., Luo, X. & Dong, Y. Effects of Chemically Modified Messenger RNA on Protein Expression. *Bioconjug. Chem.* **27,** 849–853 (2016).

148. Anderson, B. R. *et al.* Nucleoside modifications in RNA limit activation of 2'-5'-oligoadenylate synthetase and increase resistance to cleavage by RNase L. *Nucleic Acids Res.* **39,** 9329–9338 (2011).

149. Kauffman, K. J. *et al.* Optimization of Lipid Nanoparticle Formulations for mRNA Delivery in Vivo with Fractional Factorial and Definitive Screening Designs. *Nano Lett.* **15,** 7300–

7306 (2015).

150. Eltoukhy, A. A. *et al.* Effect of molecular weight of amine end-modified poly (b -amino ester) s on gene delivery efficiency and toxicity. *Biomaterials* **33,** 3594–3603 (2012).

151. Dahlman, J. E. *et al.* In vivo endothelial siRNA delivery using polymeric nanoparticles with low molecular weight. *Nat. Nanotechnol.* **19,** 648–655 (2014).

152. Pardi, N. *et al.* Expression kinetics of nucleoside-modified mRNA delivered in lipid nanoparticles to mice by various routes. *J. Control. Release* **217,** 345–351 (2015).

153. DeRosa, F. *et al.* Therapeutic efficacy in a hemophilia B model using a biosynthetic mRNA liver depot system. *Gene Ther.* **23,** 699–707 (2016).

154. Charette, M. & Gray, M. W. Pseudouridine in RNA: what, where, how, and why. *IUBMB Life* **49,** 341–351 (2000).

155. Kierzek, E. *et al.* The contribution of pseudouridine to stabilities and structure of RNAs. *Nucleic Acids Res.* **42,** 3492–501 (2014).

156. Karikó, K., Muramatsu, H., Ludwig, J. & Weissman, D. Generating the optimal mRNA for therapy: HPLC purification eliminates immune activation and improves translation of nucleoside-modified, protein-encoding mRNA. *Nucleic Acids Res.* **39,** 1–10 (2011).

157. Bakaysa, S. L. *et al.* Single- and double-stranded viral RNA generate distinct cytokine and antiviral responses in human fetal membranes. *Mol. Hum. Reprod.* **20,** 701–708 (2014).

158. Andries, O. *et al.* Innate immune response and programmed cell death following carrier-mediated delivery of unmodified mRNA to respiratory cells. *J. Control. Release* **167,** 157–166 (2013).

159. Basu, S., Hodgson, G., Katz, M. & Dunn, A. R. Evaluation of role of G-CSF in the production, survival, and release of neutrophils from bone marrow into circulation. *Blood* **100,** 854–861 (2002).

160. Deshmane, S. L., Kremlev, S., Amini, S. & Sawaya, B. E. Monocyte Chemoattractant Protein-1 (MCP-1): An Overview. *J. Interf. Cytokine Res.* **29,** 313–326 (2009).

161. von Vietinghoff, S. & Ley, K. Homeostatic regulation of blood neutrophil counts. *J. Immunol.* **181,** 5183–8 (2008).

162. King, A. M. Q., Adams, M. J., Carstens, E. B. & Lefkowitz, E. J. *Virus Taxonomy: Classification and Nomenclature of Viruses.* (Elsevier, 2012).

163. Bai, F. *et al.* A paradoxical role for neutrophils in the pathogenesis of West Nile virus. *J. Infect. Dis.* **202,** 1804–1812 (2010).

164. Lee, N. *et al.* A major outbreak of severe acute respiratory syndrome in Hong Kong. *N. Engl. J. Med.* **348,** 1986–1994 (2003).

165. Duchin, J. S. *et al.* Hantavirus Pulmonary Syndrome: A Clinical Description of 17 Patients With A Newly Recognized Disease. *N. Engl. J. Med.* **330,** 949–955 (1994).

166. Quindry, J. C., Stone, W. L., King, J. & Broeder, C. E. The effects of acute exercise on neutrophils and plasma oxidative stress. *Med. Sci. Sports Exerc.* **35,** 1139–1145 (2003).

167. Efrati, P., Presentey, B., Margalith, M., Rozenszajn, L. Leukocytes of Normal Pregnant Women. (1964).

168. Wisse, E., Jacobs, F., Topal, B., Frederik, P. & De Geest, B. The size of endothelial fenestrae in human liver sinusoids: implications for hepatocyte-directed gene transfer. *Gene Ther.* **15,** 1193–9 (2008).

169. Spiess, M. The Asialoglycoprotein Receptor : A Model for Endocytic Transport Receptors. *Biochemistry* **29,** (1990).

170. Dahlman, J. E., Kauffman, K. J., Langer, R. & Anderson, D. G. *Nanotechnology for Invivo Targeted siRNA Delivery. Advances in Genetics* **88,** (Elsevier, 2014).

171. Zhou, Z., Xu, M.-J. & Gao, B. Hepatocytes: a key cell type for innate immunity. *Cell. Mol. Immunol.* **13,** 1–15 (2015).

172. Bangel-Ruland, N. *et al.* Cystic fibrosis transmembrane conductance regulator-mRNA delivery: a novel alternative for cystic fibrosis gene therapy. *J. Gene Med.* **15,** 414–426 (2013).

173. Uchida, S. *et al.* Systemic delivery of messenger RNA for the treatment of pancreatic cancer using polyplex nanomicelles with a cholesterol moiety. *Biomaterials* **82,** 221–228 (2016).

174. Oberli, M. A. *et al.* Lipid Nanoparticle–Assisted mRNA Delivery for Potent Cancer Immunotherapy. *Nano Lett.* **17,** 1326–1335 (2017).

175. Kranz, L. M. *et al.* Systemic RNA delivery to dendritic cells exploits antiviral defence for cancer immunotherapy. *Nature* **534,** 396–401 (2016).

176. Fenton, O. S. Design, Synthesis, and Biological Evaluation of Diketopiperazine Based Ionizable Lipids for the In Vivo Delivery of Messenger RNA. (Massachusetts Institute of Technology, 2016).

177. Bronte, V. & Pittet, M. J. The spleen in local and systemic regulation of immunity. *Immunity* **39,** 806–818 (2013).

178. Kaczmarek, J. C. *et al.* Polymer-Lipid Nanoparticles for Systemic Delivery of mRNA to the Lungs. *Angew. Chem. Int. Ed. Engl.* **128,** 14012–14016 (2016).

179. Budhiraja, R., Tuder, R. M. & Hassoun, P. M. Endothelial Dysfunction in Pulmonary Hypertension. *Circulation* **109,** 159–165 (2004).

180. Dudley, A. C. Tumor endothelial cells. *Cold Spring Harb. Perspect. Med.* **2,** 1–18 (2012).

181. Reichmuth, A., Oberli, M. A., Jeklenec, A., Langer, R. & Blankschtein, D. mRNA Vaccine Delivery Using Lipid Nanoparticles. *Ther. Deliv* **7,** 117–138 (2016).

182. Chahal, J. S. *et al.* Dendrimer-RNA nanoparticles generate protective immunity against lethal Ebola, H1N1 influenza, and Toxoplasma gondii challenges with a single dose. *Proc. Natl. Acad. Sci.* **113,** E4133–E4142 (2016).

183. Khan, O. F. *et al.* Dendrimer-inspired nanomaterials for the in vivo delivery of siRNA to lung vasculature. *Nano Lett.* **15,** 3008–3016 (2015).

184. Yamaoka, K., Nakagawa, T. & Uno, T. Statistical moments in pharmacokinetics. *J. Pharmacokinet. Biopharm.* **6,** 547–558 (1978).

185. Bao, Y. *et al.* Effect of PEGylation on biodistribution and gene silencing of siRNA/lipid nanoparticle complexes. *Pharm. Res.* **30,** 342–51 (2013).

186. Tomasetti, L., Liebl, R., Wastl, D. S. & Breunig, M. Influence of PEGylation on nanoparticle mobility in different models of the extracellular matrix. *Eur. J. Pharm. Biopharm.* **108,** 145–155 (2016).

187. Blanco, E., Shen, H. & Ferrari, M. Principles of nanoparticle design for overcoming biological barriers to drug delivery. *Nat. Biotechnol.* **33,** 941–951 (2015).

188. Cheng, C. J., Tietjen, G. T., Saucier-Sawyer, J. K. & Saltzman, W. M. A holistic approach to targeting disease with polymeric nanoparticles. *Nat. Rev. Drug Discov.* **14,** 239–47 (2015).

189. Monopoli, M. P., Aberg, C., Salvati, A. & Dawson, K. a. Biomolecular coronas provide the biological identity of nanosized materials. *Nat. Nanotechnol.* **7,** 779–86 (2012).

190. Zuckerman, J. E., Choi, C. H. J., Han, H. & Davis, M. E. Polycation-siRNA nanoparticles can disassemble at the kidney glomerular basement membrane. *Proc. Natl. Acad. Sci. U. S. A.* **109,** 3137–42 (2012).

191. Aird, W. C. Endothelial cell heterogeneity. *Cold Spring Harb Perspect Med* **2,** a006429 (2012).

192. Porel, M. & Alabi, C. A. Sequence-defined polymers via orthogonal allyl acrylamide building blocks. *J. Am. Chem. Soc.* **136,** 13162–13165 (2014).

193. Hao, J. *et al.* Rapid Synthesis of a Lipocationic Polyester Library via Ring-Opening Polymerization of Functional Valerolactones for Efficacious siRNA Delivery. *J. Am. Chem. Soc.* **137,** 9206–9209 (2015).

194. Siegwart, D. J. *et al.* Combinatorial synthesis of chemically diverse core-shell nanoparticles for intracellular delivery. *Proc Natl Acad Sci U S A* **108,** 12996–13001 (2011).

195. Yamada, K. M. & Cukierman, E. Modeling Tissue Morphogenesis and Cancer in 3D. *Cell* **130,** 601–610 (2007).

196. Holt, R. A. & Jones, S. J. M. The new paradigm of flow cell sequencing. *Genome Res.* **18,** 839–846 (2008).

197. Mannocci, L. *et al.* High-throughput sequencing allows the identification of binding molecules isolated from DNA-encoded chemical libraries. *Proc. Natl. Acad. Sci. U. S. A.* **105,** 17670–17675 (2008).

198. Shendure, J. & Ji, H. Next-generation DNA sequencing. *Nat. Biotechnol.* **26,** 1135–1145 (2008).

199. Saliba, A. E., Westermann, A. J., Gorski, S. A. & Vogel, J. Single-cell RNA-seq: Advances and future challenges. *Nucleic Acids Res.* **42,** 8845–8860 (2014).

200. White, K. *et al.* Genetic and hypoxic alterations of the microRNA- 210-ISCU1/2 axis promote iron–sulfur deficiency and Pulmonary Hypertension. *EMBO Mol. Med.* **7,** 695–713 (2015).

201. Platt, R. J. *et al.* CRISPR-Cas9 knockin mice for genome editing and cancer modeling. *Cell* **159,** 440–455 (2014).

202. Herr, K. J. *et al.* Loss of α-catenin elicits a cholestatic response and impairs liver regeneration. *Sci. Rep.* **4,** 6835 (2014).

203. Otsuka, H., Nagasaki, Y. & Kataoka, K. PEGylated nanoparticles for biological and pharmaceutical applications. *Adv. Drug Deliv. Rev.* **64,** 246–255 (2012).

204. Hsu, P. D., Lander, E. S. & Zhang, F. Development and applications of CRISPR-Cas9 for genome engineering. *Cell* **157,** 1262–1278 (2014).

205. Yaari, Z. *et al.* Theranostic barcoded nanoparticles for personalized cancer medicine. *Nat. Commun.* **7,** 1–10 (2016).

206. Eustaquio, T. & Leary, J. Nanobarcoding: detecting nanoparticles in biological samples using in situ polymerase chain reaction. *Int. J. Nanomedicine* **7,** 5625–5639 (2012).

207. Eustaquio, T. & Leary, J. F. Nanobarcoded superparamagnetic iron oxide nanoparticles for nanomedicine: Quantitative studies of cell-nanoparticle interactions by scanning image cytometry. *Cytom. Part A* **89,** 207–216 (2016).

208. Stoeva, S. I., Lee, J. S., Smith, J. E., Rosen, S. T. & Mirkin, C. A. Multiplexed detection of protein cancer markers with biobarcoded nanoparticle probes. *J. Am. Chem. Soc.* **128,** 8378–8379 (2006).

209. Stoeva, S. I., Lee, J. S., Thaxton, C. S. & Mirkin, C. A. Multiplexed DNA detection with biobarcoded nanoparticle probes. *Angew. Chemie - Int. Ed.* **45,** 3303–3306 (2006).

210. Rajendran, L., Knölker, H.-J. & Simons, K. Subcellular targeting strategies for drug design and delivery. *Nat. Rev. Drug Discov.* **9,** 29–42 (2010).

211. Dahlman, J. E. *et al.* Barcoded nanoparticles for high throughput in vivo discovery of targeted therapeutics. *Proc. Natl. Acad. Sci.* **114,** 2060–2065 (2017).

212. Sager, H. B. *et al.* RNAi targeting multiple cell adhesion molecules reduces immune cell recruitment and vascular inflammation after myocardial infarction. *Sci. Transl. Med.* **8,** 1–12 (2016).

213. Sergeeva, O. V, Koteliansky, V. E. & Zatsepin, T. S. mRNA Based Therapeutics – Advances and Perspectives. *Biochem.* **81,** (2016).

214. Tolmachov, O. E. & Tolmachova, T. Design and Production of mRNA-based Gene Vectors for Therapeutic Reprogramming of Cell Fate. *Gene Technol.* **4,** e117 (2015).

215. Kim, N., Duncan, G. A., Hanes, J. & Suk, J. S. Barriers to inhaled gene therapy of obstructive lung diseases: A review. *J. Control. Release* **240,** 465–488 (2016).

216. Adams, S. T. & Miller, S. C. Beyond D-luciferin: Expanding the scope of bioluminescence imaging in vivo. *Curr. Opin. Chem. Biol.* **21,** 112–120 (2014).

217. Prescher, J. A. & Contag, C. H. Guided by the light: visualizing biomolecular processes in living animals with bioluminescence. *Curr. Opin. Chem. Biol.* **14,** 80–89 (2010).

218. Hoshino, H., Nakajima, Y. & Ohmiya, Y. Luciferase-YFP fusion tag with enhanced emission for single-cell luminescence imaging. *Nat. Methods* **4,** 637–639 (2007).

219. Saito, K. *et al.* Luminescent proteins for high-speed single-cell and whole-body imaging. *Nat. Commun.* **3,** 1262 (2012).

220. Ishikawa, T. O. & Herschman, H. R. Conditional bicistronic Cre reporter line expressing both firefly luciferase and B-galactosidase. *Mol. Imaging Biol.* **13,** 284–292 (2011).

221. Wang, Y., Sun, Z., Peng, J. & Zhan, L. Bioluminescent imaging of hepatocellular carcinoma in live mice. *Biotechnol. Lett.* **29,** 1665–1670 (2007).

222. Madisen, L. *et al.* A robust and high-throughput Cre reporting and characterization system for the whole mouse brain. *Nat. Neurosci.* **13,** 133–142 (2010).

223. Snapp, E. L. Fluorescent proteins: a cell biologist's user guide. *Trends Cell Biol.* **19,** 649–655 (2009).

224. Rubart, M. Two-photon microscopy of cells and tissue. *Circ. Res.* **95,** 1154–1166 (2004).

225. Baratta, J. L. *et al.* Cellular organization of normal mouse liver: A histological, quantitative immunocytochemical, and fine structural analysis. *Histochem. Cell Biol.* **131,** 713–726 (2009).

226. Broos, K. *et al.* Particle-mediated Intravenous Delivery of Antigen mRNA Results in Strong Antigen-specific T-cell Responses Despite the Induction of Type I Interferon. *Mol Ther Nucleic Acids* **5,** e326 (2016).

227. Park, J., Park, J., Pei, Y., Xu, J. & Yeo, Y. Pharmacokinetics and biodistribution of recently-developed siRNA nanomedicines. *Adv. Drug Deliv. Rev.* **104,** 93–109 (2015).

228. Holtkamp, S. *et al.* Modification of antigen encoding RNA increases stability , translational efficacy and T-cell stimulatory capacity of dendritic cells Modification of antigen encoding RNA increases stability , translational efficacy and T-cell stimulatory capacity of dendr. *Blood* **108,** 4009–4018 (2006).

229. Miller, J. B. *et al.* Non-Viral CRISPR/Cas Gene Editing In Vitro and In Vivo Enabled by Synthetic Nanoparticle Co-Delivery of Cas9 mRNA and sgRNA. *Angew. Chemie Int. Ed.* **56,** 1059–1063 (2016).

230. Kauffman, K. J. *et al.* Efficacy and immunogenicity of unmodified and pseudouridine-modified mRNA delivered systemically with lipid nanoparticles in vivo. *Biomaterials* **109,** 78–87 (2016).

231. Dar, S. A., Thakur, A., Qureshi, A. & Kumar, M. siRNAmod: A database of experimentally validated chemically modified siRNAs. *Sci. Rep.* **6,** 20031 (2016).

232. Holstein, J. M., Anhuser, L. & Rentmeister, A. Modifying the 5'-Cap for Click Reactions of

Eukaryotic mRNA and To Tune Translation Efficiency in Living Cells. *Angew. Chemie - Int. Ed.* **55,** 10899–10903 (2016).

233. Zuckerman, J. E. & Davis, M. E. Clinical experiences with systemically administered siRNA-based therapeutics in cancer. *Nat. Rev. Drug Discov.* **14,** 843–856 (2015).

234. Zatsepin, T. S. & Koteliansky, V. Lipid nanoparticles for targeted siRNA delivery – going from bench to bedside. *Int J Nanomedicine.* **11,** 3077–3086 (2016).

235. Pardi, N. *et al.* Administration of nucleoside-modified mRNA encoding broadly neutralizing antibody protects humanized mice from HIV-1 challenge. *Nat. Commun.* **8,** 14630 (2017).

236. Parmar, R. G. *et al.* Endosomolytic bioreducible poly(amido amine disulfide) polymer conjugates for the in vivo systemic delivery of siRNA therapeutics. *Bioconjug. Chem.* **24,** 640–7 (2013).

237. Nabhan, J. F. *et al.* Intrathecal delivery of frataxin mRNA encapsulated in lipid nanoparticles to dorsal root ganglia as a potential therapeutic for Friedreich's ataxia. *Sci. Rep.* **6,** 20019 (2016).

238. Yin, H., Kauffman, K. J. & Anderson, D. G. Delivery technologies for genome editing. *Nat. Rev. Drug Discov.* 1–13 (2017). doi:10.1038/nrd.2016.280

239. Yin, H. *et al.* Therapeutic genome editing by combined viral and non-viral delivery of CRISPR system components in vivo. *Nat. Biotechnol.* **34,** 328–33 (2016).

240. Lange, A. *et al.* Classical nuclear localization signals: Definition, function, and interaction with importin alpha. *J. Biol. Chem.* **282,** 5101–5105 (2007).